QSO ABSORPTION LINES AND THE IONIZING FIELD AT HIGH REDSHIFTS

Thesis by

Lin Zuo

In Partial Fulfillment of the Requirements
for the Degree of
Doctor of Philosophy

California Institute of Technology
Pasadena, California
1992

(Submitted November 15, 1991)

ACKNOWLEDGEMENTS

First I would like to thank my thesis adviser Dr. Sterl Phinney for his financial support, for the encouragement and for letting me free so that I could do things my way. During the last three and a half years Sterl has provided many insightful advises and made invaluable contribution to the work presented here. He is an excellent teacher and a great researcher. Many times discussion with him had helped clarify the problems. I am very impressed by his knowledge both in width and depth. His attitude towards doing research work will certainly influence my astronomy career for the years to come.

Dr. Wal Sargent was my supervisor during my first two years here at Caltech. From him I have learned a lot about observations of QSO absorption lines. It is really a great privilege to be so close with a leading expert when working in the field of QSO absorption lines and related subjects. Wal had provided financial support in the summer of 1987 and has been providing all the computer money I have been spending in these years. He has done so without asking anything for return. Because of this, I could stick in my spacious Robinson office and feel free to do things I want to do.

I would also like to thank Dr. Ray Weymann for his support and guidance during my first year in the United States. Working with him was a good start in my research career. Actually some of the concepts presented in this thesis were originated from discussion with him. I also greatly appreciate his recommendation

which brought me to Caltech. Drs. Jill Bechtold, Jim Liebert and Richard Green of University of Arizona are also thanked for their help and encouragement which made my stay in Tucson a little easier.

During the last five years at Caltech I have learned a lot from professors and fellow students of our astronomy department. I thank Drs. Roger Blandford, Nick Scoville, Peter Goldreich, George Djorgovski, Shri Kulkarni, Maarten Schmidt, Jeremy Mould and Tony Readhead for their excellent teaching and their effort on making Caltech a great place for astronomy students. I would also like to thank all my fellow students for discussion, help, encouragement and companionship. I especially wish to thank Chuck Steidel, Mingshen Han, Haiming Wang, Josh Roth, Fernando Selman, Zhong Wang and Wenge Xu. I thank our librarians for their assistance in finding important references. I'm going to miss great ping-pong games at the Robinson basement with Xiaopei Pan. He is the best opponent I've met here.

Dr. Richard McCray of University of Colorado wrote strong recommendation letters for me after his visit at Nanjing University, which made it possible for me to come to the States without having to take some examinations. I am always thankful for what he had done for me and hope that with this thesis I have not completely disappointed him.

I greatly appreciate a Li Ming scholarship award for the 1990—1991 academic year.

I also wish to thank my family for their understanding and support. I thank

my brother and sisters for taking care of mom and dad. I'm very sorry my father left this world too early. I wish I would have spent more time with him in 1989 summer when I was visiting my homeland. Finally, I would like to thank my wife Yuhua for her understanding, support and love. Being together with her has made life so enjoyable.

ABSTRACT

In this thesis we explore the relationship between the QSO absorption line systems and the metagalactic ionizing field at high redshifts.

In the first introductory chapter we describe the recent developments in the field of QSO absorption lines and the ionizing radiation background. We concentrate on compiling the new observational results and address why studies of QSO absorption line systems and ionizing field are important to our understandings of the formation and evolution of the large scale structure of the universe.

In the second chapter Markoff's method has been used to derive a general formalism to deal with the absorptions produced by randomly distributed discrete clouds, such as the QSO absorption line systems. Some analytical forms are obtained for the effective optical depth τ_{eff}, the count reduction factor f_c and the optical depth probability distribution function $P(\tau)$. We demonstrate that the spectrum of ionizing background is very different from the intrinsic source spectrum. We calculate the QSO contributions to $J_{\nu_L}(z_{obs})$ by using simple analytical expressions. We show that because of the Lyman continuum absorption produced by QSO absorption line systems, it is very difficult to find a "clear" line of sight to conduct the HeII Gunn-Peterson test. We have also found that dust grains in the QSO damped Lyα systems produce a marginally significant obscuration for $z = 3$ quasars: the count reduction factor is 1/1.7 at $z = 3$. The reddening is shown to be small for a flux limited QSO sample.

In the following two chapters we discuss fluctuations and intensity correlation in the ionizing field. We derive the intensity probability distribution function $P(J)$ for randomly distributed point sources. We show that absorptions by QSO absorption line systems reduce the total number of sources involved in producing the ionizing background and therefor enhance the fluctuation significantly, if QSOs are the main ionizing sources. We have calculated the intensity correlation function ξ_J for randomly distributed QSOs. The QSO Lyα clouds can be used as intensity indicators to reveal the intensity correlation at high redshifts. We have measured the equivalent width correlation function $\xi_{1/W}$ for several selected QSOs and have found, in some cases, strong correlation signals at small separations. Careful examination shows that such signals are mainly generated by the lines near the QSO emission redshifts. One explanation is that the high S/N near QSO emission redshifts enable us to detect very weak lines which result in the correlation signal. The other explanation is that the correlated intensities of ionizing field near QSOs have caused the observed equivalent width correlation. If this latter explanation is correct, from the affected range by QSOs we conclude that J_{ν_L} is less than 10^{-21}ergs $s^{-1}cm^{-2}Hz^{-1}sr^{-1}$ at $z \sim 3.5$.

The last two chapters deal with the ionization structure of the QSO Lyα clouds. We solve the coupled ionization balance and radiation transfer problem (the "inverse HII region" problem) for the non-uniform spherical absorbing clouds and calculate the HI column density distribution $f(N)$. We show that with an appropriate density gradient in the clouds we can reproduce the observed overall power law distribution

and the apparent excess of absorption systems with $N \geq 2 \times 10^{20} \mathrm{cm}^{-2}$. The calculated $f(N)$ is not sensitive to the input ionizing spectra and is a generic feature of the density profile. In our model all QSO absorption lines have the same origin: the ionized outer envelopes produce the Lyα forest lines while the neutral cores result in damped Lyα systems. We discuss the consequences of such models and propose star-forming dwarf galaxies as primary candidates for QSO absorption line systems. Our calculations also suggest that uniform cloud models are highly unlikely. To calculate the absorptions produced by HeI and HeII in QSO Lyα clouds we also solve the ionization structure for the clouds containing both H and He. We explore the variation of HeI and HeII distributions under different input ionizing spectra and discuss how to get a self-consistent spectral shape for the ionizing background.

TABLE OF CONTENTS

To the memory of my father

CHAPTER ONE

QSO ABSORPTION LINES AND THE IONIZING FIELD AT HIGH REDSHIFTS—AN INTRODUCTION

In this introductory chapter we describe the recent developments in the field of QSO absorption lines and the ionizing radiation background at high redshifts. We concentrate on compiling the new observational results and explore the relationship between QSO absorption line systems and the ionizing field. We address why such investigations are important to our understandings of the formation and evolution of the large scale structure of the universe.

In the past several years there have been some large surveys for QSO absorption line systems, which have spent a lot of large telescope times. Thus we have plenty of observational results to tell. On the other hand, there have been no direct observations of the ionizing background at high z. The results are indirect and subject to theoretical assumptions used to derive them.

1 QSO ABSORPTION LINES

It is now widely recognized that studies of QSO absorption line systems provide unique information about the universe at early epochs. Using luminous quasar as probe, the intervening gas clouds with very small HI column densities ($\sim 10^{13}\mathrm{cm}^{-2}$) can be detected along various lines of sight. QSO absorption spectra also show a variety of metal lines at high redshifts which are believed to be the traces of early

star formation processes. The distribution of QSO absorption line systems offer clues about how matter is distributed at redshifts back to $z > 4$ and at very large scales. Their evolution with cosmic time helps us to understand the evolution of the ionizing radiation field, the chemical composition and the fluctuation spectrum of density inhomogeneities.

It is convenient to categorize QSO absorption lines into four classes: the Lyα forest lines, the heavy element systems, the damped Lyα systems and the broad absorption line systems. We will discuss each of them in turn.

1.1 The Lyα Forest Lines

At sufficiently high spectral resolution all high redshift quasars show numerous narrow absorption lines at wavelengths shortward of Lyα emission. It is now firmly established that most of these lines are Lyα absorption features, thus the name of Lyα forest, which are produced by intervening absorbers (Lynds 1971; Sargent *et al.* 1980). New results show that in the redshift range $1.7 < z < 3.8$, the mean number of $W_{res} > 0.36\AA$ lines per unit redshift is $n(z) = 1.74(1+z)^{2.75\pm0.29}$, after excluding those lines within a distance less than 8Mpc from QSOs to avoid the "proximity effect" (Lu *et al.* 1991). This indicates significant evolution of Lyα absorbers with cosmic time, because a non-evolving population would result in $n(z) \propto (1+z)^{-2}(1+2q_0z)^{-1/2}$. The observed HI column density distribution is consistent with a power law $f(N) \propto N^{-1.5}$—$N^{-1.8}$ over the range of $13 < \log N < 16$ (Hunstead 1988; Carswell 1988; Carswell *et al.* 1991). Lyα forest lines show little,

if any, clustering on scales $\Delta v > 50$km s^{-1} (Webb 1987; Bechtold and Shectman 1989; Pettini *et al.* 1990). Most of Lyα forest lines, if not all, show no corresponding metal lines (Sargent 1988).

The best case so far for determining the characteristic size of Lyα clouds is the recent spectroscopic studies of the gravitationally lensed quasar pair UM673 A and B by Smette *et al.* (1991). They have found that all the 68 absorption lines present at 5σ in B are also present in A; there are only two anti-coincidences (present in A, not in B at 3σ), and these could be a MgII doublet. The velocity differences between corresponding lines in the two spectra are consistent with zero ($\sigma = 17$km s^{-1}). The equivalent widths are strongly correlated in the two spectra, essentially proving that the two lines of sight intersect the same clouds. From the above facts they inferred that the Lyα cloud diameters are in the range $12 < d < 160 h_{50}^{-1}$kpc (2σ limits); or, if the anti-coincidences are MgII, $d > 23 h_{50}^{-1}$kpc. The large range in d reflects the fact that while we can get a good lower limit we are not able to derive a stringent upper limit. The new analyses of the spectra of the gravitationally lensed QSO pair Q2345+007 A, B by McGill (1990), Duncan (1991) and Steidel and Sargent (1991a) also showed that the characteristic size of Lyα clouds could be considerably larger than previously quoted $\sim$ 10kpc.

Controversial conclusions have been reached regarding the Doppler widths b ($b = \sqrt{2}\sigma$, where σ is the radial dispersion of velocities) of Lyα absorption lines and cloud temperature T. Pettini *et al.* (1990) have observed a portion of the

QSO 2206–199N Lyα forest with a very high velocity resolution 6.5 km s^{-1}. They claim to have found some Lyα forest absorption lines with very small b values which correspond to T below 5000–10000K. But a more recent observation of QSO 1100–264 by Carswell *et al.* (1991) with a velocity resolution $\lesssim$ 9km s^{-1} has failed to find Lyα clouds whose temperatures must be less than 10^4K.

There are various models concerning the nature of the Lyα forest clouds (see Blades, Turnshek and Norman (1988) for comprehensive reviews). Given the facts that the Lyα clouds are large, $d > 10$kpc, and the typical absorption lines have a neutral hydrogen column density $N \sim 10^{15}$cm^{-2}, it is evident that these intervening clouds can be highly photoionized by the integrated ionizing flux from quasars and galaxies. Actually most of the models proposed for the Lyα forest clouds satisfy the photoionization assertion. In the pressure confinement model first proposed by Sargent *et al.* (1980) and later studied in more detail by Ostriker and Ikeuchi (1983) and Ikeuchi and Ostriker (1986), the Lyα clouds are primordial clumps confined by a hot and rarefied intergalactic medium (IGM). On the other hand, gravitational force either involving the dark matter or from pure baryons have been proposed to confine the Lyα clouds (Black 1981; Melott 1980; Rees 1986, 1988; Ikeuchi 1986). There are also models in which the Lyα clouds need not be confined. Bond *et al.* (1988) have argued that these clouds are pressure-driven relics which went to expansion when photoionization occurred. Fransson and Epstein (1982) have proposed that the Lyα forest lines are due to the galactic wind from high redshift dwarf galaxies. The "forest" of theoretical models reflects our poor understanding of the nature of

the Lyα absorbers at present time.

1.2 The Heavy Element Systems

The heavy element systems are metal containing narrow absorption lines. Among the numerous observed ionic line transitions the doublets of MgII$\lambda\lambda$ 2795.5, 2802.7 and CIV$\lambda\lambda$ 1548.2, 1550.8 are usually the strongest and easiest to detect. Most of the identifications of heavy element systems are based on the presence of at least one of these two doublets. At $z \gtrsim 0.3$ the MgII doublet moves into the optical domain. At redshifts above 1 the CIV doublet start to dominate the picture. The recent CIV absorption survey by Sargent, Boksenberg and Steidel (1988) and its high redshift extension by Steidel (1990a) have shown that at $z \approx 2.5$ there are about 2 CIV systems per unit redshift interval with $W_{res} > 0.15\AA$ for both doublet components. For such CIV absorption lines $n(z) \propto (1+z)^{-1.26\pm0.56}$ in the range $1.3 \leq z_{obs} \leq 3.7$, if expressed as a power law. The 2-point correlation function for the CIV redshifts shows that there is a significant clustering of the redshifts on scales up to 600km s^{-1} in the rest frame of the absorbers. A CIV system with $z_{obs} = 4.13$ has been detected (Steidel 1990a). There are about 1 MgII systems per unit redshift with $W_{res}(2796) \geq 0.3\AA$ at redshift $z_{obs} \sim 1$. $n(z) \propto (1+z)^{0.78\pm0.42}$ for such systems in the redshift range $0.2 \leq z_{obs} \leq 2.2$ (Steidel and Sargent 1991b).

By studying the absorption features in the spectra of close quasar pairs and gravitationally lensed QSO images, very important information can be obtained about the sizes of the metal absorption line clouds. The very recent observation

of the gravitationally lensed QSO pair Q2345+007 A, B by Steidel and Sargent (1991a) has clearly revealed the differences in CIV absorption line strengths along the two lines of sight. This means that the distribution of CIV varies over scales as small as 1.4—$8.5h^{-1}$ kpc, depending on the assumed lens redshift and q_0. This combined with the clustering result strongly suggests that the absorption occurs in relatively small clouds which are embedded in much larger structures.

The heavy element systems are believed to be somehow associated with galaxies. There are some observational evidences which support this view. In some cases CaII$\lambda\lambda$3933.7, 3968.5 and NaI$\lambda\lambda$5890.0, 5895.9 absorption lines in the spectra of QSOs are found to correspond to nearby galaxies which are close to quasars on the plane of the sky (Boksenberg and Sargent 1978; see also the review by Blades 1988). In some other cases mapping of QSO fields reveals galaxies at redshifts same as that of metal absorption line systems observed in the QSO spectra (Bergeron 1988; Bergeron and Boisse 1991).

One important subset of the heavy element systems is the Lyman limit systems (LLS), since most of them contain metal lines. Such systems have a neutral hydrogen column density larger than $1.6 \times 10^{17}\mathrm{cm}^{-2}$ and are optically thick to Lyman limit frequency photons. Sargent, Steidel and Boksenberg (1989) found that $n(z = 2.950) = 1.91 \pm 0.33$ for LLS with $N \geq 2.4 \times 10^{17}\mathrm{cm}^{-2}$. The more recent survey by Lanzetta *et al.* (1991) confirmed this result (Lanzetta 1991). But controversial results regarding the evolution of LLS are reached by these two groups.

Sargent, Steidel and Boksenberg found $n(z) \propto (1+z)^{0.68\pm0.54}$ in the range of $0.67 \leq z_{LLS} \leq 3.58$, while Lanzetta claimed that $n(z)$ is virtually constant over the redshift range $0.35 \leq z \lesssim 2.5$ and evolves as $n(z) \propto (1+z)^{5.7\pm1.9}$ in the redshift range $2.5 \leq z \leq 3.7$.

1.3 The Damped Lyα Systems

Damped Lyα systems have column densities greater than $10^{20}\mathrm{cm}^{-2}$. The Lyα absorption lines produced by such systems are broadened by radiation damping and have rest frame equivalent widths $> 5\mathring{A}$ (Wolfe *et al.* 1986). The recent spectroscopic survey by Lanzetta *et al.* (1991) showed that at an average redshift of $\langle z_{obs} \rangle \approx 2.5$, $0.16 \pm 0.03 \leq n(z) \leq 0.25 \pm 0.04$ for those systems with HI column density $N \geq 2 \times 10^{20}\mathrm{cm}^{-2}$. They also found that over the HI column density range $20.3 \leq \log N \leq 21.8$, $f(N) \propto N^{-1.67\pm0.19}$. From these observations it can be inferred, quite model independently, that the mean value of the cosmological mass density contributed by the damped Lyα absorbers is $\langle \Omega_D \rangle = 0.79 \pm 0.14 \times 10^{-3} h^{-1}$ for $q_0 = 0$ and $\langle \Omega_D \rangle = 1.45 \pm 0.25 \times 10^{-3} h^{-1}$ for $q_0 = 0.5$. This value is roughly equal to the entire present-day luminous matter content in the universe.

When a damped Lyα system is observed against a radio-loud quasar, 21 cm absorption is usually detected at the same redshift as the Lyα absorption. Briggs *et al* (1989) have used VLBI to show that the damped Lyα system detected in 21 cm absorption at $z = 2.04$ in front of radio source PKS 0458-020 extends across a transverse dimension exceeding $8\,h^{-1}$kpc. Foltz, Chaffee and Wolfe (1988) have found

low-ionization absorptions at $z \simeq 0.44$ in spectrum of QSO 3CR 196. This absorption redshift is only $\sim 60\text{km s}^{-1}$ away from the previously known 21 cm absorption feature observed in the same object. Since the radio emission is predominantly from extended lobes, the whole absorption system must be at least large enough to cover the optical QSO and part of one or both of the lobes. This leads directly to a lower limit on the size of the absorption system of about 6.5 kpc.

Wolfe *et al.* (1986) (see also Wolfe 1988) have proposed that damped Lyα systems may be large HI disks which are the progenitors of normal galaxies. Very recently Lowenthal *et al.* (1991) have reported the detection of a galaxy associated with the damped Lyα absorbing cloud seen at $z = 3.09$ toward the QSO PHL 957 ($z_{em} = 2.681$). This association encourages an identification of the damped Lyα systems with nearby galaxies. But the rate of incidence of damped Lyα absorbers is greater than that expected for local galaxies (Lanzetta *et al.* 1991). It is possible that two different populations of damped Lyα absorbers exist. One is associated with large sized disk galaxies, and the other may consist of a large number of small objects, such as dwarf galaxies at high z, which produce the observed high incidence rate.

1.4 The Broad Absorption Line (BAL) Systems

About 10% of all optically selected QSOs show very broad absorption troughs (Turnshek 1988). Resonance line transitions due to CIV, SiIV, NV and OVI are commonly observed, indicating high ionization states. The outflow velocities relative to QSOs

can reach as high as 30,000 km s^{-1}. It is almost certain that BAL systems are associated with quasars themselves.

2 THE INTERGALACTIC IONIZING FIELD

According to the standard picture of big bang cosmology, at early epochs the universe kept cooling while it was expanding. When it was cool enough (this happened at $z \sim 1000$) protons and electrons combined to form hydrogen atoms. Shortly after this had happened the universe was neutral. From observations of the cosmic microwave background we know it was also very smooth. Because of gravitational instability small density perturbations grew. When they became strong enough gravitational collapses occurred and stars, galaxies and quasars formed. Schneider, Schmidt and Gunn (1991) have recently discovered a quasar with $z_{em} = 4.9$. From its spectrum we can clearly see the existence of heavy elements at that epoch. These heavy elements are believed to have been formed from cooking hydrogen atoms in star formation processes.

The formation of astronomical objects, in turn, affected the IGM by depositing energy and radiation into the surrounding environment. The integrated ionizing flux from quasars and galaxies may have been responsible for the reionization of IGM, the ionization of Lyα clouds and even the metal absorption line systems. Studies of the ionizing field and its evolution with redshift provide important clues to the formation and evolution of quasars and galaxies.

2.1 The Ionizing Flux from QSOs

If we could observe all the ionizing sources in the universe we can simply add them together to get the integrated ionizing background. Of course this is only a dream. At high redshifts the only ionizing sources which are observed in large quantities are quasars. And even for these intrinsically luminous objects we still don't know enough about the luminosity function at $z \gtrsim 2.2$. The situation is further complicated by absorptions produced by QSO absorption line systems. Bechtold *et al.* (1987) and Miralda-Escudé and Ostriker (1990) have calculated QSO contributions to the ionizing field. In Chapter Two and Chapter Four we will show that for $z \geq 2.2$ the calculated Lyman limit frequency intensity is roughly constant at a level of $J_{-21} \simeq 0.4$, where J_{-21} is the Lyman limit frequency intensity of the ionizing field expressed in units of 10^{-21}ergs cm^{-2} sec^{-1}Hz^{-1}sr^{-1}. In our calculations we have assumed that the comoving space QSO luminosity function is unchanged and takes the form as determined by Boyle *et al.* (1988) at $z = 2.2$. The recent work by Schmidt, Schneider and Gunn (1991) have showed that QSOs are endangered species at early epochs and their comoving space densities decline steeply for redshifts larger than 3. Also we have used $n(z) \propto (1+z)^{\gamma}$ with $\gamma = 0.5$ or 1 for LLS, thus we may have underestimated the absorption at high z since Lanzetta (1991) showed that LLS may evolve much more rapidly at early epochs. So our results should be taken as upper limits for QSO contributions to the ionizing field.

2.2 The Gunn-Peterson Effect

The Gunn-Peterson effect states that if there were any significant smoothly distributed neutral hydrogen component, there would exist a significant trough-like absorption in the spectra of quasars shortward of the Lyα emission. The absence of such absorption feature in the observed QSO spectra indicates strongly that the reionization must have taken place at redshift larger than 4. Upper limits for the Gunn-Peterson optical depths at various redshifts have been obtained by many people (Steidel and Sargent 1987; Jenkins and Ostriker 1991; Webb *et al.* 1991). These limits are important, since they allow us to put constraints to the ionizing background and the mass density of the smooth IGM.

Since the IGM is highly ionized the time scale to recombine the small amount of IGM n_{HI} is shorter than the Hubble time (Sargent *et al.* 1980). This means the ionization equilibrium is valid and we can relate the Gunn-Peterson optical depth τ_{GP} to the smooth IGM mass density and the ionizing field intensity. We have $J_{-21} \simeq 0.3(1+z)^5(1+2q_0z)^{-1/2}\Omega_I^2h^3/\tau_{GP}$, where Ω_I is the contribution to the present day density parameter by the smooth ISM component. Steidel and Sargent have shown that at redshift $z = 2.64$, $\tau_{GP} < 0.02 \pm 0.03$. Taking $q_0 = 0.5$, $\Omega_I = 0.05$, $h = 0.5$ and $\tau_{GP} < 0.05$, we get $J_{-21}(z = 2.64) > 0.6$. Miralda-Escudé and Ostriker (1990) estimated $\tau_{GP} < 0.1$ for QSO 0000-26 ($z_{em} = 4.1$) from the spectrum taken by Webb *et al.* (1988). This means $J_{-21}(z = 4.1) > 1.4$! These results indicate that QSOs may not be the dominating ionizing sources at high z. There may be other sources, such as young galaxies (see Bechtold *et al.* 1987) with plenty of massive main sequence stars within them, which dominate the ionizing

background. With the discovery of the $z_{em} = 4.9$ quasar we hope a more stringent limit will be obtained in the near future.

We should point out that the Gunn-Peterson effect is mixed together with the Lyα forest lines and it is very hard to disentangle them, especially for high redshift QSOs (Webb *et al.* 1991). This makes the accurate determination of τ_{GP} very difficult. Also J_{-21} is very sensitive to Ω_I, which we don't know. But since the galaxy formation process is most unlikely to be perfectly efficient, Ω_I may not be very much smaller than the total baryon contribution Ω_b obtained from nucleosynthesis calculations: $0.04 \leq \Omega_b \leq 0.1$ (Boesgaard and Steingman 1985), here we have used $h = 0.5$. Further complications may involve subtraction of Lyα emission lines, accurate determination of continuum level and correction for the proximity effect (see Chapter Three). In Chapter Two and Chapter Three we will also discuss the HeII Gunn-Peterson test using *HST* and the future space observatories.

2.3 The Inverse or Proximity Effect

The proximity effect or the inverse effect, was first noticed by Carswell *et al.* (1984). It seems that the cloud number density rises less rapidly with redshift within an individual QSO, as one approaches the QSO, than in an ensample of QSO spectra at the same redshift. Using a large sample of QSO Lyα forest lines with $W_{res} \geq 0.36\AA$, Lu *et al.* (1991) recently showed that the line number density per unit redshift is $n(z) \propto (1+z)^{2.37\pm0.26}$. But when those lines within a distance less than 8Mpc

from the QSOs are excluded, they got $n(z) \propto (1+z)^{2.75\pm0.29}$, which means a more significant evolution. One explanation for such effect is that the enhanced ionizing field near QSOs ionize HI more significantly and remove week Lyα lines from the rest equivalent width limited sample. If this ionization model is correct, J_{-21} can be determined. Bajtlik *et al.* (1988) and Lu *et al.* (1991) have carried out detailed analyses to show that J_{-21} is constant for $1.7 < z < 3.8$ and equal to $\log J_{-21} = 0.0 \pm 0.5$.

A way to check the correctness of the ionization model is to search for correlations between QSO Lyman limit luminosities and the proximity effect. Bajtlik *et al.* (1988) found a weak positive correlation but Lu *et al.* (1991) found no evidence for such correlation. It should be pointed out that in these two samples most of QSO Lyman limit frequency luminosities are estimated from their visual magnitudes using a empirical fitting formula given by Tytler (1987). Such a scheme may lead to large errors. Since there are only a few $W_{res} \geq 0.36\AA$ lines within a typical bright QSO influence range in which the enhanced ionizing field is at least two times larger than the mean background, we expect large fluctuations. Regarding the QSO emission redshifts an additional complication should also be considered. It has been found that the high-ionization lines, such as CIVλ1549, and Lyα emission lines have lower redshifts by around 1000km s^{-1} compared to the low-ionization lines and Hα (see Carswell *et al.* (1991) and references therein). Carswell *et al.* (1991) have argued that the redshift of low-ionization lines represents the systematic quasar redshift, because in the spectrum of QSO 1331+170 the detected [OIII]λ5007 emission line,

which is expected to arise in the extended emission region and thus represents the systematic quasar redshift, has a redshift similar to that of low-ionization lines. This means that in the two QSO samples used by Bajtlik *et al.* (1988) and Lu *et al.* (1991) the systematic emission redshifts for the quasars have been underestimated, since they are mainly derived from CIV emission lines. All these caveats make the determination of J_{-21} a very hard task and the uncertainties may be larger than quoted by Bajtlik *et al.* and Lu *et al.*.

Very recently Dobrzycki and Bechtold (1991) have discovered a large ($\sim$ 10Mpc) void in the spectrum of QSO 0302-003. From the assumption that the void is due to the proximity effect generated by the observed nearby quasar, they derived the background UV flux at $z \approx 3.2$ to be $J_{-21} = 0.1$. But this result can be further complicated by the possible quasar anisotropic emission and luminosity variation in the time scale of a few times 10^7 years.

2.4 Other Constraints to the Ionizing Background

While the Gunn-Peterson effect and the proximity effect seem to set important constraints to the Lyman limit frequency intensity of ionizing field, the observed relative column densities of metal ions in QSO heavy element systems may be used to constrain the shape of the ionizing flux spectrum. This assumes that the metal line systems are photoionized by the ionizing background. Steidel and Sargent (1989) and Steidel (1990b) have argued that one can rule out young galaxies as the main source of ionization, because their spectrum is too soft. This soft spectrum

leads to the result that metal line systems are dominated by low-ionization species, in clear contradiction with the observations. But there are two factors which should be considered before this conclusion is confirmed. One is that although QSOs may not be the dominating source for ionizing HI, they may be important contributors to the ionizing flux at shorter wavelengths. Another factor one should consider is that QSO absorption line systems produce significant absorption to the ionizing flux, especially at high redshift. Since the absorption is frequency dependent, photons with energies just above 13.6eV can travel only a small distance before they are absorbed while higher energy photons can contribute to the ionizing field from a much larger volume. The resulting ionizing spectrum is then flatter then the intrinsic spectrum of ionizing sources (see Chapter Two and Chapter Three). More recently Giroux and Shapiro (1991) and Madau (1991) have shown that when this frequency dependent absorption effect is taken into account, the ionizing field generated by young, star-forming galaxies can reproduce the observed results.

An interesting upper limit for J_{-21} is obtained by Songaila, Cowie and Lilly (1990). They noticed that observations so far have failed to detect significant Lyα emission from damped Lyα clouds. They argued that the surfaces of damped Lyα systems must absorb the incident ionizing photons and emit roughly one Lyα photon per ionization. Therefor the 3σ upper limits of 10^{-17}ergs cm^{-2}s^{-1}arcsec^{-2} around the four damped Lyα systems observed by Smith *et al.* (1989) leads to $J_{-21} < 53[(1+z)/3.5]^4$ in the redshift range $z = 2.3$—2.8.

Locally direct measurements of diffuse far ultraviolet background have been carried out with detectors on sounding rockets or spacecraft (see Bowyer 1991 and Henry 1991 for comprehensive reviews). The intensity of the diffuse background is estimated to be $J_\nu(z = 0) \sim 2.7 \times 10^{-21}[\lambda/(10^3 \mathring{A})]$ergs cm^{-2}s^{-1}Hz^{-1}sr^{-1} in the wavelength range $\sim$ 1216 to 3200$\mathring{A}$ (and possibly beyond). This background is not detected at wavelengths below 1216$\mathring{A}$. The upper limit is $\sim 8.2 \times 10^{-22}$ergs cm^{-2}s^{-1}Hz^{-1}sr^{-1}. But this background may primarily Galactic in origin (Bowyer 1991; Henry 1991). An indirect upper limit for the local ionizing field intensity was obtained by Songaila *et al.* (1989). They have measured an H_α surface brightness of 30 mR at two positions on high-velocity neutral hydrogen cloud complex C. They argued that each incident ionizing photon onto the system must be matched by one recombination which in turn produces 0.46 H_α photons (case B). Thus the observed surface brightness means $J_{-21}(z = 0) \leq 0.06$. Our calculations in Chapter Two show that the observed QSOs contribute a $J_{-21}(z = 0) \sim 1.4 \times 10^{-2}$.

REFERENCES

Bajtlik, S., Duncan, R. C. & Ostriker, J. P., 1988. *Astrophys. J.*, **327**, 570.

Bechtold, J. & Shectman, S. A., 1989. *IAU Symp. 134: Active Galactic Nuclei*, P549, eds Osterbrock, D. E. & Miller, J. S., Kluwer Academic Publishers, Dordrecht.

Bechtold, J., Weymann, R. J., Lin, Z. & Malkan, M. A., 1987. *Astrophys. J.*, **315**, 180.

Bergeron, J., 1988. In: *Quasar Absorption Lines: Probing the Universe*, P127, eds. Blades, C. *et al.*, Cambridge University Press.

Bergeron, J., Boisse, P., 1991. *Astron. Astrophys.*, **243**, 344.

Black, J. H., 1981. *Mon. Not. R. astr. Soc.*, **197**, 553.

Blades, J. C., Norman, C. & Turnshek, D., 1988. *Quasar Absorption Lines: Probing the Universe*, eds., Cambridge University Press.

Blades, J. C., 1988. In: *Quasar Absorption Lines: Probing the Universe*, P147, eds. Blades, C. *et al.*, Cambridge University Press.

Boesgaard, A. M. & Steingman, G. A., 1985. *Ann. Rev. Astr. Astrophys.*, **23**, 319.

Boksenberg, A. & Sargent, W. L. W., 1978. *Astrophys. J.*, **220**, 42.

Bond, J. R., Szalay, A. S. & Silk, J., 1988. *Astrophys. J.*, **324**, 627.

Bowyer, S., 1991. In: *Annu. Rev. Astron. Astrophys.*, **29**, p29.

Boyle, B. J., Shanks, T. & Peterson, B. A., 1988. *Mon. Not. R. astr. Soc.*, **235**, 935.

Briggs, F. H., Wolfe, A. M., Lisct, H. S., Davis, M. M., & Turner, K. L., 1989. *Astrophys. J.*, **341**, 650.

Carswell *et al.*, 1991. *Astrophys. J. Lett.*, **381**, L5.

Carswell, R. F., Lanzetta, K. M., Parnell, H. C. & Webb, J. K., 1991. *Astrophys. J.*, **371**, 36.

Carswell, R. F., 1988. In: *Quasar Absorption Lines: Probing the Universe*, p91, eds Blades, C. *et al.*, Cambridge University Press.

Carswell, R. F., Morton, D. C., Smith, M. G., Stockton, A. N., Turnshek, D. A. & Weymann, R. J., 1984. *Astrophys. J.*, **278**, 486.

Dobrzycki, A. & Bechtold, J., 1991. *Astrophys. J. Lett.*, **377**, L69.

Duncan, R. C., 1991. *Astrophys. J. Lett.*, **375**, L41.

Foltz, C. B., Chaffee, Jr., F. H. & Wolfe, A. M., 1988. *Astrophys. J.*, **335**, 35.

Fransson, C. & Epstein, R., 1982. *Mon. Not. R. astr. Soc.*, **198**, 1127.

Giroux, M. L., & Shapiro, P. R., 1991. In: *After the First Three Minutes*, eds. S. S. Holt, C. L. Bennet, & V. Trimble (AIP), p352.

Henry, R. C., 1991. In: *Annu. Rev. Astron. Astrophys.*, **29**, p89.

Hunstead, R. W., 1988. In: ***Quasar Absorption Lines***, p71, eds Blades, C. *et al.*, Cambridge University Press.

Ikeuchi, S., 1986. *Astrophys. Space Sci.*, **118**, 509.

Ikeuchi, S. & Ostriker, J. P., 1986. *Astrophys. J.*, **301**, 522.

Jenkins, E. B. & Ostriker, J. P., 1991. *Astrophys. J.*, **375**, in press.

Lanzetta, K. M., 1991. *Astrophys. J.*, **375**, 1.

Lanzetta, K. M., Wolfe, A. M., Turnshek, D. A., Lu, L., McMahon, R. G. & Harzard, C., 1991. *Astrophys. J. Suppl. Ser.*, **77**, 1.

Lowenthal, J. D., Hogan, C. J., Green, R. F., Caulet, A., Woodgate, B. E., Brown, L. & Foltz, C. B., 1991. *Astrophys. J. Lett.*, **377**, L73.

Lu, L., Wolfe, A. M. & Turnshek, D. A., 1991. *Astrophys. J.*, **367**, 19.

Lynds, C. R., 1971. *Astrophys. J. Lett.*, **164**, L73.

Madau, P., 1991. *Astrophys. J. Lett.*, **376**, L33.

McGill, C., 1990. *Mon. Not. R. astr. Soc.*, **242**, 544.

Mellot, A. L., 1980. *Astrophys. J.*, **241**, 889.

Miralda-Escudé, J. & Ostriker, J. P., 1990. *Astrophys. J.*, **350**, 1.

Ostriker, P. J. & Ikeuchi, S., 1983. *Astrophys. J. Lett.*, **268**, L63.

Pettini, M., Hunstead, R. W., Smith, L. J. & Mar, D. P., 1990. *Mon. Not. R. astr. Soc.*, **246**, 545.

Rees, M. J., 1986. *Mon. Not. R. astr. Soc.*, **218**, 25p.

Rees, M. J., 1988. In: *Quasar Absorption Lines*, p107, eds. Blades, C. *et al.*, Cambridge University Press.

Sargent, W. L. W., 1988. In: *Quasar Absorption Lines*, p1, eds. Blades, C. *et al.*, Cambridge University Press.

Sargent, W. L. W., Boksenberg, A. & Steidel, C. C., 1988. *Astrophys. J. Suppl. Ser.*, **68**, 539.

Sargent, W. L. W., Steidel, C. C. & Boksenberg, A., 1989. *Astrophys. J. Suppl. Ser.*, **69**, 703.

Sargent, W. L. W., Young, P. J., Boksenberg, A. & Tytler, D., 1980. *Astrophys. J. Suppl. Ser.*, **42**, 41.

Schmidt, M., Schneider, D. P. & Gunn, G. E., 1991. Paper presented at the workshop on: *Space Distribution of Quasars.*

Schneider, D. P., Schmidt, M. & Gunn, G. E., 1991. *Astron. J.*, **102**, 837.

Smette, A., Surdej, J., Shaver, P., Foltz, C. B., Chaffee, F. H., Weymann, R. J., Williams, R. E. & Magain, P., 1991. In: *Proceedings of the ESO Mini-Workshop on Quasar Absorption Lines*, ESO scientific Report #9.

Smith, H. E., Cohen, R. D., Burns, J. E., Moore, D. J. & Uchida, B. A., 1989. *Astrophys. J.*, **347**, 87.

Songaila, A., Bryant, W. & Cowie, L. L., 1989. *Astrophys. J. Lett.*, **345**, L71.

Songaila, A., Cowie, L. L. & Lilly, S. J., 1990. *Astrophys. J.*, **348**, 371.

Steidel, C. C., 1990a. *Astrophys. J. Suppl. Ser.*, **72**, 1.

Steidel, C. C., 1990b. *Astrophys. J. Suppl. Ser.*, **74**, 37.

Steidel, C. C. & Sargent, W. L. W., 1987. *Astrophys. J. Lett.*, **318**, L11.

Steidel, C. C. & Sargent, W. L. W., 1989. *Astrophys. J. Lett.*, **343**, L33.

Steidel, C. C. & Sargent, W. L. W., 1991a. *Astron. J.*, in press.

Steidel, C. C. & Sargent, W. L. W., 1991b. *Astron. J. Suppl. Ser.*, in press.

Turnshek, D. A., 1988. In: *Quasar Absorption Lines: Probing the Universe*, p17, eds. Blades, C. *et al.*, Cambridge University Press.

Tytler, D., 1987. *Astrophys. J.*, **321**, 69.

Webb, J. K., 1987. *IAU Symp. 124: Observational Cosmology*, p803, eds. Hewitt, A., Burbidge, G. & Fang, L., Reidel, Dordrecht.

Webb, J. K., Parnell, H. C., Carswell, R, F., McMahon, R. G., Irwin, M. J., Hazard, C., Ferlet, R. & Vidal-Madjar, A., 1988. *ESO Messenger*, **51**, 15.

Webb, J. K., Barcons, X., Carswell, R, F. & Parnell, H. C., 1991. preprint.

Wolfe, A. M., 1988. In: *Quasar Absorption Lines: Probing the Universe*, p298, eds. Blades, C. *et al.*, Cambridge University Press.

Wolfe, A. M., Turnshek, D. A., Smith, H. E. & Cohen, R. D., 1986. *Astrophys. J. Suppl. Ser.*, **61**, 249.

CHAPTER TWO

ABSORPTION BY RANDOMLY DISTRIBUTED CLOUDS —THEORY AND SOME APPLICATIONS

SUMMARY. Using Markoff's method we have derived a general formalism to deal with the absorptions produced by randomly distributed discrete clouds, such as the QSO absorption line systems. Some analytical forms are obtained for the effective optical depth τ_{eff}, the count reduction factor f_c and the optical depth probability distribution function $P(\tau)$. We demonstrate that the spectrum of ionizing background is very different from the intrinsic source spectrum. We calculate $J_{\nu_L}(z_{obs})$ by using simple analytical expressions. We show that because of the Lyman continuum absorption produced by QSO absorption line systems, it is very difficult to find a "clear" line of sight to conduct the HeII Gunn-Peterson test. We have also found that dust grains in the damped Lyα systems produce a marginally significant obscuration for $z = 3$ quasars: the count reduction factor is 1/1.7 at $z = 3$. The reddening is shown to be small for a flux limited QSO sample.

1 INTRODUCTION

The spectra of high redshift quasars show numerous absorption lines. It is now widely accepted that most of these absorption lines are produced by intervening discrete objects. The Lyα forest lines are believed to have been produced by primordial gas clumps; the narrow metal line absorption systems are thought to be somehow related with galaxies; and the damped Lyα systems may even be the primeval disk galaxies in the making (see Blades, Turnshek and Norman (1988) for comprehensive reviews about these QSO absorption line systems). The Lyα forest lines show little, if any, clustering on scales $\Delta v > 50\text{km sec}^{-1}$ (Webb 1987; Bechtold and Shectman 1989; and Pettini *et al.* 1990). By contrast, the distribution of velocity splittings for CIV absorbers shows a strong excess of pairs with splittings of $\Delta v \simeq 500\text{km sec}^{-1}$ (Sargent, Boksenberg and Steidel 1988). These absorption systems contain enough neutral hydrogen atoms to significantly absorb the ionizing flux from distant sources, and some of them may have a significant amount of dust grains to redden background quasars or even remove them from a flux limited sample. Thus they have important consequences to our understanding of the universe at early epochs. In this paper, as the first order approximation, we neglect any deviation from Poisson randomness and derive a general formalism to deal with the absorptions produced by randomly distributed discrete absorbers in an expanding universe. The previous works on this subject include studies of dusty galaxy obscuration of distant quasars by Ostriker and Heisler (1984), Heisler and Ostriker (1988) and Wright (1986, 1990), and the Monte Carlo simulation of the

"Lyman valley" transmission by Møller and Jakobsen (1990).

2 FORMULATION

2.1 Optical Depth Distribution $P_k(\tau)$

Assume that along a line of sight there are k clouds between redshifts z_{obs} and z_u. The probability distribution for a cloud being at redshift z and with a neutral hydrogen column density N is $f(z,N)$. We observe at z_{obs} and at the wavelength λ_{obs}. Let the optical depth produced by a cloud of column density N at z be $\tau_c(z,N)$. We want to know the probability distribution function of the total optical depth $\tau = \sum_{i=1}^{k} \tau_c^i$. Using Markoff's method (see Chandrasekhar 1943) we can easily write down the probability distribution:

$$P_k(\tau) = \frac{1}{2\pi} \int_{-\infty}^{\infty} e^{-is\tau} A_k(s) ds, \tag{2.1}$$

where N_l and N_u are the lower and upper column density limits, respectively, and

$$A_k(s) = \left[\int_{N_l}^{N_u} dN \int_{z_{obs}}^{z_u} e^{is\tau_c(z,N)} f(z,N) dz \right]^k. \tag{2.2}$$

For $k = 1$ we have

$$P_1(\tau) = \int\int f(z,N) \delta[\tau - \tau_c(z,N)] dz dN. \tag{2.3}$$

Let $\eta(z,N)dzdN$ be the mean number of absorbing clouds in the redshift interval $z \rightarrow z + dz$ and with a neutral column density in the range $N \rightarrow N + dN$, we

have $f(N,z) = \eta(z,N)/\overline{n}$, where $\overline{n} = \int\int \eta(z,N)dzdN$ is the mean total number of clouds between z_{obs} and z_u.

For a simple example we consider the case of face-on uniform disks used by Ostriker and Heisler (1984) in exploring the dust grain obscuration of high redshift quasars. In this case $z_{obs} = 0$ and $\eta(z,N) = \pi r_d^2 n_g (c/H_0)(1+z)^{1/2}\delta(N-N_0)$, where N_0 is column density of the face-on disks, which are assumed to be identical, n_g is the assumed constant galaxy comoving space density and r_d is the disk radius. For the local selective dust grain extinction Ostriker and Heisler adopted $\tau_c \propto N\lambda^{-1}$. At the observed wavelength if we denote the optical depth produced by a local disk as τ_0 then we have $\tau_c = \tau_0(1+z)$ for an intervening disk at z. Let $t = \tau/\tau_0$, i.e., we measure the optical depth in units of τ_0, we can easily show that

$$P_1(t) = \begin{cases} D\sqrt{t} & \text{if } 1 < t < 1 + z_u \\ 0 & \text{elsewhere,} \end{cases} \tag{2.4}$$

where $D = 1.5\left[(1+z_u)^{1.5} - 1\right]^{-1}$. In this simple case a closed form for $P_2(t)$ can also be obtained. Denoting $t_u = 1 + z_u$ we have

$$P_2(t) = \begin{cases} 0 & \text{for } t < 2 \\ D^2\left[\left(\frac{t}{2} - 1\right)\sqrt{t-1} + \frac{t^2}{4}\arcsin\left(1 - \frac{2}{t}\right)\right] & \text{for } 2 < t < 2 + z_u \\ D^2\left[\left(t_u - \frac{t}{2}\right)\sqrt{t_u t - t_u^2} + \frac{t^2}{4}\arcsin\left(\frac{2t_u}{t} - 1\right)\right] & \text{for } 2 + z_u < t < 2t_u \\ 0 & \text{for } t > 2t_u. \end{cases} \tag{2.5}$$

$P_k(\tau)$ with $k > 2$ may be obtained by convolving lower k value distributions. For example, we have

$$P_3(t) = \int_2^{2(1+z_u)} P_1(t-u)P_2(u)du, \tag{2.6}$$

$$P_4(t) = \int_2^{2(1+z_u)} P_2(t-u)P_2(u)du, \tag{2.7}$$

and so on. Some of our calculated results are shown in Fig. 1.

2.2 Optical Depth Distribution $P(\tau)$ and Effective Optical Depth τ_{eff}

Now consider that the total number of clouds between z_{obs} and z_u is not a fixed number but obeys Poisson distribution with a mean total number $\overline{n}$, that is,

$$P(k,\overline{n}) = \frac{\overline{n}^k}{k!}e^{-\overline{n}}. \tag{2.8}$$

In this case the optical depth probability distribution is

$$P(\tau) = \sum_{k=0}^{\infty} P(k,\overline{n})P_k(\tau) = \frac{1}{2\pi}\int_{-\infty}^{\infty} e^{-is\tau}e^{-\overline{n}[1-I(s)]}ds, \tag{2.9}$$

where

$$\overline{n}[1-I(s)] = \int_{z_{obs}}^{z_u} dz \int_{N_l}^{N_u} \eta(z,N)\left[1-e^{is\tau_c(z,N)}\right]dN. \tag{2.10}$$

We see that $\tilde{p}(s) \equiv e^{-\overline{n}[1-I(s)]}$ is actually the Fourier transform of $P(\tau)$.

In studying the effect produced by discrete absorbing clouds a very useful concept is the effective optical depth τ_{eff}. τ_{eff} is defined by $e^{-\tau_{eff}} \equiv \langle e^{-\tau}\rangle$. From Eqs. (2.9) and (2.10) we have, for $b > 0$,

$$\begin{aligned}\langle e^{-b\tau}\rangle &= \frac{1}{2\pi}\int_{-\infty}^{\infty} ds e^{-\overline{n}[1-I(s)]}\int_0^{\infty} e^{-b\tau}e^{-is\tau}d\tau \\ &= \frac{1}{2\pi i}\int_{-\infty}^{\infty} e^{-\overline{n}[1-I(s)]}\frac{1}{(s-ib)}ds = e^{-\overline{n}[1-I(s=ib)]}.\end{aligned} \tag{2.11}$$

In the last step we have used the theorem of residues to evaluate the integral. Therefore the effective optical depth at λ_{obs} produced by absorbing clouds from z_{obs} to z_u along a line of sight is

$$\tau_{eff}(z_{obs}, z_u, \lambda_{obs}) = \overline{n}[1 - I(s = i)] = \int_{z_{obs}}^{z_u} dz \int_{N_l}^{N_u} \eta(z, N) \left(1 - e^{-\tau_c(z,N)}\right) dN. \tag{2.12}$$

The physical meaning of the effective optical depth is very clear. When all $\tau_c \ll 1$, we have $\tau_{eff} \simeq \langle\tau\rangle$, where

$$\langle\tau(z_{obs}, z_u, \lambda_{obs})\rangle = \int_{z_{obs}}^{z_u} dz \int_{N_l}^{N_u} \tau_c(z, N)\eta(z, N)dN \tag{2.13}$$

is the mean optical depth. For all $\tau_c \gg 1$ we have $\tau_{eff} \simeq \overline{n}$, the mean total number of optically thick clouds. The variance of $e^{-\tau}$ is

$$\sigma^2(e^{-\tau}) \equiv \left\langle \left(e^{-\tau} - \langle e^{-\tau}\rangle\right)^2 \right\rangle = \langle e^{-2\tau}\rangle - e^{-2\tau_{eff}}. \tag{2.14}$$

Another powerful concept is the count reduction factor introduced by Wright (1986). Assume that at a given redshift z_u (here $z_{obs} = 0$) the QSO luminosity function can be described by a power law of the form $\Phi(> L) \propto L^{-\alpha}$, the count reduction factor is then (Wright 1986)

$$f_c(z_u, \alpha) = \langle e^{-\alpha\tau}\rangle = \int_0^\infty e^{-\alpha\tau} P(\tau)d\tau. \tag{2.15}$$

This means that the QSOs at z_u will be reduced by a factor of $f_c(z_u, \alpha)$ on average in a flux limited sample when looking through dusty absorbers. As we have seen before this quantity may be readily calculated. Notice that here the flux limit is for the wavelength λ_{obs} at which we calculate the optical depth τ.

For the Ostriker and Heisler uniform face-on disks discussed in §2.1, we have ($z_{obs} = 0$ and $b > 0$)

$$\overline{n}[1 - I(s = ib)] = \frac{2}{3}A\left[(1 + z_u)^{3/2} - 1\right] - A(b\tau_0)^{-1.5}\left[\gamma\left(\frac{2}{3}, b\tau_0(1 + z_u)\right) - \gamma\left(\frac{2}{3}, b\tau_0\right)\right], \quad (2.16)$$

where $A = n_g \pi r_0^2 (c/H_0)$ and $\gamma(a, x)$ is the incomplete gamma function.

Spectroscopic observations of bright quasars have shown that the HI column density distribution of QSO absorption line systems can be well fitted by a power law of the form $f(N) \propto N^{-\beta}$ with $\beta \simeq 1.5$. Therefore it is of great interest to calculate τ_{eff} for $\eta(z, N) = A(1 + z)^{\gamma} N^{-\beta}$, where A and γ are two constants. Assume that the absorption produced by a single cloud is proportional to its neutral column density N, this is usually true for the cases we are interested in, we can write $\tau_c = N\xi(z)$. We then get

$$\tau_{eff} = \int_{z_{obs}}^{z_u} A(1 + z)^{\gamma} \xi^{\beta - 1} dz \int_{N_l \xi(z)}^{N_u \xi(z)} u^{-\beta}(1 - e^{-u}) du. \quad (2.17)$$

If $1 < \beta < 2$ and $\xi(z) > 0$ we can extend the u integration from 0 to ∞. For $\beta = 1.5$ we have the effective optical depth

$$\tau_{eff} = 2A\sqrt{\pi} \int_{z_{obs}}^{z_u} (1 + z)^{\gamma} \sqrt{\xi(z)} dz \quad (2.18)$$

and the count reduction factor (for $z_{obs} = 0$)

$$f_c(z_u, \alpha) = e^{-\sqrt{\alpha}\tau_{eff}}. \quad (2.19)$$

From Boyle, Shanks and Peterson (1988) we know that for $z < 2.2$ optically selected quasars $\alpha \simeq 0.4$ at the low luminosity end and $\alpha \simeq 2.7$ at the high luminosity end. Thus the reduction fraction f_c is larger if the flux limit is set to detect only intrinsically bright quasars. In the case of Lyman continuum absorption we have, for $\lambda_{obs} \leq 912\mathring{A}$, $\xi(z) = b(1+z)^{-3}$, where $b = \sigma_0(1+z_{obs})^3(\lambda_{obs}/912\mathring{A})^3$ with $\sigma_0 = 6.3 \times 10^{-18}\mathrm{cm}^2$ denoting the threshold HI photoionization cross section. The effective optical depth is

$$\tau_{eff} = \begin{cases} 2A\sqrt{\pi b}\frac{1}{\gamma-0.5}\left[(1+z_u)^{\gamma-0.5} - (1+z_{obs})^{\gamma-0.5}\right] & \text{for } \gamma \neq 0.5 \\ 2A\sqrt{\pi b}\ln\left(\frac{1+z_u}{1+z_{obs}}\right) & \text{for } \gamma = 0.5. \end{cases} \tag{2.20}$$

For dust grain obscuration with a local extinction curve $\tau_c \propto N\lambda^{-1}$ we have

$$\xi(z) = \frac{k}{10^{21}}\left(\frac{1+z}{1+z_{obs}}\right)\left(\frac{4400}{\lambda_{obs}}\right), \tag{2.21}$$

where $k \equiv 10^{21}(\tau_B/N)\mathrm{cm}^{-2}$ is the dimensionless "dust-to-gas ratio" (Pei, Fall and Bechtold 1991) with τ_B denoting the local optical depth at $\lambda_B = 4400\mathring{A}$ produced by a neutral column density N. The ratio k is assumed to be the same for all clouds. In this case we get

$$\tau_{eff} = \frac{2\times 10^{-11}A}{\gamma+1.5}\sqrt{\frac{4400\pi k}{0.1(1+z_{obs})\lambda_{obs}}}\left[(1+z_u)^{\gamma+1.5} - (1+z_{obs})^{\gamma+1.5}\right]. \tag{2.22}$$

For $\eta(z,N) = A(1+z)^\gamma N^{-1.5}$ and $\tau_c = N\xi(z)$ it is also possible to get a closed form of the optical depth distribution $P(\tau)$. We have in this case (for real s)

$$\overline{n}[1-I(s)] = \frac{\tau_{eff}}{2\sqrt{\pi}}\int_0^\infty u^{-1.5}(1-e^{isu})du = \tau_{eff}\sqrt{\frac{|s|}{2}}(1-is/|s|), \tag{2.23}$$

and (Phinney 1989, private communication)

$$P(\tau) = \frac{\tau_{eff}}{2\sqrt{\pi}} \frac{e^{-\frac{\tau_{eff}^2}{4\tau}}}{\tau^{3/2}}. \tag{2.24}$$

The above $P(\tau)$ expression is easily checked by using ($s > 0$ and $a > 0$; see Erdélyi *et al.* 1954)

$$\int_0^\infty x^{-3/2} e^{-a/x} \cos(sx) dx = \sqrt{\pi/a} e^{-\sqrt{2as}} \cos\sqrt{2as}, \tag{2.25}$$

and

$$\int_0^\infty x^{-3/2} e^{-a/x} \sin(sx) dx = \sqrt{\pi/a} e^{-\sqrt{2as}} \sin\sqrt{2as}. \tag{2.26}$$

The cumulative probability for the total optical depth being smaller than a certain value τ is (Phinney 1989, private communication)

$$P(<\tau) = 1 - \mathrm{erf}\left(\frac{\tau_{eff}}{2\sqrt{\tau}}\right), \tag{2.27}$$

where $\mathrm{erf}(x)$ is the error function. We have plotted $P(<\tau)$ as a function of τ in Fig. 2 for several selected τ_{eff} values. Since $\mathrm{erf}(0.48) = 0.5$, the 50% probable value is $\tau_* \simeq \tau_{eff}^2$.

For more complicated $\eta(z, N)$ form an analytical expression of $P(\tau)$ is generally not available. In this case we may first calculate the Fourier transform $\tilde{p}(s)$ and then use FFT to get $P(\tau)$ (Wright 1986). For the Ostriker and Heisler uniform face-on disks discussed in §2.1, however, when the mean total number of absorbers along a line of sight is small, say $\overline{n} < 5$, it is best to calculate first a few low k

valued $P_k(\tau)$, weighted by their Poisson factor, and then add them together to form an approximation of $P(\tau)$.

2.3 Joint Optical Depth Probability Distribution $W(\tau_1, \tau_2)$

In exploring the possible existence of dust obscuration of distant quasars it is very important to know the joint probability distribution for the reddening and extinction of quasars by dusty galaxies along the line of sight. This is because usually quasar candidates are selected to satisfy both flux and color criteria. In a Euclidean space if we know the total optical depth τ_1 along the line of sight at wavelength λ_1, we also know the total optical depth τ_2 at wavelength λ_2, adopting a certain wavelength dependent extinction law. But in an expanding universe the situation is very different. Generally the same total optical depth τ_1 at observed wavelength λ_1, generated in different realizations of dusty galaxy distribution along the line of sight, corresponds to different τ_2 values at a different observed wavelength λ_2. For the special case in which extinction is described by a power law of the form $\tau_c \propto \lambda^{-\alpha}$, τ_{c1}/τ_{c2} is independent of redshift z, and we have $\tau_1/\tau_2 = (\lambda_2/\lambda_1)^{\alpha}$. Only in this case the extinction and reddening are the same thing and we do not need the joint probability distribution.

Recently Wright (1990) has developed a Monte Carlo technique to calculate the joint probability for color and extinction. In this section we introduce a new method which, like the method used for calculating $P(\tau)$ in the previous section, is based on the evaluation of the Fourier transform of the joint probability distribution. Suppose

there are k clouds along the line of sight between z_{obs} and z_u. Let $\tau_{1c}(z,N)$ and $\tau_{2c}(z,N)$ be the optical depths produced by a cloud at the observed wavelengths λ_1 and λ_2, respectively. Using Markoff's method the joint probability distribution of the total optical depths τ_1 and τ_2 along the line of sight can be write down directly:

$$W_k(\tau_1,\tau_2)=\frac{1}{(2\pi)^2}\int_{-\infty}^{\infty}d\rho\int_{-\infty}^{\infty}e^{-i\rho\tau_1}e^{-i\sigma\tau_2}A_k(\rho,\sigma)d\sigma, \tag{2.28}$$

where

$$A_k(\rho,\sigma)=\left[\int\int e^{i\rho\tau_{1c}(z,N)}e^{i\sigma\tau_{2c}(z,N)}f(z,N)dzdN\right]^k. \tag{2.29}$$

For Poisson distribution of the total number of absorbers between z_{obs} and z_u with a mean total number of $\overline{n}$, the joint distribution is given by

$$\begin{aligned}W(\tau_1,\tau_2)&=\sum_{k=0}^{\infty}P(k;\overline{n})W_k(\tau_1,\tau_2)\\&=\frac{1}{(2\pi)^2}\int_{-\infty}^{\infty}d\rho\int_{-\infty}^{\infty}e^{-i\rho\tau_1}e^{-i\sigma\tau_2}e^{-C_1(\rho)-C_2(\rho,\sigma)}d\sigma,\end{aligned} \tag{2.30}$$

where

$$C_1(\rho)=\int\int\left(1-e^{i\rho\tau_{1c}(z,N)}\right)\eta(z,N)dzdN, \tag{2.31}$$

and

$$C_2(\rho,\sigma)=\int\int e^{i\rho\tau_{1c}(z,N)}\left(1-e^{i\sigma\tau_{2c}(z,N)}\right)\eta(z,N)dzdN. \tag{2.32}$$

From Eqs. (2.30), (2.31) and (2.32) we can show that

$$\int_0^{\infty}\tau_2W(\tau_1,\tau_2)d\tau_2=\frac{1}{2\pi}\int_{z_{obs}}^{z_u}dz\int_{N_l}^{N_u}\tau_{2c}\eta(z,N)dN\int_{-\infty}^{\infty}e^{-i\rho\tau_1-C_1(\rho)+i\rho\tau_{1c}}d\rho, \tag{2.33}$$

and

$$\langle \tau_1 \tau_2 \rangle \equiv \int_0^\infty d\tau_1 \int_0^\infty \tau_1 \tau_2 W(\tau_1, \tau_2) d\tau_2 = \langle \tau_{1c} \tau_{2c} \rangle + \langle \tau_{1c} \rangle \langle \tau_{2c} \rangle, \tag{2.34}$$

where

$$\langle \tau_{1c} \tau_{2c} \rangle = \int \int \tau_{1c} \tau_{2c} \eta(z, N) dz dN, \tag{2.35}$$

and

$$\langle \tau_{1,2c} \rangle = \int \int \tau_{1,2c} \eta(z, N) dz dN. \tag{2.36}$$

3 SOME APPLICATIONS

3.1 Lyman Continuum Absorptions by QSO Absorption Line Systems

3.1.1 The Effective Optical Depth τ_{eff}

The effective optical depth $\tau_{eff}(z_{obs}, z_u, \lambda_{obs})$ due to HI Lyman continuum absorption can be readily calculated by using the observed HI column density distribution $\eta(z, N)$. We adopt the conventional form of $\eta(z, N) = A(1+z)^\gamma N^{-\beta}$ with $\beta = 1.5$. Since $\tau_c(z, N) \propto N$, it is clear from Eq. (2.12) that the major contributors to the τ_{eff} integration are those clouds with $\tau_c(z, N) \simeq 1$, i.e., the clouds with HI column densities a few times 10^{17}cm^{-2}—the Lyman limit systems (LLS). The survey of LLS in the spectra of 59 high redshift QSOs by Sargent, Steidel and Boksenberg (1989) showed that there are 1.91 ± 0.33 Lyman limit systems with $N > 2.38 \times 10^{17}\text{cm}^{-2}$ per unit redshift at a mean redshift $\langle z \rangle = 2.950$. This result is confirmed by a new spectroscopic survey for high redshift LLS (Lanzetta 1991). But controversial

results regarding γ for the Lyman limit systems are reached. Sargent, Steidel and Boksenberg found that $\gamma = 0.68 \pm 0.54$ for $0.67 \leq z \leq 3.58$. Lanzetta claimed that $\gamma = 5.7 \pm 1.9$ over the redshift range $2.5 \leq z \leq 3.7$ and the rate of incidence of LLS is virtually constant over the range $0.35 \leq z \lesssim 2.5$. In our calculations we consider two models. We adopt $\gamma = 0.5$ for our Model 1 and $\gamma = 1.0$ for Model 2. The constant A is obtained by normalizing to get 1.91 $N > 2.38 \times 10^{17}\mathrm{cm}^{-2}$ systems per unit redshift at $z = 2.950$. We get $A = 2.3 \times 10^8$ for the Model 1 and $A = 1.2 \times 10^8$ for the Model 2. So our Model 1 is basically the same as the Miralda-Escudé and Ostriker (1990) Model A2, except that we extrapolate the LLS expression to lower HI column densities to approximate the Lyα forest contribution. Since the weak Lyα forest systems evolve like $n(z) \propto (1+z)^{2.75}$ (Lu *et al.* 1991), we may have underestimated their contribution to τ_{eff} at high redshifts.

For $\lambda_{obs} \leq 912\mathring{A}$ we use Eq. (2.20) to calculate τ_{eff}. For $912\mathring{A} < \lambda_{obs} < 912(1+z_u)\mathring{A}$ and $z_{obs} = 0$, we have

$$\tau_{eff} = \begin{cases} 2A\sqrt{\pi\sigma_0}\,\frac{(1+z_c)^{1.5}}{\gamma-0.5}\left[(1+z_u)^{\gamma-0.5} - (1+z_c)^{\gamma-0.5}\right] & \text{for } \gamma \neq 0.5 \\ 2A\sqrt{\pi\sigma_0}\,(1+z_c)^{1.5}\ln\left(\frac{1+z_u}{1+z_c}\right) & \text{for } \gamma = 0.5, \end{cases} \tag{3.1}$$

where $1 + z_c = \lambda_{obs}/912$. For $\lambda_{obs} \geq 912(1+z_u)\mathring{A}$, τ_{eff} due to the HI Lyman continuum absorption is zero. Our calculated results for $z_{obs} = 0$ are shown in Fig. 3. The results for $\lambda_{obs} \leq 912\mathring{A}$ and $z_{obs} > 0$ are given in Fig. 4. In both the figures the Model 1 results are shown in solid lines, while the Model 2 results in dashed lines.

Now we discuss the β value, $\beta = 1.5$, which we have used in our calculations. We must point out that the β value for the neutral column density N in the range $\gtrsim 10^{16}\mathrm{cm}^{-2}$ to $2.38 \times 10^{17}\mathrm{cm}^{-2}$ is very uncertain, because we cannot measure the Lyman limit discontinuity accurately for these column densities. Since the flux level shortward of the Lyman limit is indistinguishable from zero for the absorptions with HI column densities larger than $4.8 \times 10^{17}\mathrm{cm}^{-2}$, it is also impossible to get accurate column density measurements for these clouds from the Lyman limit discontinuity (Sargent, Steidel and Boksenberg 1989). Sargent, Steidel and Boksenberg (1989) claimed $\beta \simeq 1.39$ for $\log N > 17.38$ and Lanzetta estimated $\beta = 1.25 \pm 0.03$ for $17.2 \leq \log N \leq 21.8$. We think the β value for column densities a few times $10^{17}\mathrm{cm}^{-2}$ is still not well determined. More observations are needed to improve the determination.

3.1.2 Spectral Index of Ionizing Flux at High z

From Figs. 3 and 4 we see that the effective optical depth τ_{eff} due to the Lyman continuum absorption is large, especially at high redshifts or for high redshift objects. The absorption can significantly attenuate the ionizing flux from distant ionizing sources and thus has important consequences to the ionizing background (see Chapter Three and Chapter Four). Besides reducing the magnitude of the ionizing field, the frequency dependent Lyman continuum absorption also changes the shape of the resulting ionizing spectrum. This effect can easily be demonstrated as below. Let $\phi(M, z)$ be the proper space density of ionizing sources per unit absolute magnitude at redshift z and let $L(M, \nu_z) \propto \nu_z^{-\alpha}$ be the source luminosity at the

frequency $\nu_z = (1+z)\nu_{obs}/(1+z_{obs})$, the mean intensity of the ionizing field is

$$J_{\nu_{obs}}(z_{obs}) = \frac{1}{4\pi}\frac{c}{H_0}\int_{z_{obs}}^{\infty} dz \left(\frac{1+z_{obs}}{1+z}\right)^3 \frac{\epsilon e^{-\tau_{eff}}}{(1+z)^2(1+2q_0 z)^{1/2}}, \qquad (3.2)$$

where

$$\epsilon \equiv \int \phi(M,z)L(M,\nu_z)dM \qquad (3.3)$$

is the proper volume emissivity at redshift z. We now define z_1 by demanding $\tau_{eff}(z_{obs}, z_1, \nu_{obs}) = 1$. For large z_{obs} and at $\nu_{obs} \gtrsim \nu_L$, where ν_L is the Lyman limit frequency, the absorption is significant as we can see from Fig. 4. In this case z_1 is close to z_{obs}, and we have

$$J_{\nu_{obs}}(z_{obs}) \simeq \frac{1}{4\pi}\frac{c}{H_0}\frac{\epsilon(z_1 - z_{obs})}{(1+z_{obs})^2(1+2q_0 z_{obs})^{1/2}} \propto \epsilon(z_1 - z_{obs}). \qquad (3.4)$$

From Eq. (2.20) we see that when $z_1 - z_{obs}$ is small, $z_1 - z_{obs} \propto \nu_{obs}^{1.5}$, independent of γ. Since $\epsilon \propto \nu_{obs}^{-\alpha}$, we have $J_{\nu_{obs}} \propto \nu_{obs}^{1.5-\alpha}$. The resulting spectral index is changed from the intrinsic source spectral index α to $\alpha - 1.5$. We should point out that the above analysis is valid only for $\nu_{obs} \gtrsim \nu_L$. For higher frequencies the absorptions generated by HeI continuum absorption (threshold rest frame wavelength $504\mathring{A}$), HeII Lyα ($\lambda 304\mathring{A}$) forest line blanketing and HeII Lyman continuum absorption (threshold rest frame wavelength $228\mathring{A}$) in QSO absorption systems should also be taken into account.

3.1.3 $J_{\nu_L}(z_{obs})$ as a Function of z_{obs}

In this section we calculate $J_{\nu_L}(z_{obs})$ produced by QSOs as a function of z_{obs},

including the Lyman continuum absorption. At $\nu_{obs} = \nu_L$, we have

$$1 + z_1 = (1 + z_{obs}) e^{0.489\,(1+z_{obs})^{-3/2}} \tag{3.5a}$$

for Model 1 absorption; and

$$1 + z_1 = \left[0.468\,(1 + z_{obs})^{-3/2} + (1 + z_{obs})^{1/2}\right]^2 \tag{3.5b}$$

for Model 2 absorption. We make the approximation that for $z < z_1$ the absorption can be neglected, and for $z > z_1$ the flux from QSOs is significantly attenuated and makes negligible contribution to J_{ν_L} at z_{obs}. We adopt $q_0 = 1/2$ and $H_0 = 50$km s^{-1}Mpc^{-1} in our calculations below. We then have

$$J_{\nu_L}(z_{obs}) \simeq \frac{1}{4\pi}\frac{c}{H_0}\int_{z_{obs}}^{z_1} dz \left(\frac{1+z_{obs}}{1+z}\right)^3 \frac{\epsilon}{(1+z)^{5/2}}. \tag{3.6}$$

For the QSO intrinsic spectrum we adopt $L(M_B, \nu) \propto \nu^{-0.5}$ for $\lambda > 1216\mathring{A}$ and $L(M_B, \nu) = L(\nu/\nu_L)^{-1}$ for $\lambda < 1216\mathring{A}$. Thus the Lyman limit frequency luminosity L is related with the absolute B magnitude M_B by $L = 10^{-0.4M_B+20.33}$. The observed *proper* QSO luminosity function at $z \leq 2.2$ can be fairly represented by a two power law form (Boyle *et al.* 1987; Boyle *al.* 1988)

$$\phi(M_B, z) = \begin{cases} \Phi^*(1+z)^3 \left[\frac{L}{L^*(z)}\right]^{\alpha+1} & \text{for } L \geq L^*(z) \\ \Phi^*(1+z)^3 \left[\frac{L}{L^*(z)}\right]^{\beta+1} & \text{for } L \leq L^*(z), \end{cases} \tag{3.7}$$

where $L^*(z) = 10^{-0.4M_B(z)+20.33}$ with $M_B(z) = M_B^* - 2.5k_L\log(1+z)$. In our calculations we have adopted (Boyle *et al.* 1987; Boyle *al.* 1988 model B) $\alpha = -3.79$,

$\beta = -1.44$, $M_B^* = -22.42$, $k_L = 3.15$ and $\Phi^* = 10^{-6}\mathrm{Mpc}^{-3}\mathrm{mag}^{-1}$. Since $z_1 = 2.2$ for $z_{obs} = 1.898$ and $\nu_{obs} = \nu_L$, we have

$$J_{\nu_L}(z_{obs}) \simeq 3.9 \times 10^{-23}(1+z_{obs})^4 \left[(1+z_1)^{0.65} - (1+z_{obs})^{0.65}\right] \qquad (3.8)$$

for $z_{obs} \leq 1.898$. For $z_{obs} \geq 2.2$, the QSO luminosity function is not well determined. We assume that the *comoving* QSO luminosity function is the same as that at $z = 2.2$. We then get

$$J_{\nu_L}(z_{obs}) \simeq 3.97 \times 10^{-22}(1+z_{obs})^{1.5} \left[1 - \left(\frac{1+z_{obs}}{1+z_1}\right)^{2.5}\right] \qquad (3.9)$$

for $z_{obs} \geq 2.2$. In Eqs. (3.8) and (3.9) J_{ν_L} is in the unit of ergs $\mathrm{s}^{-1}\mathrm{cm}^{-2}\mathrm{Hz}^{-1}\mathrm{sr}^{-1}$. Our calculated results are plotted in Fig. 5. The solid line is for Model 1 absorption and the dashed line for Model 2 absorption.

For $z_{obs} = 0$ we see that $z_1 = 0.63$ (1.16) and $\log(J_{\nu_L}) = -22.84$ (-22.60) for Model 1 (Model 2) absorption. An indirect upper limit for the local ionizing field intensity was obtained by Songaila *et al.* (1989). They have measured an Hα surface brightness of 30 mR at two positions on high-velocity neutral hydrogen cloud complex C. They argued that each incident ionizing photon onto the system must be matched by one recombination which in turn produces 0.46 Hα photons (case B). Thus the observed surface brightness means $\log(J_{\nu_L}) \leq -22.22$ at $z_{obs} = 0$, which is consistent with our calculated result.

The flatness of the $J_{\nu_L}(z_{obs})$ curve at $z_{obs} > 2.2$ is due to the combined effects of the increasing of proper QSO space density and the increasing of Lyman continuum

absorption at early epochs. We should point out that we may have overestimated J_{ν_L} at high z_{obs}, since according to Lanzetta (1991) the absorption should be more significant at $z \geq 2.5$ and according to Schmidt, Schneider and Gunn (1991) the luminous QSO comoving space densities decline steeply for redshifts larger than 3.

3.1.4 On the Difficulty of Detecting HeII Gunn-Peterson Effect

One of the key projects of the *Hubble Space Telescope (HST)* is to observe high redshift quasars shortward of the HeII Lyα emission to carry out the HeII Gunn-Peterson test. Positive detection of the HeII Gunn-Peterson effect will not only help to check the Big Bang nucleosynthesis theory, but will also provide important information about the physical conditions of the intergalactic medium and the spectral shape of the ionizing background (Møller and Jakobsen 1990; Miralda-Escudé and Ostriker 1990). Since a typical line of sight intersects many Lyα clouds, we expect the Lyman continuum absorption to be significant. For quasars with emission redshift $z_{em} \geq 3.1$, the $\lambda 304\mathring{A}$ line is observable by *HST* optics (Møller and Jakobsen) at $\lambda_{obs} = 304\,(1 + z_{em})\mathring{A}$. We have calculated the effective optical depths for some selected z_{em} at $\lambda_{obs} = 304\,(1 + z_{em})\mathring{A}$. From these τ_{eff} values the probability that along the line of sight the total optical depth τ is less than unity, $P(< \tau = 1)$, is calculated. The results for our Model 1 and Model 2 are shown in Table 1. We see that $P(< \tau = 1)$ is small for $z_{em} \geq 3.1$ quasars, especially for the Model 1 parameters (for $z_{em} = 3.1$, $P(< \tau = 1) = 1\%$). This means that it is difficult to find a line of sight which is "clear" to conduct the HeII Gunn-Peterson test. Our

chances improve if we observe the relatively low redshift quasars. The future space observatories, such as the *Hopkins Ultraviolet Telescope*, *Orfeus* and *Lyman/FUSE*, can probe QSOs with emission redshift z_{em} as low as 2.1 (Møller and Jakobsen 1990). We see that for our Model 2 parameters and $z_{em} = 2.1$, $P(< \tau = 1) = 24\%$. One good way to improve the chances is to observe those quasars which are known from the ground observations to show no LLS and damped Lyα systems, or quasars which contain only weak LLS with absorption redshift z_{abs} high enough so that the Lyman continuum flux recovers after going through the "Lyman valley" (Møller and Jakobsen 1990).

We notice that there are only two QSOs observed to date with the *International Ultraviolet Explorer Satellite (IUE)* which have an EUV continuum that is not severely depressed by intervening absorbers at the short wavelength end. These are QSO HS1700+6416 ($z_{em} = 2.72$) reported by Reimers *et al.* (1989) and PG 1115+080 ($z_{em} = 1.722$) by Green *et al.* (1980) (see also Tripp *et al.* 1991). The former is detected down to $\lambda_{obs} \simeq 1228\mathring{A}$ and the latter down to $\lambda_{obs} \gtrsim 1300\mathring{A}$. Very recently Beaver *et al.* (1991) reported the detection of EUV flux down to $1630\mathring{A}$ for QSO UM 675 ($z_{em} = 2.148$) using the *HST*. But this QSO was chosen for observation because it is known to show no strong absorptions from the ground based spectrophotometry. We have calculated $P(< \tau = 1)$ for these three QSOs at the lowest λ_{obs}. $P(< \tau = 1)$ for HS1700+6416 is 2% and 7% from our Model 1 and Model 2, respectively; for PG1115+080, $P(< \tau = 1)$ is 11% (Model 1) and 24% (Model 2); for UM 675, $P(< \tau = 1)$ is 5% (Model 1) and 11% (Model 2). We

consider these are lucky cases, but we see that these three cases are not inconsistent with our calculations.

We have neglected in the above calculations the line blanketing by HI Lyα forest, the higher Lyman series lines and the HeI continuum absorption of QSO Lyα clouds. Like in the HI Gunn-Peterson test, the HeII Gunn-Peterson test may also face the similar difficulty of separating the real effect and the HeII Lyα forest line blanketing.

3.2 QSOs and Dust Grain Extinction

3.2.1 Dust Grain Extinction from Observed Damped Lyα Systems

Dust grain extinction is significant only when the line of sight intersects very large column density clouds, i.e., we need only to consider the damped Lyα systems. We use the new results published by Lanzetta *et al.* (1991). They showed that the mean number per unit redshift of the damped Lyα systems with HI column density $N \geq 2\times10^{20}\mathrm{cm}^{-2}$ is $0.16\pm0.03 \leq n(z) \leq 0.25\pm0.04$ at an average redshift $z_{abs} = 2.5$. We assume the distribution function is of the form $\eta(z, N) = A(1+z)^{\gamma}N^{-\beta}$. According to Lanzetta *et al.*, $\beta = 1.67 \pm 0.19$ for $20.3 \leq \log N \leq 21.8$ and $\gamma = 0.3 \pm 1.4$. We use $\beta = 1.5$ and $\gamma = 0.5$ in our calculations. Adopting $n(z = 2.5) = 0.25$, we get the normalization constant $A = 1.2\times10^{9}$. We adopt the $1/\lambda$ extinction law and use the dimensionless "dust-to-gas ratio" k defined by Pei, Fall and Bechtold (1991),

From Eq. (2.22) we get the effective optical depth due to the dust grain extinction:

$$\tau_{eff}(0, z_u, \lambda_{obs}) = 2.1 \times 10^{-2} \sqrt{\frac{4400\,k}{0.1\,\lambda_{obs}}} \left[(1+z_u)^2 - 1\right]. \qquad (3.10)$$

Adopting $k = 0.1$ (Pei, Fall and Bechtold 1991) and observing at $\lambda_{obs} = 4400\mathring{A}$, τ_{eff} is 0.32, 0.50 and 0.74 for $z_u = 3$, 4 and 5; the corresponding count reduction factor $f_c = e^{-\sqrt{\alpha}\tau_{eff}}$ is 1/1.7, 1/2.3 and 1/3.4 for $\alpha = 2.7$.

Following Wright (1990) we also calculate the quasar rest frame color excess $E([1770]-[4220])$ which is produced by dust grain reddening. Neglecting the observational complications such as the transmissions of band passes and using the $1/\lambda$ extinction law, we have $E([1770]-[4220]) = 0.63\tau_1$, where τ_1 is the optical depth at $1770(1+z_u)\mathring{A}$ to a z_u quasar. For a flux limited QSO sample with redshift z_u, we get the mean rest frame color excess

$$\begin{aligned}\langle E([1770]-[4220])\rangle &= \frac{0.63\lambda_{obs}}{1770(1+z_u)} e^{-\sqrt{\alpha}\tau_{eff}} \int \tau e^{-\alpha\tau} P(\tau) d\tau \\ &= \frac{0.63\lambda}{1770(1+z_u)} \times \frac{\tau_{eff}}{2\sqrt{\alpha}}. \qquad (3.11)\end{aligned}$$

In the above equation the flux limit is at λ_{obs}, τ and τ_{eff} are both calculated at λ_{obs} and they are produced by the dust grain extinction. The QSO luminosity function at z_u is assumed to be $\Phi(>L) \propto L^{-\alpha}$ and all QSOs have the same spectrum. For $\lambda_{obs} = 4400\mathring{A}$ and $\alpha = 2.7$, the mean rest frame color excess is $\langle E([1770]-[4220])\rangle$=0.04, 0.05 and 0.06 for $z_u = 3$, 4 and 5; for $\alpha = 0.4$, $\langle E([1770]-[4220])\rangle$ is increased to 0.10, 0.12 and 0.15.

We must point out that there are several complications which we have overlooked. One is that we have extended our integration to include very large clouds

which are not observed. The main contributors in τ_{eff} integration are those clouds with $\tau_c \simeq 1$. For $k = 0.1$ and $\lambda_{obs} = 4400\AA$, these are the clouds which have column densities a few times $10^{21}\mathrm{cm}^{-2}$. Since the maximum observed column density in Lanzetta *et al.* (1991) sample is about $6 \times 10^{21}\mathrm{cm}^{-2}$, we may have overestimated τ_{eff}. We note that the extrapolation to very large column densities will lead to an infinite total mass of gas, so the distribution at very high column densities must go down very rapidly. The second complication is that for $z > 2.6$ the Lyα forest moves into the B band, and for $z > 3.8$ the Lyman continuum absorption should also be taken into account, as we have seen in the above section. These two absorption mechanisms are far more important than the dust grain extinction when they play roles in removing quasars. The third complication is observational. Quasar candidates are based mainly on color photometry or multi-object spectroscopy. Variability and absence of proper motions are also used as complementary information. The detailed analysis including these complications is beyond the scope of this paper.

3.2.2 Discussion

Ostriker and Heisler (1984) (see also Heisler and Ostriker 1988) first suggested that clouds (or intervening dusty galaxies) may produce enough extinction at high redshifts to remove background quasars from a flux-limited sample. This is because of the crowding of galaxies at early epochs and the increasing of dust opacity with decreasing wavelength. These intervening dusty objects should imprint absorption features on the background quasar spectra. The damped Lyα systems are natural

places to search for dust. Pei, Fall and Bechtold (1991) have indeed found that quasars with damped Lyα systems in the foreground are stochastically redder than those without damped Lyα systems in the foreground. They claimed that the significance level of reddening is at least 4σ. But we notice that there is no significant correlation between the neutral column densities of the damped Lyα systems and the quasar spectral indices. The Galactic-type dust appears to be ruled out by the absence of strong extinction near 2175$\AA$ in the rest frame of of several damped Lyα systems. By using the observed neutral column density distribution of Lanzetta *et al.* (1991) and also adopting the dust-to-gas ratio determined by Pei, Fall and Bechtold, we have seen in the previous section that the resulting obscuration is marginally significant and the reddening in a flux limited sample is small.

As Ostriker and Heisler have argued there may be a bias against detecting optically thick clouds, since the spectroscopy required to measure the column densities requires a fairly bright optical continuum, very few quasars will be luminous enough to remain observable behind such optically thick clouds. As we have seen in the above section that adding in more very high column density clouds will not help a lot and is restricted by the total mass of gas clouds. The dust-to-gas ratio for the observed damped Lyα systems determined by Pei, Fall and Bechtold (1991) seems too low to significantly remove the background QSOs. So the only possibility for dust obscuration to be very significant is to introduce a new population of optically thick absorbers with high dust-to-gas ratio. Very recently Wright (1990) has indeed constructed models which match both the observed quasar reddening trend and

the Lyα absorber column density distribution and at the same time can still have significant effects on quasar counts: count reduction factors at $z = 3$ of 2.7—4.

4 CONCLUSIONS

Using Markoff's method we have derived a general formalism to deal with the absorptions produced by randomly distributed discrete clouds, such as the QSO absorption line systems. Some analytical forms are given for the effective optical depth τ_{eff}, the count reduction factor f_c and the optical depth probability distribution function $P(\tau)$. We then use these results to address problems of the attenuation of ionizing background by QSO absorption line systems, the difficulty of conducting the HeII Gunn-Peterson test using *HST* and the dust grain obscuration of distant quasars.

The Lyman continuum absorption from QSO absorption line systems not only reduces the magnitude of ionizing field significantly, but also tilts the intrinsic source spectrum to result in a flat background spectrum near the Lyman limit frequency. For sources with an intrinsic spectral index α, the resulting ionizing background spectrum near ν_L is $\alpha - 1.5$.

With a few reasonable approximations we have derived analytical expressions for $J_{\nu_L}(z_{obs})$. We have obtained an upper limit $J_{\nu_L} \sim 4 \times 10^{-22}$ergs $s^{-1}cm^{-2}Hz^{-1}sr^{-1}$ for QSO contributions to the ionizing background at redshifts larger than 2.2.

We have shown that it is very difficult to find a line of sight which is "clear" of the Lyman continuum absorption for $z_{em} \geq 3.1$ quasars. For our Model 1 parameters, the probability that along a line of sight the total optical depth is less than unity is only 1%. In order to carry out the HeII Gunn-Peterson test successfully, it is necessary for *HST* to observe those quasars which are known from the ground observations to display no LLS and damped Lyα systems, or quasars which contain only weak LLS with z_{abs} high enough so that the Lyman continuum flux recovers after going through the "Lyman valley".

We have shown that the observed damped Lyα systems combined with the dust-to-gas ratio determined by Pei, Fall and Bechtold (1991) produce a marginally significant obscuration for $z = 3$ quasars. The count reduction factor is calculated to be 1/1.7 at $z = 3$. The reddening is shown to be small for a flux limited QSO sample. We point out some complications which have been overlooked in such calculations. We have also shown that in order to boost dust grain obscuration more significantly, it is necessary to introduce a new population of optically thick absorbers with a high dust-to-gas ratio. Such dusty absorbers may have escaped spectroscopic detection so far, simply because quasars behind them have too faint continuum levels to be studied spectroscopically.

ACKNOWLEDGMENT

This work was supported in part by NSF Grant AST84-51725.

REFERENCES

Beaver, E. A., Burbidge, E. M., Cohen, R. D., Junkkarinen, V. T., Lyons, R. W., Rosenblatt, E. I., Hartig, G. F., Margon, B. & Davidsen, A. F., 1991. *Astrophys. J. Lett*, **377**, L1.

Bechtold, J. & Shectman, S. A., 1989. *IAU Symp. 134: Active Galactic Nuclei*, p549, eds. Osterbrock, D. E. & Miller, J. S., Kluwer Academic Publishers, Fang, Dordrecht.

Blades, J. C., Norman, C. & Turnshek, D., 1988. *Quasar Absorption Lines: Probing the Universe*, eds., Cambridge University Press.

Boyle, B. J., Shanks, T. & Peterson, B. A., 1988. *Mon. Not. R. astr. Soc.*, **235**, 935.

Boyle, B. J., Fong, R., Shanks, T. & Peterson, B. A., 1987. *Mon. Not. R. astr. Soc.*, **227**, 717.

Chandrasekhar, S., 1943. *Rev. Mod. Phys.*, **15**, 1.

Erdélyi, A., Magnus, W., Oberhettinger, F. & Tricomi, F. G., 1954. *Tables of Integral Transforms*, McGraw-Hill, New York.

Green, R. F., Pier, J. R., Schmidt, M., Estabrook, F. B., Lane, A. L. & Wahlquist, H. D., 1980. *Astrophys. J.*, **239**, 483.

Heisler, J. & Ostriker, J. P., 1988. *Astrophys. J.*, **332**, 543.

Lanzetta, K. M., 1991. *Astrophys. J.*, **375**, 1.

Lanzetta, K. M., Wolfe, A. M., Turnshek, D. A., Lu, L., McMahon, R. G. & Hazard, C., 1991. *Astrophys. J. Suppl. Ser.*, **77**, 1.

Lu, L., Wolfe, A. M. & Turnshek, D. A., 1991. *Astrophys. J.*, **367**, 19.

Miralda-Escudé, J. & Ostriker, J. P., 1990. *Astrophys. J.*, **350**, 1.

Møller, P. & Jakobsen, P., 1990. *Astron. Astrophys.*, **228**, 299.

Ostriker, J. P. & Heisler, J., 1984. *Astrophys. J.*, **278**, 1.

Pei, Y., Fall, M. & Bechtold, J. 1991. *Astrophys. J.*, **378**, 6.

Pettini, M., Hunstead, R. W., Smith, L. J. & Mar, D. P., 1990. *Mon. Not. R. astr. Soc.*, **246**, 545.

Reimers, D., Clavel, J., Groote, D., Engels, D., Hagen, H. J., Naylor, T., Wamsteker, W. & Hopp, U., 1989. *Astron. Astrophys.*, **218**, 71.

Sargent, W. L. W., Boksenberg, A. & Steidel, C. C., 1988. *Astrophys. J. Suppl. Ser.*, **68**, 539.

Sargent, W. L. W., Steidel, C. C. & Boksenberg, A., 1989. *Astrophys. J. Suppl. Ser.*, **69**, 703.

Schmidt, M., Schneider, D. P. & Gunn, G. E., 1991. Paper presented at the workshop on: *Space Distribution of Quasars.*

Songaila, A., Bryant, W. & Cowie, L., L., 1989. *Astrophys. J. Lett*, **345**, L71.

Tripp, T. M., Green, R. F. & Bechtold, J., 1991. *Astrophys. J. Lett*, **364**, L29.

Webb, J. K., 1987. *IAU Symp. 124: Observational Cosmology*, p803, eds Hewitt, A., Burbidge, G. & Fang, L., Reidel, Dordrecht.

Wright, E. L., 1986. *Astrophys. J.*, **311**, 156.

Wright, E. L., 1990. *Astrophys. J.*, **353**, 411.

Table 1. Calculated $P(<\tau=1)$ for HeII Gunn-Peterson test.

z_{em}	$\lambda_{obs}(\AA)$	τ_{eff} (M1)	τ_{eff} (M2)	$P(<\tau=1)$ (M1)	$P(<\tau=1)$ (M2)
2.1	942.4	2.36	1.67	0.10	0.24
2.7	1124.8	3.08	2.38	0.03	0.09
3.1	1246.4	3.59	2.92	0.01	0.04
3.5	1368.0	4.13	3.52	0.003	0.01
4.0	1520.0	4.84	4.34	0.0006	0.002

FIGURE CAPTIONS

Figure 1. Optical depth probability distribution $P_k(t)$ as a function $t = \tau/\tau_0$ for Ostriker-Heisler hard edged, face-on uniform dusty disks. (a)$z_u = 0.5$; (b)$z_u = 4.0$.

Figure 2. The cumulative probability distribution $P(< \tau)$ as a function of τ for various τ_{eff} values.

Figure 3. The effective optical depth $\tau_{eff}(0, z_u, \lambda_{obs})$ as a function of λ_{obs} produced by HI Lyman continuum absorption of QSO Lyα clouds. $z_{obs} = 0$. Solid lines are for the Model 1 absorption and dashed lines the Model 2 absorption.

Figure 4. Same as Fig. 3, but for $z_{obs} = 1$, 2, 3 and 4. For $\lambda_{obs} \leq 912\mathring{A}$ only.

Figure 5. $J_{\nu_L}(z_{obs})$ as a function of z_{obs} for Model 1 absorption (solid line) and Model 2 absorption (dashed line).

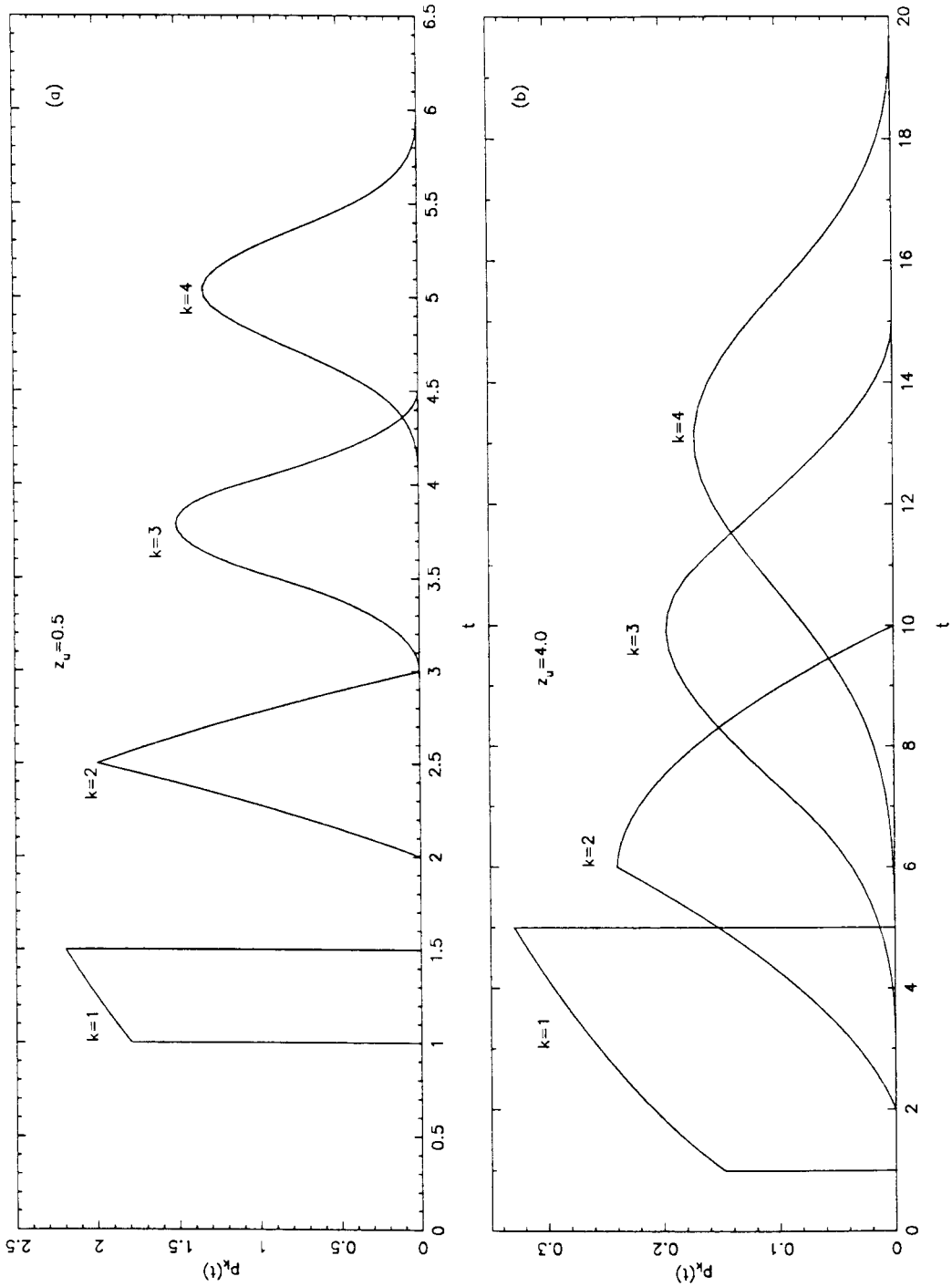

Figure 1

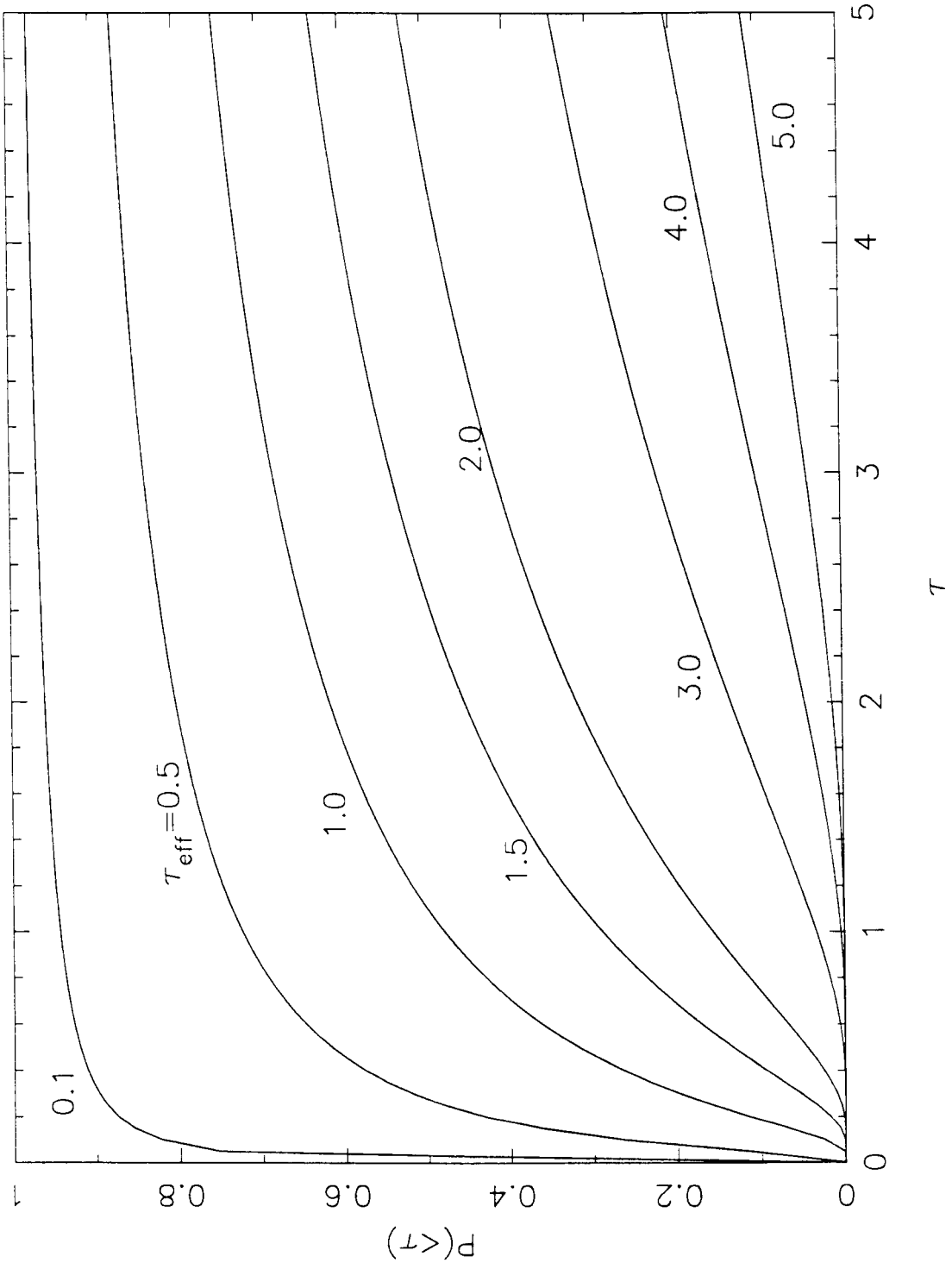

Figure 2

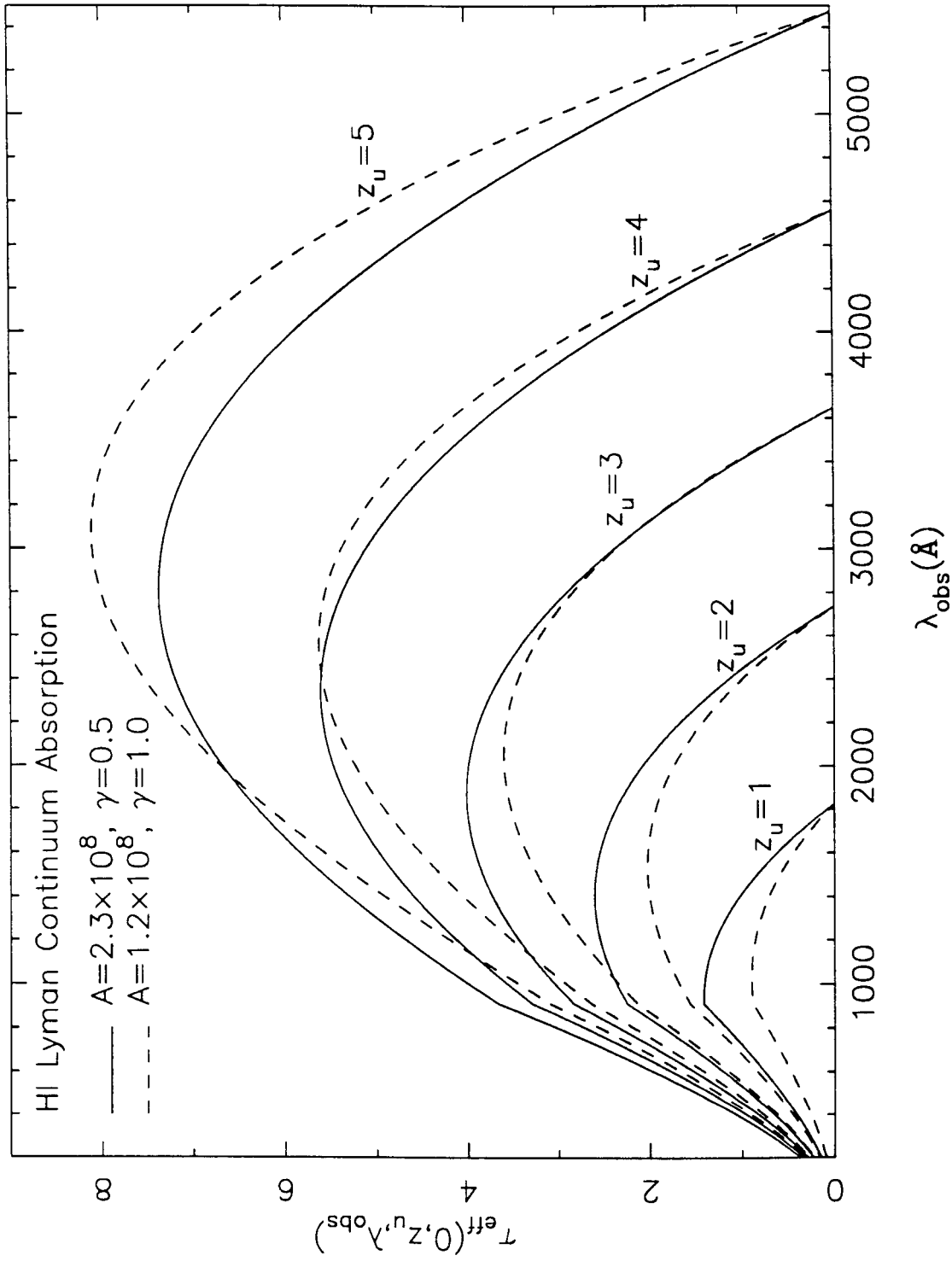
HI Lyman Continuum Absorption
A=2.3×10^8, γ=0.5
A=1.2×10^8, γ=1.0
z_u=5
z_u=4
z_u=3
z_u=2
z_u=1
τ_eff(0,z_u,λ_obs)
λ_obs(Å)
0
2
4
6
8
1000
2000
3000
4000
5000

Figure 3

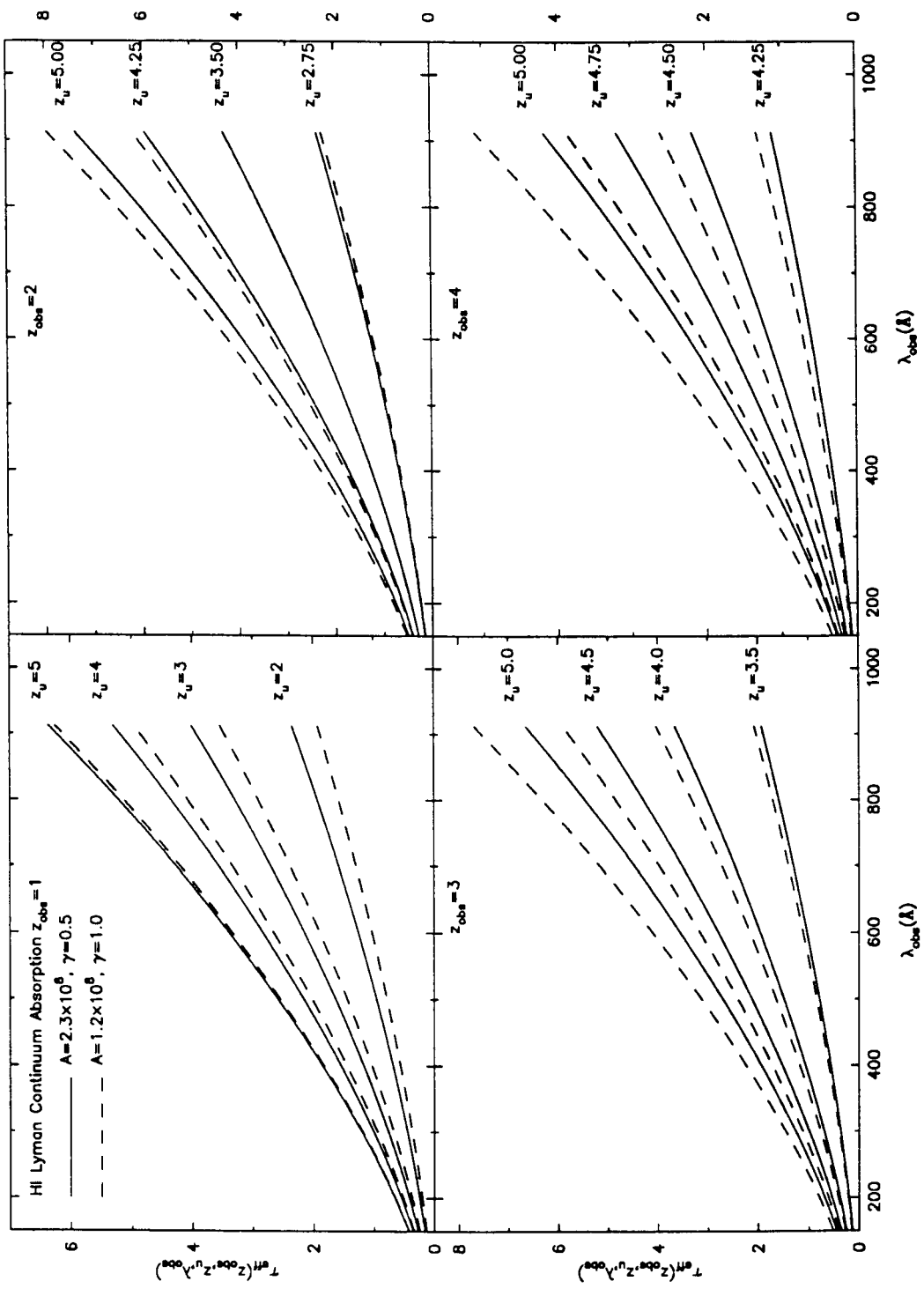
HI Lyman Continuum Absorption $z_{obs}=1$
A=2.3×10^8, γ=0.5
A=1.2×10^8, γ=1.0
z_u=5
z_u=4
z_u=3
z_u=2
z_{obs}=2
z_u=5.00
z_u=4.25
z_u=3.50
z_u=2.75
z_{obs}=3
z_u=5.0
z_u=4.5
z_u=4.0
z_u=3.5
z_{obs}=4
z_u=5.00
z_u=4.75
z_u=4.50
z_u=4.25
$\tau_{eff}(z_{obs},z_u,\lambda_{obs})$
λ_{obs}(Å)

Figure 4

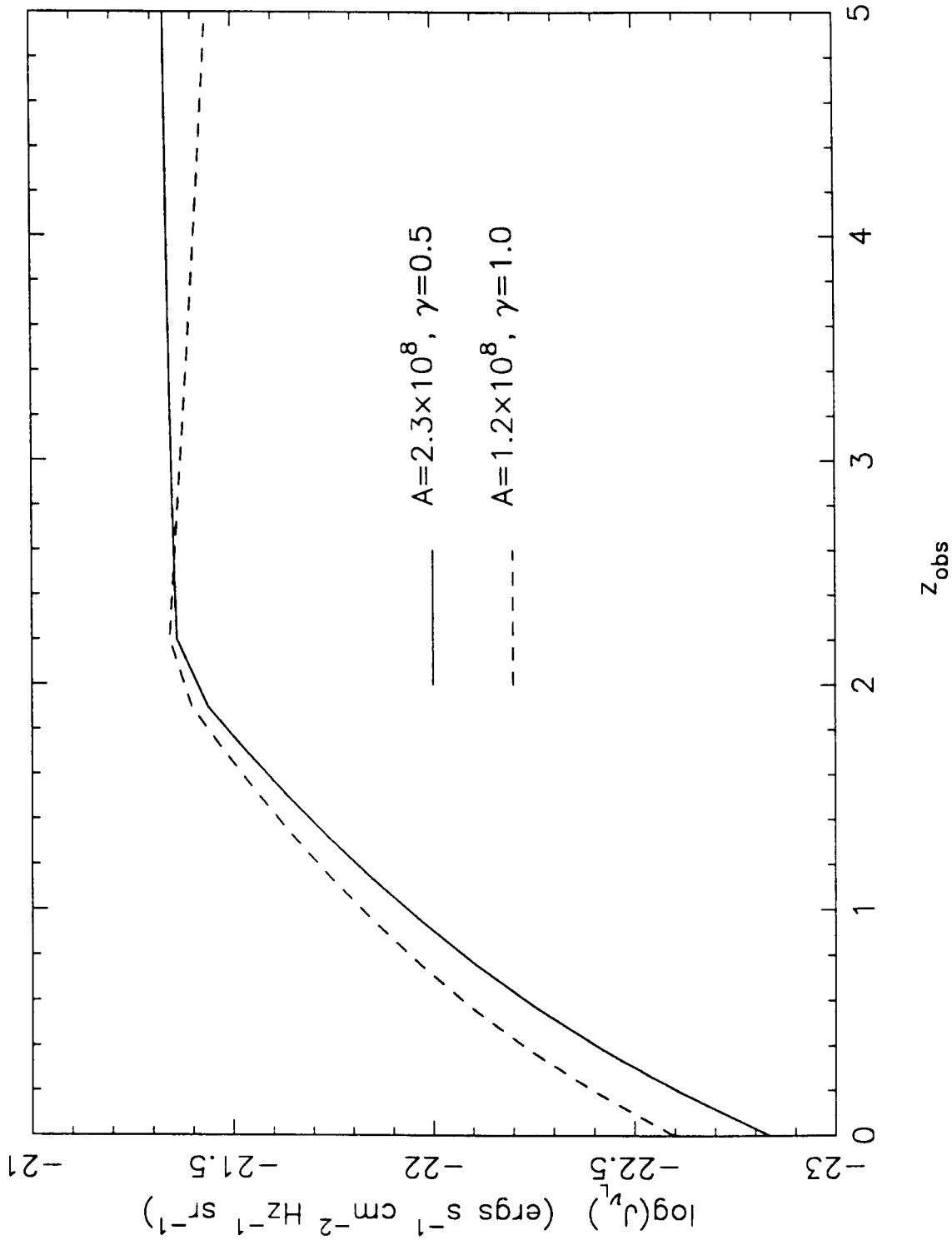
log(J$_{\nu_L}$) (ergs s^{-1} cm^{-2} Hz^{-1} sr^{-1})
−23
−22.5
−22
−21.5
−21
0
1
2
3
4
5
z_{obs}
A=2.3×10^8, γ=0.5
A=1.2×10^8, γ=1.0

Figure 5

CHAPTER THREE

FLUCTUATIONS IN THE IONIZING BACKGROUND

SUMMARY. We have derived a formalism to deal with fluctuations in the ionizing field produced by randomly distributed sources in an expanding universe, as well as in a Euclidean space. The probability distribution function $P(J)$ has been calculated for some models. Absorption by QSO absorption line systems reduces the total number of sources involved in producing J and therefore enhances the fluctuations significantly. We explore the possibility of detecting the "clearings" or "voids" in Lyα forests. We show that it is very difficult to distinguish statistically between a real clearing and a large gap produced merely by fluctuations in the line distribution. We also examine the HI and HeII Gunn-Peterson effect under the influence of the enhanced ionizing filed near a quasar. We show that a luminous quasar can reduce the Gunn-Peterson optical depth significantly out to a large wavelength interval.

1 INTRODUCTION

The studies of QSO absorption spectra offer important information on the dominating ionizing sources at high redshifts. If QSO metal absorption line systems are photoionized by a metagalactic ionizing field, as believed to be the case by many people, then the observed relative column densities of the most abundant ions can be used to set constraints to the possible spectral shape of ionizing flux. This in turn may tell us about the spectral shape of ionizing sources, although it is further complicated by the frequency dependent absorption of hydrogen and helium ions contained in intervening absorbing clouds (Madau 1991; Giroux and Shapiro 1991; Steidel 1990; Steidel and Sargent 1989). On the other hand the absence of the Gunn-Peterson effect in the spectra of high-redshift quasars and the decline of the counted number of Lyα forest lines with rest equivalent widths larger than a limiting value, the so called "inverse" or "proximity" effect, can be used to set a lower limit to the amplitude of the Lyman limit intensity of the ionizing background. The results thus obtained indicate that the observed QSOs cannot provide the required ionizing photons at high redshifts (Shapiro and Giroux 1987; Bajtlik, Duncan and Ostriker 1988; Lu *et al.* 1991). Other sources, such as young, star-forming galaxies (Bechtold *et al.* 1987), may be the main sources of the ionizing field at early epochs. There are also other ways to get information about the dominating ionizing sources. Since the space densities of different ionizing sources are expected to be very different, we expect that the fluctuations they produce in the ionizing field to also differ considerably. By studying the intensity fluctuations and exploring its

influence upon QSO Lyα absorption lines we can get some clues about the nature of the main contributors of the ionizing field at high z.

In this paper we develop a theory to deal with the fluctuations produced by randomly distributed sources in an expanding universe, as well as in a Euclidean space. We first apply a similar method used by Wright (1986) and Fall and Pei (1988) in dealing with cloudy absorption to derive the intensity distribution $P(J_\nu)$. We then show that application of Markoff's method leads to a more general formulation. A related subject, the correlation of the ionizing field at high redshifts is discussed in another paper (Chapter Four). We will adopt an Einstein-de Sitter universe (q_0=1/2) and use H_0 = 50km s^{-1}Mpc^{-1} throughout this paper unless otherwise specified.

2 FORMULATION

2.1 Divergence of $\sigma(J_{\nu_{obs}})$

Suppose we have ionizing sources and absorbers in an expanding universe. We assume that these sources and absorbers are distributed randomly and are independent of each other. We observe, at redshift z_{obs}, the mean specific intensity $J_{\nu_{obs}}$, which is defined by

$$J_{\nu_{obs}} \equiv \frac{\int I_{\nu_{obs}} d\omega}{4\pi}, \tag{2.1}$$

where $I_{\nu_{obs}}$ is the usual direction dependent specific intensity. At epoch z, the frequency ν_z, which will be redshifted to ν_{obs} at z_{obs}, is given by the following

expression

$$\nu_z = \frac{1+z}{1+z_{obs}}\nu_{obs}. \tag{2.2}$$

Now suppose we divide the universe into numerous thin "onion layers" of thickness Δz_i (i = 1, 2, ..., ∞), and denote z_i as the mean redshift of the i^{th} layer. Then in one realization of the distribution of both sources and absorbers, we have

$$J_{\nu_{obs}} = \frac{1}{4\pi}\sum_{i=1}^{\infty}\frac{1}{4\pi r_{L_i}^2}\frac{1+z_i}{1+z_{obs}}\sum_{j=1}^{N_i}L_{ij}e^{-\tau_{ij}}, \tag{2.3}$$

where N_i is the number of sources in the i^{th} layer, r_{L_i} is the luminosity distance from z_{obs} to z_i as measured at z_{obs}, L_{ij} is the luminosity of the j^{th} source in the i^{th} layer at frequency ν_{z_i}, and τ_{ij} is the optical depth to this source. The proper volume of the i^{th} layer as measured at z_i, ΔV_i, is given by

$$\Delta V_i = 4\pi r_{p_i}^2\frac{c}{H_0}\frac{1}{(1+z_i)^{3/2}}\left(\frac{1+z_{obs}}{1+z_i}\right)^3\frac{\Delta z_i}{1+z_{obs}} \equiv B(z_i)\Delta z_i, \tag{2.4}$$

where

$$r_{p_i} = \frac{2c}{H_0}\left[(1+z_{obs})^{-1/2} - (1+z_i)^{-1/2}\right]\frac{1}{1+z_{obs}} \tag{2.5}$$

is the proper distance to the i^{th} layer as measured at z_{obs}. The luminosity distance r_{L_i} is related to r_{p_i} by the following expression:

$$r_{L_i} = \left(\frac{1+z_i}{1+z_{obs}}\right)r_{p_i}. \tag{2.6}$$

Let $\phi(M,z)$ be the proper space density of sources per unit absolute magnitude at redshift z, it can be shown that the ensemble mean of Eq. (2.3) is

$$\langle J_{\nu_{obs}}\rangle = \frac{1}{4\pi}\frac{c}{H_0}\int_{z_{obs}}^{\infty}dz\left(\frac{1+z_{obs}}{1+z}\right)^3\frac{\epsilon e^{-\tau_{eff}}}{(1+z)^{5/2}}, \tag{2.7}$$

where

$$\epsilon \equiv \int \phi(M,z)L(M,\nu_z)dM \tag{2.8}$$

is the proper volume emissivity at redshift z and $\tau_{eff}(\nu_{obs}, z_{obs}, z)$, which is defined as $e^{-\tau_{eff}} \equiv \langle e^{-\tau} \rangle$, is the effective optical depth between z and z_{obs} at frequency ν_{obs}.

If we square Eq. (2.3) and then take the ensemble average, we can calculate variance of $J_{\nu_{obs}}$:

$$\sigma^2(J_{\nu_{obs}}) \equiv \langle (J_{\nu_{obs}} - \langle J_{\nu_{obs}} \rangle)^2 \rangle = \langle J^2_{\nu_{obs}} \rangle - \langle J_{\nu_{obs}} \rangle^2. \tag{2.9}$$

After some algebra, we have

$$\sigma^2(J_{\nu_{obs}}) = \frac{1}{(4\pi)^3}\frac{c}{H_0}\int_{z_{obs}}^{\infty} dz \int \phi(M,z)L^2(M,\nu_z)dM \frac{\langle e^{-2\tau} \rangle}{r_L^2}(1+z_{obs})^2(1+z)^{-4.5}. \tag{2.10}$$

Since $r_L^{-2} \propto (z - z_{obs})^{-2}$, it is clear that $\sigma^2(J_{\nu_{obs}})$ diverges.

2.2 The Probability Distribution Function $P(J_\nu|z)$

The formal expression (2.10) for $\sigma^2(J_{\nu_{obs}})$ diverges. A moment description is therefore not useful. Instead we calculate the probability distribution of J_ν. We define $P(J_\nu|z)dJ_\nu$ as the probability that sources between z_{obs} and z will produce a specific intensity in the range $J_\nu \rightarrow J_\nu + dJ_\nu$ at z_{obs}. For simplicity we neglect absorption effect in this section. Let $\rho(j_\nu, z)dj_\nu dz$ be the mean number of sources in the redshift interval $z \rightarrow z + dz$ which produce a specific intensity in the range $j_\nu \rightarrow j_\nu + dj_\nu$ at

z_{obs}; and let $q(J_\nu|z, z+\delta z)dJ_\nu$ be the probability that the sources between z and $z+\delta z$ will produce a specific intensity in the range $J_\nu \to J_\nu + dJ_\nu$ at z_{obs}. When δz is very small, we have

$$q(J_\nu|z, z+\delta z) \simeq \delta(J_\nu)\left[1 - \delta z \int_0^\infty dj_\nu \rho(j_\nu, z)\right] + \rho(J_\nu, z)\delta z, \tag{2.11}$$

neglecting the higher order small quantities.

The J_ν probability distribution produced by sources between z_{obs} and $z \to z+dz$ is

$$P(J_\nu|z+\delta z) = \int_0^{J_\nu} dJ'_\nu P(J_\nu - J'_\nu|z) q(J'_\nu|z, z+\delta z). \tag{2.12}$$

Using Eq. (2.11), we get

$$\frac{\partial P(J_\nu|z)}{\partial z} = -P(J_\nu|z)\int_0^\infty dj_\nu \rho(j_\nu, z) + \int_0^{J_\nu} dJ'_\nu P(J_\nu - J'_\nu|z)\rho(J'_\nu, z). \tag{2.13}$$

The Fourier transform of a function $y(x)$, $\tilde{y}(s)$, is defined by

$$\tilde{y}(s) = \int_{-\infty}^{\infty} dx y(x) e^{2\pi i s x}. \tag{2.14}$$

Since $P(x|z) = 0$ and $\rho(x, z) = 0$ when $x < 0$, we have

$$\int_0^{J_\nu} dJ'_\nu P(J_\nu - J'_\nu|z)\rho(J'_\nu, z) = \int_{-\infty}^{\infty} ds \tilde{P}(s|z) e^{-2\pi i s J_\nu} \tilde{\rho}(s, z). \tag{2.15}$$

The Fourier transform of Eq. (2.13) leads to

$$\frac{\partial \tilde{P}(s|z)}{\partial z} = \tilde{P}(s|z)[\tilde{\rho}(s, z) - \tilde{\rho}(0, z)]. \tag{2.16}$$

The boundary condition $P(J_\nu|z_{obs}) = \delta(J_\nu)$ means $\tilde{P}(s|z_{obs}) = 1$. This leads to

$$\tilde{P}(s|z) = \exp\left\{\int_{z_{obs}}^{z} dz'[\tilde{\rho}(s, z') - \tilde{\rho}(0, z')]\right\}. \tag{2.17}$$

From the definition of Fourier transform, we get

$$\langle J_\nu^n \rangle \equiv \int_0^\infty dJ_\nu J_\nu^n P(J_\nu|z) = \frac{1}{(2\pi i)^n} \frac{\partial^n}{\partial s^n} \tilde{P}(s|z)\Big|_{s=0}. \tag{2.18}$$

Notice that at redshift z, a single source with a luminosity spectrum $L(M, \nu_z)$ produces a

$$j_{\nu_{obs}} = \frac{1}{4\pi} \frac{L(M, \nu_z)}{4\pi r_L^2} \frac{1+z}{1+z_{obs}} \tag{2.19}$$

at z_{obs}. So $\rho(J_\nu, z)$ is related with $\phi(M, z)$ by

$$\rho(j_\nu, z) = \phi(M, z) B(z) \left(\frac{\partial j_\nu}{\partial M} \right)^{-1}, \tag{2.20}$$

where $B(z)$ is defined by Eq. (2.4). It is now easy to show that Eq. (2.18) gives the same $\langle J_\nu \rangle$ and $\langle J_\nu^2 \rangle$ as in the previous section (if absorption is neglected). The inverse Fourier transform of $\tilde{P}(s|z)$ gives

$$P(J_\nu|z) = \int_{-\infty}^{\infty} ds \tilde{P}(s, z) e^{-2\pi i s J_\nu}. \tag{2.21}$$

We can also use Laplace transform to get $P(J_\nu|z)$. The Laplace transform of a function $y(x)$ is defined as

$$\hat{y}(s) = \int_0^\infty y(x) e^{-sx} dx. \tag{2.22}$$

The similar method as in deriving $\tilde{P}(s|z)$ leads to the following expression for the Laplace transform of $P(J_\nu|z)$:

$$\hat{P}(s|z) = \exp\left\{ \int_{z_{obs}}^{z} dz' [\hat{\rho}(s, z') - \hat{\rho}(0, z')] \right\}, \tag{2.23}$$

where $\hat{\rho}(s,z)$ is Laplace transform of $\rho(J_\nu,z)$. The inverse Laplace transform of $\hat{P}(s|z)$ leads to (see Mathews and Walker, 1970)

$$P(J_\nu|z)=\frac{1}{2\pi i}\int_{C-i\infty}^{C+i\infty}e^{sJ_\nu}\hat{P}(s|z)ds. \tag{2.24}$$

2.3 J_ν Fluctuations in a Euclidean Space and Markoff's Method

In a Euclidean space there is no frequency redshift, so we drop the subscript ν in J_ν. Let $P(J|r)$ be the probability that sources between $r=0$ and r will produce a specific intensity (neglecting absorption) in the range of $J\rightarrow J+dJ$ at $r=0$. Denote $\rho(j,r)djdr$ as the mean number of sources in the interval $r\rightarrow r+dr$ which produce a specific intensity in the range $j\rightarrow j+dj$ at $r=0$. Using the similar arguments as in §2.2 we get

$$\frac{\partial P(J|r)}{\partial r}=-P(J|r)\int_0^\infty dj\rho(j,r)+\int_0^J dJ'P(J-J'|r)\rho(J',r). \tag{2.25}$$

We can use either Fourier or Laplace transform to solve the above equation as in §2.2.

Actually there is a more general method which can be used to derive the $P(J|r)$ distribution. This is Markoff's method (see Chandrasekhar 1943). Consider this problem first: given N uncorrelated sources in a spherical region of radius R, and given $f(L,r)dLdr$, the probability of finding a source at a radius between $r\rightarrow r+dr$ and with a luminosity in the range of $L\rightarrow L+dL$, what is $P_N(J|R)$, the probability distribution of intensity J at the center $r=0$? The contribution to J from a single

source at a radius r and with a luminosity L is $j(L,r) = L/(4\pi r)^2$. Using markoff's method, we can write down $P_N(J|R)$ directly (Chandrasekhar 1943):

$$P_N(J|R) = \frac{1}{2\pi}\int_{-\infty}^{\infty} e^{-isJ} I^N(s) ds, \tag{2.26}$$

where $I(s)$ is given by

$$I(s) = \int_0^R dr \int e^{isj(L,r)} f(L,r) dL. \tag{2.27}$$

To understand this new scheme better we now consider the situation in which N identical sources are uniformly (randomly) distributed in the spherical region. In this case we have

$$f(L,r) = \frac{3r^2}{R^3}\delta(L - L_s), \tag{2.28}$$

where L_s is the source luminosity. We then get

$$I(s) = \int_0^R e^{isL_s/(4\pi r)^2} \frac{3r^2}{R^3} dr. \tag{2.29}$$

Let $u = J/[L_s/(4\pi R)^2]$, we can easily calculate $P_N(u|R)$ for $N = 1$:

$$P_1(u|R) = \begin{cases} \frac{3}{2}u^{-5/2} & \text{for } u \geq 1; \\ 0 & \text{for } u < 1. \end{cases} \tag{2.30}$$

For $N = 2$ we have

$$P_2(u|R) = \begin{cases} \frac{3}{u^4}\frac{u-2}{(u-1)^{3/2}}(u^2 + 8u - 8) & \text{for } u \geq 2; \\ 0 & \text{for } u < 2. \end{cases} \tag{2.31}$$

For larger N, $P_N(u|R)$ can be obtained by convolving the lower N value distributions. For example, we have

$$P_3(u|R) = \int P_1(t|R) P_2(u - t|R) dt, \tag{2.32}$$

and

$$P_4(u|R) = \int P_2(t|R)P_2(u-t|R)dt, \tag{2.33}$$

and so on.

Now let us consider the situation in which the total number of sources in the spherical region is not fixed but obeys Poisson distribution, i.e., the probability of finding N sources, $N = 0, 1, 2, \ldots, \infty$, within the spherical volume is

$$p(N;\bar{N}) = \frac{\bar{N}^N}{N!}e^{-\bar{N}}, \tag{2.34}$$

where $\bar{N}$ is the total mean number of sources. In this case the intensity probability distribution is

$$P(J|R) = \sum_{N=0}^{\infty} p(N;\bar{N})P_N(J|R) = \frac{1}{2\pi}e^{-\bar{N}}\int_{-\infty}^{\infty} e^{-isJ}e^{\bar{N}I(s)}ds, \tag{2.35}$$

where $I(s)$ is given by Eq. (2.27). It can be shown that this $P(J|R)$ expression is the same as the one given by Eq. (2.25).

3 SOME NUMERICAL CALCULATIONS

3.1 Calculations in an Expanding Universe

For simplicity we assume in this section that all sources are identical and their proper space density is given by the following expression:

$$n(z) = \begin{cases} 0 & \text{if } z > z_{on}; \\ n_0(1+z)^3 & \text{if } z \leq z_{on}. \end{cases} \tag{3.1}$$

We further assume that the spectrum of ionizing sources is of a power law form, that is,

$$L_\nu = L\left(\frac{\nu}{\nu_L}\right)^{-\alpha}, \tag{3.2}$$

where ν_L is the Lyman limit frequency and L is the luminosity at ν_L. For definiteness we take $\alpha = 1$. In this case the mean specific intensity at the Lyman limit, $\langle J\rangle$ (hereafter we drop the subscript ν_L for the Lyman limit frequency), is given by

$$\langle J\rangle = \frac{n_0 L}{4\pi}\frac{c}{H_0}\frac{(1+z_{obs})^4}{2.5}\left[\frac{1}{(1+z_{obs})^{2.5}} - \frac{1}{(1+z_{on})^{2.5}}\right]. \tag{3.3}$$

We have, for $\nu_{obs} = \nu_L$,

$$\rho(j,z) = \delta[j - j^s(z)]B(z)n(z), \tag{3.4}$$

where

$$j^s(z) = \frac{1}{4\pi}\frac{L}{4\pi r_L^2} \tag{3.5}$$

is the specific intensity at the Lyman limit frequency produced by a single source at redshift z. We then get from Eq. (2.17)

$$\tilde{P}(s|z_{on}) = \exp\left[I_i - \frac{F\beta^3}{3}\right], \tag{3.6}$$

where

$$I_i = \int_{z_{obs}}^{z_{on}} B(z)n(z)e^{2\pi i s j^s(z)}dz = F\int_0^\beta dr r^2 e^{iEs\frac{(1-r)^4}{r^2}}, \tag{3.7}$$

$$E = \frac{L}{32\pi}\left(\frac{c}{H_0}\right)^{-2}(1+z_{obs})^3, \tag{3.8}$$

$$F = 32\pi n_0\left(\frac{c}{H_0}\right)^3(1+z_{obs})^{-1.5}, \tag{3.9}$$

and $\beta = 1 - [(1+z_{obs})/(1+z_{on})]^{0.5}$. It is clear that for $z \geq z_{on}$ we have $P(J|z) = P(J|z_{on})$; and for $J < j^s(z_{on})$ we get

$$P(J|z_{on}) = \delta(J)\exp\left[-\int_{z_{obs}}^{z_{on}} B(z)n(z)dz\right]. \tag{3.10}$$

This leads to

$$P_0 \equiv \int_0^{j^s(z_{on})} P(J|z_{on})dJ = \exp\left[-\int_{z_{obs}}^{z_{on}} B(z)n(z)dz\right]. \tag{3.11}$$

The physical meaning of the above equation is very clear: the probability of finding no sources between z and z_{on} is the probability of observing $J \leq j^s(z_{on})$. It is interesting to note that when $z_{on} \to \infty$, $j^s(z_{on}) \to 0$, but P_0 approaches a non-zero value, although it may be very small. This is because in a flat Einstein–de Sitter universe the mean total number of ionizing sources we can see at z_{obs} is finite.

Since we have neglected absorption, all photons have their energy reduced by the same fractional amount. The scaling in frequency for $P(J)$ is thus very simple. We have, for $\alpha = 1$,

$$\langle J_{\nu_{obs}}\rangle = \langle J\rangle \left(\frac{\nu_{obs}}{\nu_L}\right)^{-\alpha} = \langle J\rangle \left(\frac{\nu_{obs}}{\nu_L}\right)^{-1}, \tag{3.12}$$

and

$$j^s_{\nu_{obs}}(z) = j^s(z)\left(\frac{\nu_{obs}}{\nu_L}\right)^{-\alpha} = j^s(z)\left(\frac{\nu_{obs}}{\nu_L}\right)^{-1}. \tag{3.13}$$

In $\tilde{P}(s|z_{on})$, the only thing we should change for a frequency ν_{obs} is to replace $j^s(z)$ in Eq. (3.7) by $j^s(z)(\nu_{obs}/\nu_L)^{-1}$. This replacement leads to

$$P(J_{\nu_{obs}}|z_{on}) = P(J|z_{on})\left(\frac{\nu_{obs}}{\nu_L}\right). \tag{3.14}$$

The scaling with L can be done in the same way. If L is replaced by aL, where a is a constant, then the probability density is simply replaced by $P(J/a)/a$.

We have carried out some numerical calculations for $P(J)$. The input model parameters are given in Table 1. Notice that a Lyman limit luminosity $L = 10^{30}$ergs $s^{-1}Hz^{-1}$ corresponds to an absolute B magnitude of $M_B = -24.2$, if we adopt $L_\nu \propto \nu^{-1}$ for $\lambda < 1216\mathring{A}$ and $L_\nu \propto \nu^{-0.5}$ for $\lambda > 1216\mathring{A}$. Our six models are so constructed that $n_0 L$ is big enough to produce a $\langle J \rangle \gtrsim 10^{-21}$ergs $sec^{-1}cm^{-2}Hz^{-1}sr^{-1}$ at $z_{obs} = 3$, the value estimated by Bajtlik *et al.* (1987) and Lu *et al.* (1991) from the so called "proximity" or "inverse" effect. In our calculations we have used the inverse FFT to convert $\tilde{P}(s|z_{on})$. Our calculated results are shown in Fig. 1 and Fig. 2. In these figures, as well as in Table 1, J_{-21} is the mean intensity at the Lyman limit frequency in unit of 10^{-21} ergs $s^{-1}cm^{-2}Hz^{-1}sr^{-1}$. In all our six models $j^s(z_{on})$ and P_0 are very small and we have neglected them.

3.2 Calculations in a Euclidean Space

As in §3.1 we assume that all ionizing sources are identical and have the same luminosity L at the frequency we are interested in. Let sources be randomly distributed in a sphere of radius r_m, which is finite to avoid the Olbers' Paradox. We observe at $r = 0$. The mean number density of these ionizing sources is denoted as n and we neglect absorption effect. The mean total number of ionizing sources is $n_t = (4/3)\pi r_m^3 n$. The intensity produced by a source at distance r is

$$j^s(r) = \frac{1}{4\pi}\frac{L}{4\pi r^2}. \tag{3.15}$$

The mean intensity at $r = 0$ is

$$\langle J \rangle = \frac{nL}{4\pi} r_m. \tag{3.16}$$

We now introduce a new variable $x = J/\langle J \rangle$, i.e., we measure J in unit of $\langle J \rangle$. From §2 we know that Fourier transform of the probability distribution $P(x|r_m)$ is

$$\tilde{P}(s|r_m) = \exp\left\{ \int_0^{r_m} dr[\tilde{\rho}(s,r) - \tilde{\rho}(0,r)] \right\}, \tag{3.17}$$

where $\tilde{\rho}(s,r)$ is Fourier transform of $\rho(x,r)$, which is given by

$$\rho(x,r) = 4\pi r^2 n \langle J \rangle \delta[x\langle J \rangle - j^s(r)]. \tag{3.18}$$

Denote $\omega = 2\pi s/(3n_t)$, we can show that

$$\tilde{P}(s|r_m) = e^{I1}, \tag{3.19}$$

where the real and the imaginary parts of $I1$ are, for $s \geq 0$,

$$\mathrm{Re}(I1) = [\cos\omega - 2\omega\sin\omega - 2\omega^{1.5}\sqrt{\frac{\pi}{2}} + 2\sqrt{2\pi}\omega^{1.5}C(\omega) - 1]n_t, \tag{3.20}$$

and

$$\mathrm{Im}(I1) = [\sin\omega + 2\omega\cos\omega - 2\omega^{1.5}\sqrt{\frac{\pi}{2}} + 2\sqrt{2\pi}\omega^{1.5}S(\omega)]n_t. \tag{3.21}$$

In the above two expressions $C(x)$ and $S(x)$ are the Fresnel's sine and cosine integrals which are defined by

$$C(x) = \frac{1}{\sqrt{2\pi}} \int_0^x \frac{\cos(s)}{\sqrt{s}} ds, \tag{3.22}$$

and

$$S(x) = \frac{1}{\sqrt{2\pi}} \int_0^x \frac{\sin(s)}{\sqrt{s}} ds. \tag{3.23}$$

We also have Re($I1(-s)$)=Re($I1(s)$) and Im($I1(-s)$) = $-$Im($I1(s)$). We see from the above equations that $\tilde{P}(s|r_m)$, thus $P(x|r_m)$, depends only on the total mean source number n_t. Our calculations for n_t=10, 100, 1000 and 10000 are shown in Fig. 3. As expected the peak of distribution function for $n_t = 10000$ is quite narrow while for n_t=10 it is pretty wide. We see from Fig. 3 that the probability of $J < \langle J \rangle/2$ is $\sim 20\%$ and the probability of $J > \langle J \rangle$ is only $sim30\%$ in the case of $n_t = 10$, indicating significant fluctuations.

By rescaling $P(x|r_m)$ curve we can easily get intensity distribution $P(J|r_m)$. For $n = 3.2 \times 10^6 \mathrm{Gpc}^{-3}$ and $L = 10^{30}$ergs $\mathrm{s}^{-1}\mathrm{Hz}^{-1}$, these are the proper space density at z_{obs}=3 and the Lyman limit luminosity in our model #2 of §3.1, we choose r_m to match n_t =10, 100, 1000 and 10000. The $P(J_{-21}|r_m)$ curves obtained by rescaling the corresponding curves in Fig. 3 are plotted in Fig. 4. We see that the widths of $P(J_{-21}|r_m)$ peaks are roughly the same for all four curves while the peak positions are shifted to different places for different n_t values. This indicates that for a fixed source space density the absolute width of $P(J_{-21}|r_m)$ curve is not sensitive to r_m and is actually dominated by a few (< 10) local sources.

The fluctuations in J caused by the nearest neighbors from an observer at $r = 0$ can be readily calculated. Suppose we generate various realizations of source distribution in the spherical region. Let r_1, r_2, ... be the distances to the nearest

random source, the second nearest random source, and so on, the distribution of r_s $(s = 1, 2, \ldots)$ is

$$p(r_s)dr_s = \frac{n_s^{s-1}}{(s-1)!} e^{-n_s} 4\pi r_s^2 n dr_s, \tag{3.24}$$

where $n_s = 4\pi r_s^3 n/3$. The above distribution can be understood directly by observing that the probability that $(s-1)$ sources are within the spherical region of radius r_s is $n_s^{s-1}e^{-n_s}/(s-1)!$, and the probability of a source being in the shell $(r_s, r_s + dr_s)$ is $4\pi r_s^2 n dr_s$, since these two are independent events, product of their probabilities leads to $p(r_s)dr_s$. The probability distribution of J, $P_s(J)$, produced by the s^{th} neighbor, can be calculated using the following expression:

$$P_s(J) = -p(r_s)\frac{dr_s}{dJ}, \tag{3.25}$$

where J is related with r_s by $J = L/(4\pi r_s)^2$. For $n = 3.2 \times 10^6 \mathrm{Gpc}^{-3}$ and $L = 10^{30}$ergs $\mathrm{s}^{-1}\mathrm{Hz}^{-1}$, the calculated results are shown in Fig. 5. For $s = 1$, $P_1(J)$ reaches its maximum value of $40.11 n^{-2/3} L^{-1}$ at $J = 1.17 \times 10^{-2} n^{2/3} L$. Since $\langle J \rangle$ converges and $\langle J^2 \rangle$ diverges, when J is large the asymptotic form of $P(J) \propto J^{-\alpha}$ must satisfy the condition: $2 < \alpha \leq 3$. From Eq. (3.25) we can show that $P_1(J)$ goes like $P_1(J) \propto nL^{1.5}J^{-2.5}$ when J is large. This means that the closest source dominates the behavior of $P(J)$ at very large J (see Appendix A).

3.3 A Simplified Treatment for Absorption Effect

In the above $P(J)$ calculations we have completely neglected absorption effect. We now give a simplified treatment for this effect. We define $z_c(\nu_{obs})$ by demanding

$\tau_{eff}(\nu_{obs}, z_{obs}, z_c) \equiv 1$, i.e., the effective optical depth between z_{obs} and z_c is unity. We approximate the absorption effect by simply dropping the ionizing sources with redshift $z > z_c(\nu_{obs})$ and neglecting absorption for those sources with $z < z_c(\nu_{obs})$. Adopting our Model 1 absorption discussed in Chapter Two we have (see Eq. (3.5a) of Chapter Two), for $\nu_{obs} = \nu_L$,

$$1 + z_c(\nu_L) \simeq (1 + z_{obs}) e^{0.489(1+z_{obs})^{-3/2}}. \tag{3.26}$$

From the above expression we get, for $z_{obs} = 3$, $z_c(\nu_L) \simeq 3.25$. So our model 2, 4 and 6 in §3.1, in which $z_{obs} = 3$ and $z_{on} = 3.2$, should be good approximations for the absorption effect. It is also clear that for $\nu_{obs} = \nu_L$, since $z_{obs} - z_c$ is small at high z_{obs}, we can use the results derived in a Euclidean space. We should point out that the recent result by Lanzetta (1991) showed that the line number per unit redshift of the optically thick Lyman limit systems may evolve much faster at high z than what we have assumed $(1+z)^{0.5}$. This means that we may have considerably underestimated the absorption at early epochs.

We now examine how many ionizing sources are involved in producing the ionizing background at ν_L. We define the absorption length scale $r_0(z_{obs})$ as the proper distance between z_{obs} and z_c as measured at z_{obs}. At $z_{obs} = 3$, we have $r_0 \simeq 45$Mpc. The sources which are responsible for producing J_{ν_L} are contained in a spherical region of radius r_0. According to Boyle, Shanks and Peterson (1988) the QSO luminosity function at $z < 2.2$ is most simply parameterised by two power laws, with $\Phi(L) \propto L^{-3.7\pm0.1}$ at high luminosities and $\Phi(L) \propto L^{-1.4\pm0.2}$ at low

luminosities. The knee luminosity L^* evolves with redshift z. Those QSOs with $L \sim L^*$ dominate the ionizing flux. At $z = 2.2$, $L^* \simeq 10^{31}$ergs sec^{-1}Hz^{-1}, which corresponds to an absolute B magnitude $M_B = -26.5$. The comoving space density of QSOs with M_B bright than -26.5 is roughly 10^3Gpc^{-3} at $z = 2.2$. Let us assume quasars are non-evolving at $z > 2.2$ and have a constant comoving space density. We then see that there are about 20 QSOs with M_B brighter than -26.5 at $z = 3$, and there are about 4 such QSOs at $z = 4$. Very recently Schmidt, Schneider and Gunn (1991) have shown that the luminous QSOs are endangered species at early epochs and their comoving space densities decline steeply for redshifts larger than 3. This combined with the result regarding the evolution of Lyman limit absorption systems by Lanzetta (1991) suggests significant fluctuations in the ionizing field at high redshifts, if QSOs are the major ionizing sources at early epochs.

4 Lyα CLOUDS AND $P(J)$

4.1 Neutral Hydrogen Column Density Distribution and $P(J)$

It is now widely believed that the forest absorption lines observed in quasar spectra blueward of Lyα emission are produced by highly ionized intervening clouds. If this is true the neutral hydrogen column density N may be written as $N = A/J$, where A depends on the intrinsic properties of an absorbing cloud. Let the probability distribution of A be $f(A)$, the neutral hydrogen column density distribution is

$$\eta(N) = \int_0^\infty f(NJ)JP(J)dJ. \tag{4.1}$$

We see that the observed $\eta(N)$ has been modulated by $P(J)$. For $f(A) = \delta(A - A_0)$ we have $\eta(N) = A_0 P(A_0/N)/N^2$. In this case $\eta(N)$ distribution is completely determined by $P(J)$. On the other hand if $f(A)$ is of a power law form, i.e., $f(A) \propto A^{-\beta}$, we get $\eta(N) \propto N^{-\beta}$, no matter what $P(J)$ is. As we have seen in §3.2 the observed $\eta(N)$ may be best described as a power law distribution and despite the line number per unit redshift evolves as a function of z this power law form seems to remain unchanged. This argues for a power law distribution of A, with the same power index as observed for $\eta(N)$.

When a cutoff neutral column density N_c is imposed by observational limitation, the probability of observing an absorption line with $N > N_c$ are different at places with different J values. For a fixed J the column density distribution is $\eta(N) \propto J^{-\beta+1} N^{-\beta}$ for $f(A) \propto A^{-\beta}$. Suppose that at place 1 the intensity is J_1 and at place 2 we have J_2. If the mean number of lines per unit redshift interval is n_1 at place 1 and n_2 at place 2, we have $n_1/n_2 = (J_2/J_1)^{\beta-1}$. When observed near a QSO at the end of the line of sight, this effect is the so called inverse effect. The "clearings" in Lyα forests, which we will discuss below, is another form of this effect.

4.2 Clearings in Lyα Forests

We define a clearing as a region around an ionizing source within which the Lyman limit frequency intensity of ionizing field is enhanced by at least a factor of 2 over

the mean intensity $\langle J_{\nu_L} \rangle$. By this definition the radius of a clearing, r_{cl}, is given by

$$r_{cl}^2(z) = \frac{1}{(4\pi)^2} \frac{L}{\langle J_{\nu_L}(z) \rangle}, \tag{4.2}$$

for a source at redshift z and with a Lyman limit luminosity L.

For ionizing sources with an intrinsic, non-evolving luminosity spectrum $L_\nu = L(\nu/\nu_L)^{-\alpha}$ and a constant comoving luminosity function $\Phi(L)$, we have

$$\langle J_{\nu_L}(z_{obs}) \rangle \simeq \frac{1}{4\pi} \frac{c}{H_0} \int \Phi(L) L dL \frac{(1+z_{obs})^{3+\alpha}}{1.5+\alpha} \times \left[\frac{1}{(1+z_{obs})^{1.5+\alpha}} - \frac{1}{(1+z_c)^{1.5+\alpha}} \right]. \tag{4.3}$$

At high redshifts the absorption is strong and we have, from Eq. (3.26),

$$z_c - z_{obs} \simeq 0.25 \left(\frac{1+z_{obs}}{4} \right)^{-1/2}. \tag{4.4}$$

Using the above approximation Eq. (4.3) becomes

$$\langle J_{\nu_{obs}} \rangle \simeq \frac{1}{8\pi} \frac{c}{H_0} \int \Phi(L) L dL. \tag{4.5}$$

The expected number of clearings per unit redshift interval, which a line of sight intersects, is given by

$$\frac{dN_{cl}}{dz} \simeq \frac{1.5+\alpha}{4} (1+z)^{-1} \left[1 - \left(\frac{1+z_c}{1+z} \right)^{-(1.5+\alpha)} \right]^{-1}. \tag{4.6}$$

dN_{cl}/dz does not depend on $\Phi(L)$. At high z Eq. (4.4) can be used, and we get

$$\frac{dN_{cl}}{dz} \simeq 1 \left(\frac{1+z}{4} \right)^{0.5}. \tag{4.7}$$

The expected number of clearings along a line of sight between z_1 and z_2 is easily obtained by integrating the above equation:

$$N_{cl} \simeq 0.3\,[(1+z_2)^{1.5} - (1+z_1)^{1.5})]. \tag{4.8}$$

For $z_1 = 2$ and $z_2 = 4$, $N_{cl} \sim 2$. Note that this includes all kinds of clearings with various sizes.

As pointed out by Kovner and Rees (1989), at sufficient resolution, QSO spectra can be examined for patches of reduced HI column density in Lyα clouds. We now explore the possibility of detecting such clearings in Lyα forests. The detection of a clearing depends critically on the clearing size. After correction for the inverse effect, the observed number density of Lyα forest lines with a rest equivalent width $W > 0.36\mathring{A}$ is $dN_{Ly\alpha}/dz \simeq 1.74(1+z)^{2.75}$ (see Lu *et al.* 1991). The mean separation of $W > 0.36\mathring{A}$ lines is thus $\Delta l_{Ly\alpha} \sim 2.4((1+z)/4)^{-5.25}$Mpc. If a clearing is much larger than this then it is more likely to be detected. Since the ionizing sources which contribute most to $\langle J_\nu \rangle$ also create most clearings' cross-sections, if faint sources such as young galaxies dominate the ionizing field then the typical clearing size is small and we are not expected to detect these galaxy clearings. Bright QSOs create big clearings which can contain many Lyα clouds. Put in numerical values we have $r_{cl} \simeq 2.7 J_{-21}(L/10^{31}\mathrm{ergs\,s^{-1}Hz^{-1}})$Mpc. We see that it is still very difficult even to detect QSO clearings, unless $J_{-21} < 1$. But we know that there are numerous weaker ($W < 0.36\mathring{A}$) Lyα forest lines per unit redshift interval. Counting these weak lines will help to identify clearings more

easily.

Another difficulty in detecting clearings is that the absorption lines in a clearing are not necessarily removed from observations, and even when they are removed it is still very difficult to distinguish statistically between a clearing and a large gap produced merely by random fluctuations in the line distribution (see Appendix B). For a Lyα forest having 100 lines, which would be the case for a $z_{em} \simeq 4$ quasar, the probability that a random gap has a size larger than six times the mean separation is $\sim 20\%$ (see Appendix B)! We think that the best strategy to detect clearings is to observe weak lines and to observe at high redshifts ($z \gtrsim 4$), because a clearing there contains many lines. In fact we suspect that at very high redshifts the Lyα forest lines may become so dense that they may blend together to destroy the forest. Should this happen a clearing may take the form of an isolated "Lyα hill" and be easily recognized. A line of sight may sometimes penetrate at least two clearings. In this case it is better to check the probability of finding more than one large gap due to random fluctuations in the line distribution. We have worked out a relevant statistics in Appendix B.

5 PROXIMITY EFFECT AND GUNN-PETERSON TEST

The Gunn-Peterson test addresses the cumulative line absorption effect produced by a smoothly distributed component of intergalactic medium (IGM). Since it was first proposed in 1965 by Gunn and Peterson, spectra of distant quasars shortward of the HI Lyα ($\lambda 1215.7\mathring{A}$) emission, and very recently shortward of the HeI Lyα ($\lambda 584.3\mathring{A}$)

emission probed with the *IUE* and *HST*, have been searched for absorption troughs produced by smoothly distributed intergalactic HI and HeI (Gunn and Peterson 1965; Steidel and Sargent 1987; Jenkins and Ostriker 1991; Tripp *et al.* 1990; Beaver *et al.* 1991). So far all attempts have failed to find positive evidence of the Gunn-Peterson effect. But very important upper limits have been set for the IGM number densities n_{HI} and n_{HeI} at various redshifts. These limits are important, since they allow us to put constraints to the ionizing background and the mass density of the smooth IGM component. With the launch of the *HST* we may also be able to conduct the HeII Lyα ($\lambda 303.8\mathring{A}$) Gunn-Peterson test for distant ($z_{em} \geq 3.1$) quasars, if we are lucky enough to find "clear" lines of sight which do not display significant Lyman continuum absorption to destroy the flux level at the wavelengths corresponding to HeII Lyα emissions (see Møller and Jakobsen 1990; Chapter Two).

Similar as in the cases of clearings in Lyα forest and the decline of number density of Lyα forest lines near QSO emission redshifts, we expect the Gunn-Peterson optical depths be reduced by the enhanced ionizing field near QSOs. We examine this effect quantitatively below.

The Gunn-Peterson optical depth at redshift z is

$$\tau_i(z) = \frac{n_i(z)}{H_0(1+z)(1+2q_0z)^{1/2}} \left(\frac{\pi e^2 f_i}{m_e \nu_i}\right), \tag{5.1}$$

where the subscript i means HI, or HeI, or HeII. $n_i(z)$ is the proper number density of the smoothly distributed HI, HeI and HeII species at redshift z. The oscillator

strength $f_i = 0.4162$ for HI and HeII, and $f_{HeI} = 0.2762$ for HeI.

The number density n_i can be calculated from the ionization equilibrium equations. The ionization balance is valid because the IGM is highly ionized and the time scale to recombine the small amount of n_{HI}, n_{HeI} and n_{HeII} is shorter than the Hubble time (Sargent *et al.* 1980). To solve the ionization balance for n_i we assume that $n_H/n_{He} = 12$, $n_H(z) \propto (1+z)^3$ and the smoothly distributed IGM component contributes Ω_I to the present density parameter. We adopt the following broken power law form for the background ionizing field:

$$J_\nu = \begin{cases} J_1 \left(\frac{\nu}{\nu_L}\right)^{-s_1} & \text{for } \nu_L < \nu < \nu_2; \\ J_2 \left(\frac{\nu}{\nu_2}\right)^{-s_2} & \text{for } \nu_2 < \nu < 4\nu_L; \\ J_3 \left(\frac{\nu}{4\nu_L}\right)^{-s_3} & \text{for } \nu > 4\nu_L. \end{cases} \tag{5.2}$$

The Lyman limit frequency has been denoted as ν_L. $h\nu_2 = 24.6$eV is the threshold energy for ionizing HeI. The photoionization cross-sections for HI, HeI and HeII have been taken as (Osterbrock 1989) $\sigma_\nu(HI) = 6.3 \times 10^{-18}(\nu/\nu_L)^{-3}\text{cm}^2$, $\sigma_\nu(HeI) = 7.8 \times 10^{-18}(\nu/\nu_2)^{-2}\text{cm}^2$ and $\sigma_\nu(HeII) = 1.58 \times 10^{-18}(\nu/4\nu_L)^{-3}\text{cm}^2$. For the recombination coefficients we use $\alpha_A(HI) = 2.51 \times 10^{-13}$, $\alpha_A(HeI) = 2.69 \times 10^{-13}$ and $\alpha_A(HeII) = 1.36 \times 10^{-12}$, all in units of $\text{cm}^3\ \text{sec}^{-1}$. These values are appropriate for IGM temperature $T = 2 \times 10^4$K (Osterbrock 1989). The Monochromatic QSO luminosity is assumed to be $L_\nu = L_0(\nu/\nu_L)^{-\alpha}$.

Since the IGM is highly ionized, there is little HeI, and its Gunn-Peterson optical depth is negligible for reasonable input parameters. So in what follows we

only consider HI and HeII. The ionization equations can be easily solved to get n_{HI} and n_{HeII} (see Osterbrock 1989). Inserting the n_{HI} and n_{HeII} results into the Gunn-Peterson optical depth expressions we get

$$\tau_{HI}(z) \simeq 9.75 \times 10^{-2} \frac{(3+s_1)h^3\Omega_I^2(1+z)^5\,(1+2q_0z)^{-1/2}}{J_{-21}(HI)[1+\omega_{HI}]} \tag{5.3}$$

and

$$\tau_{HeII}(z) \simeq 4.41 \times 10^{-2} \frac{(3+s_3)h^3\Omega_I^2(1+z)^5\,(1+2q_0z)^{-1/2}}{J_{-21}(HeII)[1+\omega_{HeII}]}. \tag{5.4}$$

For $q_0 = 1/2$, we have

$$\omega_{HI} = 1.85 \times 10^{-7}\, L_{31} J_{-21}(HI) h^2 \left(\frac{3+s_1}{3+\alpha}\right) \times$$

$$(1+z)^3 \left(\frac{1+z}{1+z_{em}}\right)^{1+\alpha} \left[1 - \sqrt{\frac{1+z}{1+z_{em}}}\right]^{-2} \tag{5.5}$$

and

$$\omega_{HeII} = 4^{-\alpha} \left(\frac{3+s_3}{3+s_1}\right) \frac{J_{-21}(HeII)}{J_{-21}(HI)}\, \omega_{HI}. \tag{5.6}$$

In the above equations L_{31} is defined by $L_0 = L_{31}$ergs sec^{-1}cm^{-2}; and $J_{-21}(HI)$ and $J_{-21}(HeII)$ are J_1 and J_3 expressed in units of 10^{-21}ergs cm^{-2}sec^{-1}Hz^{-1}sr^{-1}, respectively. The flux from a distant (z_{em}) quasar is attenuated by a factor of $e^{-\tau_i(z)}$, where $1+z = \lambda_{obs}/(1215.7\mathring{A})$ for HI and $1+z = \lambda_{obs}/(303.8\mathring{A})$ for HeII.

We have calculated some numerical results. For definiteness we have used $s_1 = s_3 = 0$ and $\alpha = 0.7$. We adopt $q_0 = 0.5$, $h = 0.5$ and $\Omega_I = 0.02$. We have neglected the complications due to the HI and HeII Lyα emissions and the HI and HeII Lyα forests produced by discrete absorbers. Our results are shown in solid

lines in Fig. 6. The dashed lines represent the results without the Gunn-Peterson absorption. The input parameters z_{em}, L_{31}, $J_{-21}(HI)$ and $J_{-21}(HeII)$ are shown in the same figure. Notice that $\lambda_{obs} \leq 912\mathring{A}$ is not observable due to the Galactic Lyman continuum absorption.

6 DISCUSSION AND CONCLUSIONS

We have developed a theory to deal with fluctuations of the ionizing field produced by randomly distributed point sources in an expanding universe, as well as in a Euclidean space. The probability distribution $P(J)$ has been calculated for some models. At high redshifts absorption by quasar absorption line systems reduces the total number of sources involved in producing J and therefore greatly enhances fluctuations.

We have explored the possibility of detecting the "clearings" or "voids" in Lyα forests. We have shown that it is very difficult to distinguish statistically between a real clearing and a large gap produced merely by fluctuations in the line distribution.

We have also examined the HI and HeII Gunn-Peterson effect under the influence of the enhanced ionizing filed near a quasar. We have shown that a luminous quasar can reduce the Gunn-Peterson optical depth significantly out to a large wavelength interval.

ACKNOWLEDGMENT

This work was supported in part by NSF Grant AST84-51725.

REFERENCES

Bajtlik, S., Duncan, R. C. & Ostriker, J. P., 1988. *Astrophys. J.*, **327**, 570.

Beaver, E. A., Burbidge, E. M., Cohen, R. D., Junkkarinen, V. T., Lyons, R. W., Rosenblatt, E., I., Hartig, G. F., Margon, B. & Davidsen, A. F., 1991. *Astrophys. J. Lett.*, **377**, L1.

Bechtold, J., Weymann, R. J., Lin, Z. & Malkan, M., A., 1987. *Astrophys. J.*, **315**, 180.

Boyle, B. J., Shanks, T. & Peterson, B. A., 1988. *Mon. Not. R. astr. Soc.*, **235**, 935.

Chandrasekhar, S., 1943. *Rev. Mod. Phys.*, **15**, 1.

Fall, M. & Pei, Y., 1988. *Astrophys. J.*, **337**, 7.

Giroux, M. L., & Shapiro, P. R., 1991. in *After the First Three Minutes*, eds. S. S. Holt, C. L. Bennet, & V. Trimble (AIP), p352.

Gunn, J. E. & Peterson, B. A., 1965. *Astrophys. J.*, **142**, 1633.

Jenkins, E. B. & Ostriker, J. P., 1991. *Astrophys. J.*, **375**, in press.

Kendall, M. G. & Moran, P. A. P., 1963. *Geometrical Probability* (Hafner Publishing Company, New York), p32.

Kovner, I. & Rees, M. J., 1989. *Astrophys. J.*, **345**, 52.

Lanzetta, K. M., 1991. *Astrophys. J.*, **375**, 1.

Lu, L., Wolfe, A. M. & Turnshek, D. A., 1991. *Astrophys. J.*, **367**, 19.

Madau, P., 1991. *Astrophys. J. Lett.*, **376**, L33.

Mathews, J. & Walker, R. L., 1970. *Mathematical Methods of Physics* (The Benjamin/Cummings Publishing Company), p108.

Møller, P. & Jakobsen, P., 1990. *Astron. Astrophys.*, **228**, 299.

Osterbrock, D. E., 1989. *Astrophysics of Gaseous Nebulae and Active Galactic Nuclei*, University Science Books, California.

Ostriker, J. P., Bajtlik, S. & Duncan, R. C., 1988. *Astrophys. J. Lett.*, **327**, L35.

Sargent, W. L. W., Young, P. J., Boksenberg, A. & Tytler, D., 1980. *Astrophys. J. Suppl. Ser.*, **42**, 41.

Shapiro, P. R. & Giroux, M. L., 1987. *Astrophys. J. Lett*, **321**, L107.

Schmidt, M., Schneider, D. P. and Gunn, G. E., 1991. Paper presented at the workshop on: *Space Distribution of Quasars.*

Steidel, C. C. & Sargent, W. L. W., 1987. *Astrophys. J. Lett*, **318**, L11.

Steidel, C. C. & Sargent, W. L. W., 1989. *Astrophys. J. Lett*, **343**, L33.

Steidel, C. C., 1990. *Astrophys. J. Suppl. Ser.*, **74**, 37.

Tripp, T. M., Green, R. F. & Bechtold, J., 1990. *Astrophys. J. Lett*, **364**, L29.

Wright, E. L., 1986. *Astrophys. J.*, **311**, 156.

APPENDIX A: ASYMPTOTIC EXPANSION OF $P(x|r_m)$

We will use the same symbols as defined in §3.2. The probability distribution of $x = J/\langle J\rangle$ is (in a Euclidean space)

$$P(x|r_m) = \int_{-\infty}^{\infty} ds e^{-2\pi i s x} e^{I1}, \tag{A1}$$

where $I1$ is given in §3.2. Denoting $C_R(\omega) = \mathrm{Re}[e^{I1(\omega)}]$ and $C_I(\omega) = \mathrm{Im}[e^{I1(\omega)}]$, where $\omega = 2\pi s/(3n_t)$, Eq. $(A1)$ can be written as

$$P(x|r_m) = \frac{1}{\pi x}\int_0^{\infty}\left[C_R\left(\frac{u}{3n_t x}\right)\cos u + C_I\left(\frac{u}{3n_t x}\right)\sin u\right] du. \tag{A2}$$

From Eqs. (3.20) and (3.21) we find

$$\mathrm{Re}(I1) = [-\sqrt{2\pi}\omega^{3/2} + \frac{3}{2}\omega^2 - \frac{1}{40}\omega^4]n_t + o(\omega^4), \tag{A3}$$

and

$$\mathrm{Im}(I1) = [3\omega - \sqrt{2\pi}\omega^{3/2} + \frac{1}{6}\omega^3]n_t + o(\omega^4). \tag{A4}$$

Using the above expressions we get

$$C_R(\omega) = 1 - \sqrt{2\pi}n_t\omega^{3/2} + o(\omega^{3/2}), \tag{A5}$$

and

$$C_I(\omega) = 3n_t\omega - \sqrt{2\pi}n_t\omega^{3/2} + o(\omega^{3/2}). \tag{A6}$$

We then have

$$P(x|r_m) = \frac{1}{2\sqrt{3}}n_t^{-1/2}x^{-5/2} + o(x^{-5/2}). \tag{A7}$$

Converting the above expression to the intensity distribution $P(J|r_m)$, we get

$$P(J|r_m) = \frac{1}{32\pi^2} nL^{3/2} J^{-5/2} + o(J^{-5/2}). \qquad (A8)$$

Comparing this with the distribution due to the closest source,

$$P_1(J) = \frac{1}{32\pi^2} nL^{3/2} J^{-5/2} + o(J^{-5/2}), \qquad (A9)$$

we see that at very large J the closest source dominates the $P(J|r_m)$ behaviour.

APPENDIX B: LARGE GAPS IN Lyα FORESTS DUE TO FLUCTUATIONS IN LINE DISTRIBUTION

Spectroscopic observations of bright quasars show that mean number density of Lyα forest lines, which satisfy certain criteria, evolves like $dN/dz = A(1+z)^{\gamma}$, where A and γ are two constants. Given the above intrinsic line distribution we examine the probability of finding large gaps in the Lyα forests. We concentrate here only on the statistics and neglect all observational complications such as the line blending effect (see Ostriker *et al.* 1988).

Suppose we have observed a Lyα forest between redshifts z_1 and z_2 and found $N-1$ lines. For high redshift quasars usually z_2 is the emission redshift z_{em} and z_1 is set to $(\lambda_{Ly\beta}/\lambda_{Ly\alpha})(1+z_{em}) = 0.844(1+z_{em})$ to avoid contaminations by Lyβ lines. We want to know whether the largest gaps observed in the forest are significantly inconsistent with the above line distribution. To do this we introduce a new variable x:

$$x = \frac{(1+z)^{\gamma+1} - (1+z_1)^{\gamma+1}}{(1+z_2)^{\gamma+1} - (1+z_1)^{\gamma+1}}. \qquad (B1)$$

x varies from 0 to 1. We then have $dN/dx = \lambda$, where λ is the mean number of lines between z_1 and z_2 and is given by

$$\lambda \equiv \frac{A[(1+z_2)^{\gamma+1} - (1+z_1)^{\gamma+1}]}{\gamma+1}. \qquad (B2)$$

This means that the Lyα forest lines are uniformly distributed in x. The probability of finding $N-1$ lines between z_1 and z_2, P_{N-1}, is assumed to be the Poisson

distribution:

$$P_{N-1}(\lambda) = \frac{\lambda^{N-1}}{(N-1)!}e^{-\lambda}. \qquad (B3)$$

Here we assume this probability is not significantly small and assume these $N-1$ lines are randomly distributed in accordance with the underlying distribution law. The $N-1$ random lines along with the two end points $x = 0$ and $x = 1$ form N intervals. From Kendall and Moran (1963) we know that the probability that exactly k intervals are larger than an assigned value of x_{gap} ($k = 0, 1, 2, ...$ and $kx_{gap} \leq 1$), $P(N,k)$, is given by

$$P_{N,k} = \binom{N}{k}[(1-kx_{gap})^{N-1} - \binom{N-k}{1}(1-(k+1)x_{gap})^{N-1} + ...$$

$$+ (-)^s\binom{N-k}{s}(1-(k+s)x_{gap})^{N-1}], \qquad (B4)$$

where the series stops at the last term for which $1-(k+s)x_{gap}$ is positive. $P_{N,0}$ is the probability that the largest interval is less than x_{gap}. The probability that the largest exceeds x_{gap} is then

$$P(> x_{gap}) = 1 - P_{N,0} = \binom{N}{1}(1-x_{gap})^{N-1} - \binom{N}{2}(1-2x_{gap})^{N-1} + ...$$

$$= N(1-x_{gap})^{N-1} - N(N-1)\frac{(1-2x_{gap})^{N-1}}{2} + ... \qquad (B5)$$

We plot in Fig. B1 $P(> x_{gap})$ for several N values. We see that for $N = 100$ and $x_{gap} = 0.06$, $P(> 0.06) \approx 20\%$. This means that the probability of finding a gap with a size larger than six times the mean separation is not significantly small. When the mean number of lines is large, $\lambda \sim N \gg 1$, our $P(> x_{gap})$ approaches the

result obtained by Ostriker *et al.* (1988) for small (but still very large if measured in unit of the mean separation) x_{gap}, i.e., $P(> x_{gap}) \sim N(1 - x_{gap})^{N-1} \sim Ne^{-\lambda x_{gap}}$.

Sometimes a line of sight may penetrate more than one clearing. To test this it is better to calculate the probability that more than one gaps exceed x_{gap}, $P_{m1}(> x_{gap})$. This is given by $P_{m1}(> x_{gap}) = P(> x_{gap}) - P_{N,1}$. In our Fig. B2 we plot $P_{m1}(> x_{gap})$ for the same N values used in Fig. B1. For $N = 100$ $P_{m1}(> 0.06) \approx 1\%$.

Table 1. Model parameters.

Model #	z_{obs}	z_{on}	L(ergs s^{-1}Hz^{-1})	M_B	n_0(Gpc^{-3})	$\langle J_{-21} \rangle$
1	3	6.0	10^{30}	–24.2	5×10^4	6.39
2	3	3.2	10^{30}	–24.2	5×10^4	0.98
3	3	6.0	10^{31}	–26.7	5×10^3	6.39
4	3	3.2	10^{31}	–26.7	5×10^3	0.98
5	3	4.0	10^{29}	–21.7	5×10^5	3.63
6	3	3.2	10^{29}	–21.7	5×10^5	0.98

FIGURE CAPTIONS

Figure 1. $P(J_{-21})$ as a function of J_{-21} for #1, #3 and #5 models in an expanding universe.

Figure 2. $P(J_{-21})$ as a function of J_{-21} for #2, #4 and #6 models in an expanding universe.

Figure 3. $P_n(x)$ in a Euclidean space for the mean total source number n=10, 100, 1000 and 10000.

Figure 4. $P_n(J_{-21})$ in a Euclidean space (see the text for details).

Figure 5. $P_s(J_{-21})$ as a functions of J_{-21} for the s^{th} neighbor; the input parameters are the same as in Fig. 4.

Figure 6. The Gunn-Peterson absorption of the flux of a z_{em} quasar, including the proximity effect, for various assumed ionizing field intensities. (a) HI Lyα absorption for a $z_{em} = 4.5$ quasar with $L_{31} = 5$; (b) same as in (a) except z_{em}=5.0; (c) HeII Lyα absorption for a $z_{em} = 2.2$ quasar with $L_{31} = 2$; (d) same as in (c) except $z_{em} = 3.2$.

Figure B1. $P(> x_{gap})$ as a function x_{gap} for, from left to right, N = 160, 150, 140, 110, 100, 90, 50, 45 and 40.

Figure B2. $P_{m1}(> x_{gap})$ as a function x_{gap} for, from left to right, N = 160, 150, 140, 110, 100, 90, 50, 45 and 40.

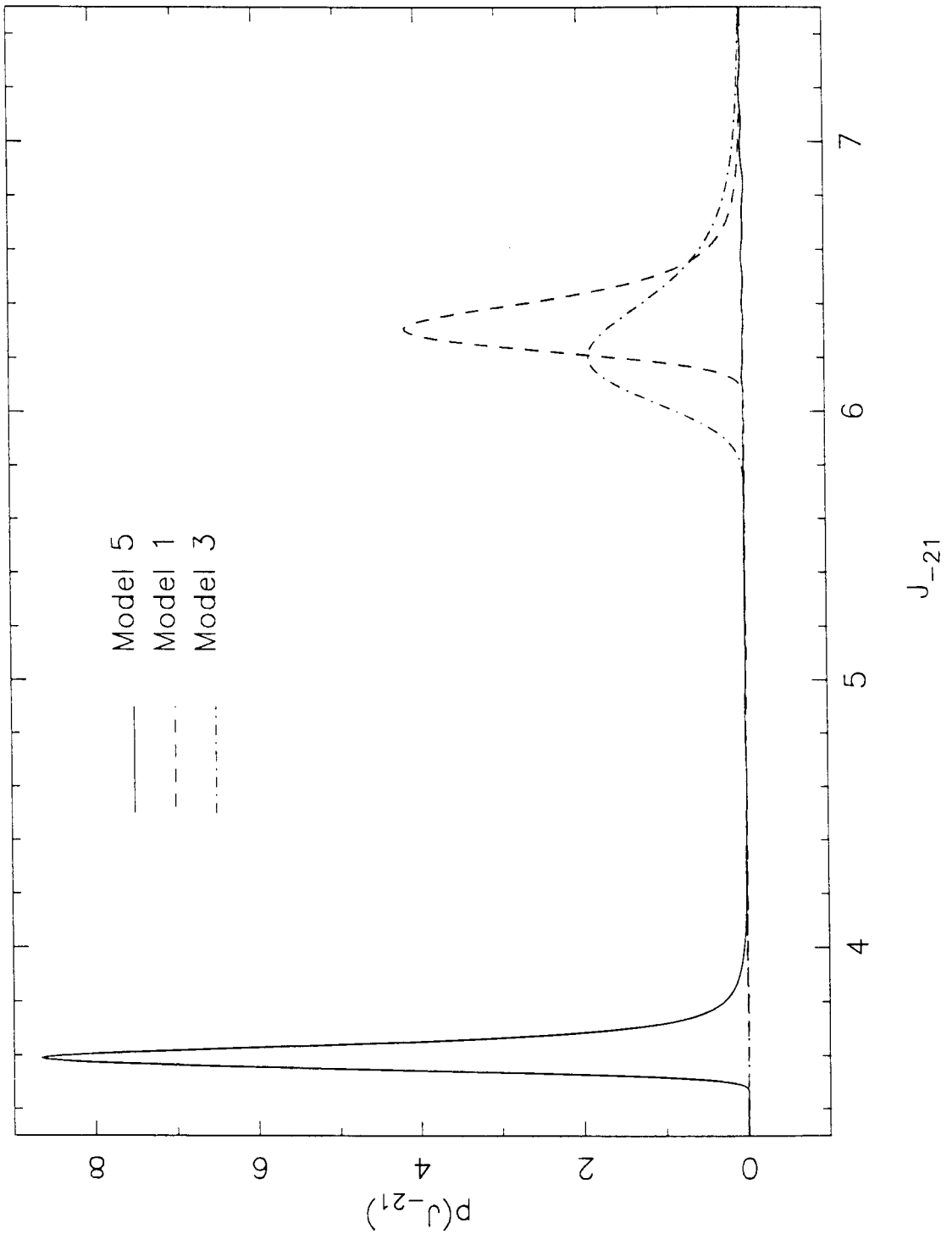

Figure 1

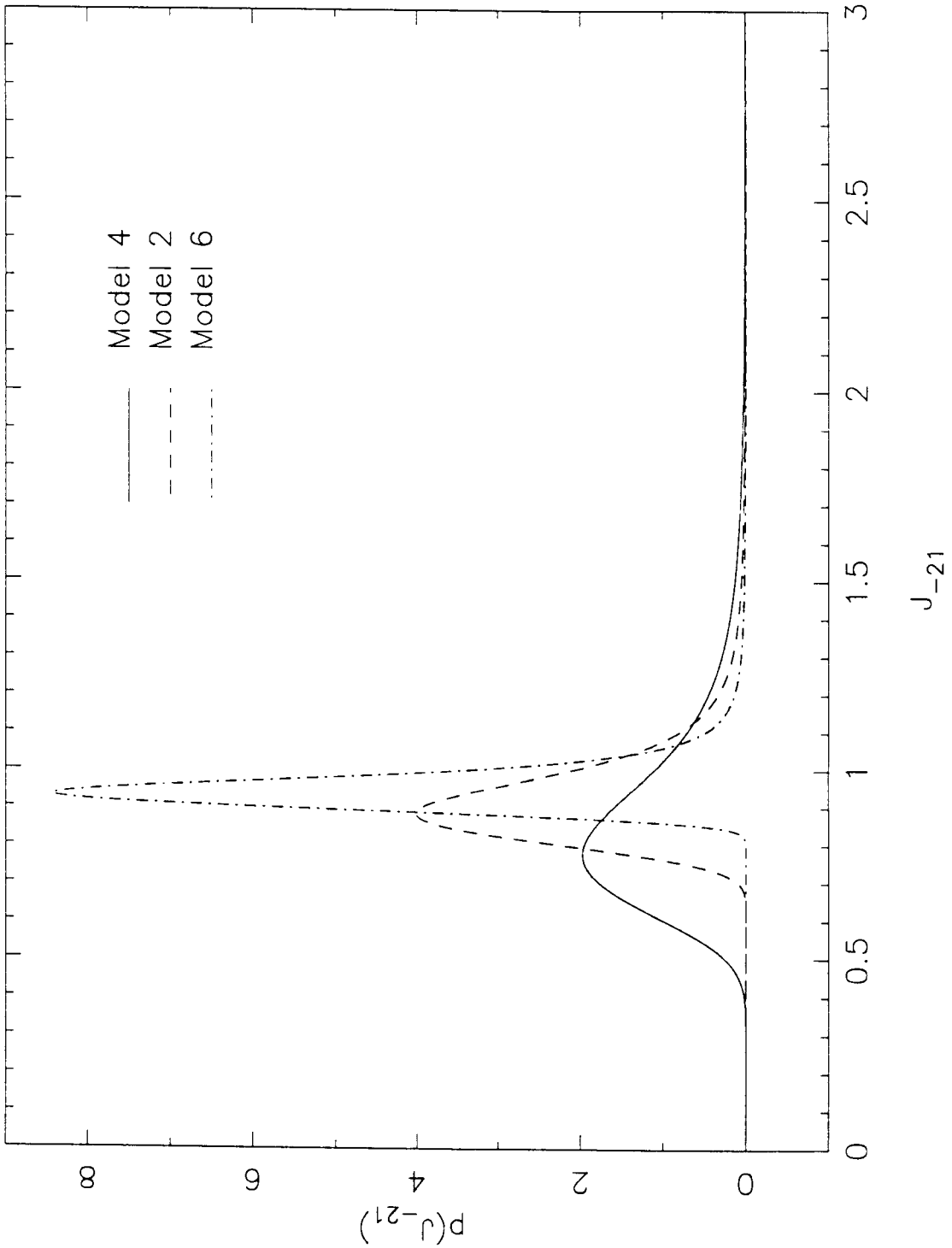

Figure 2

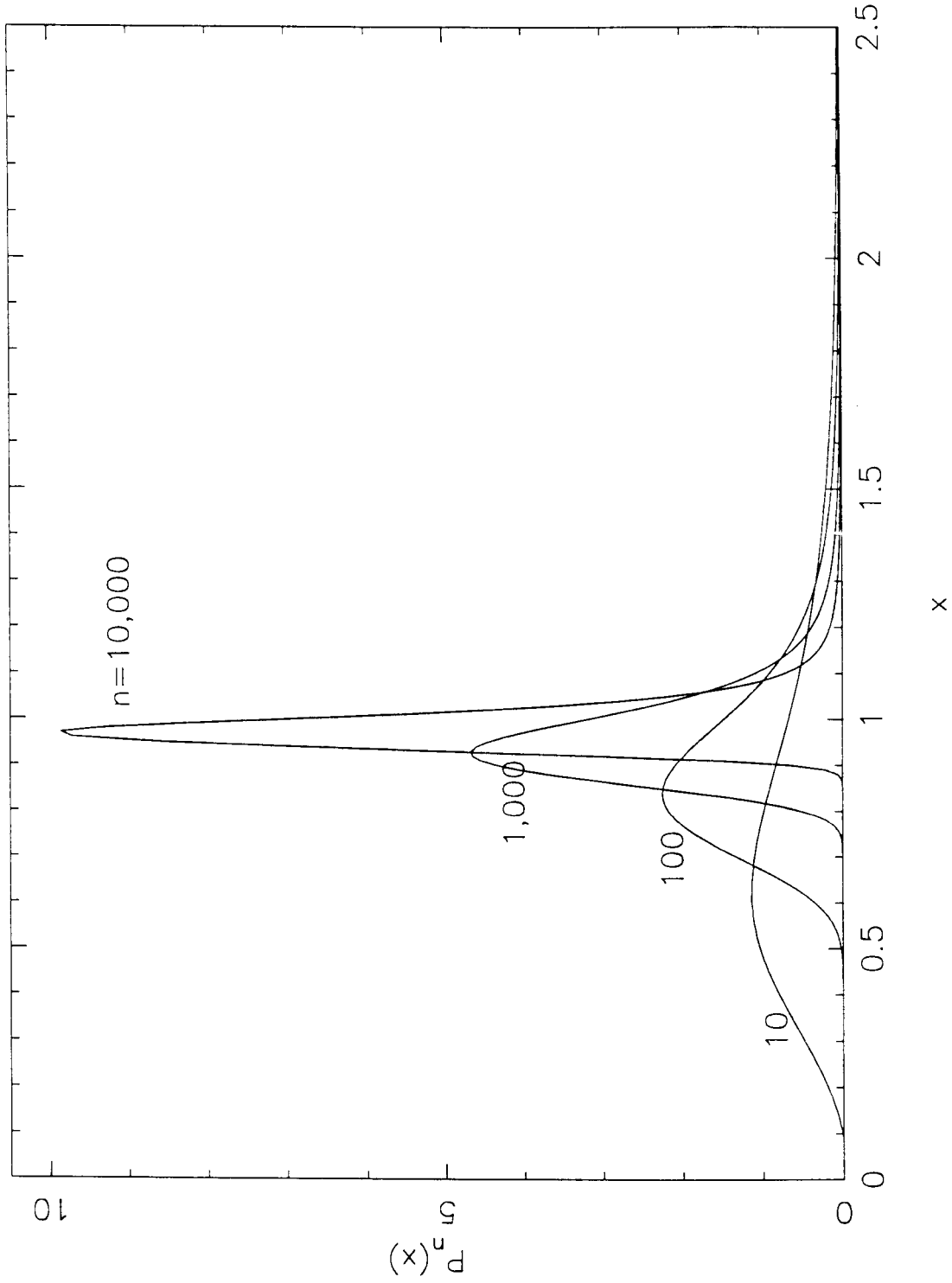

Figure 3

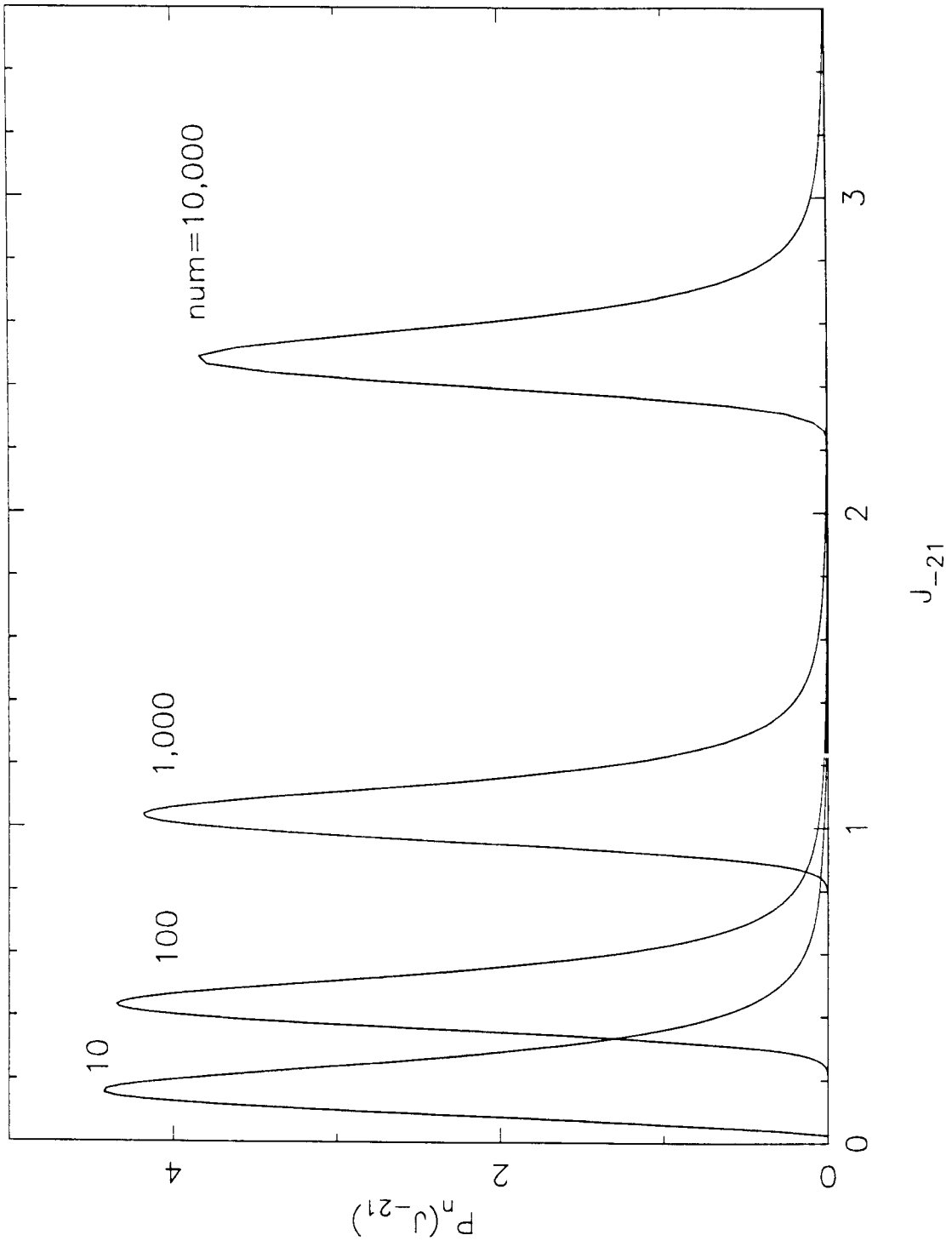

Figure 4

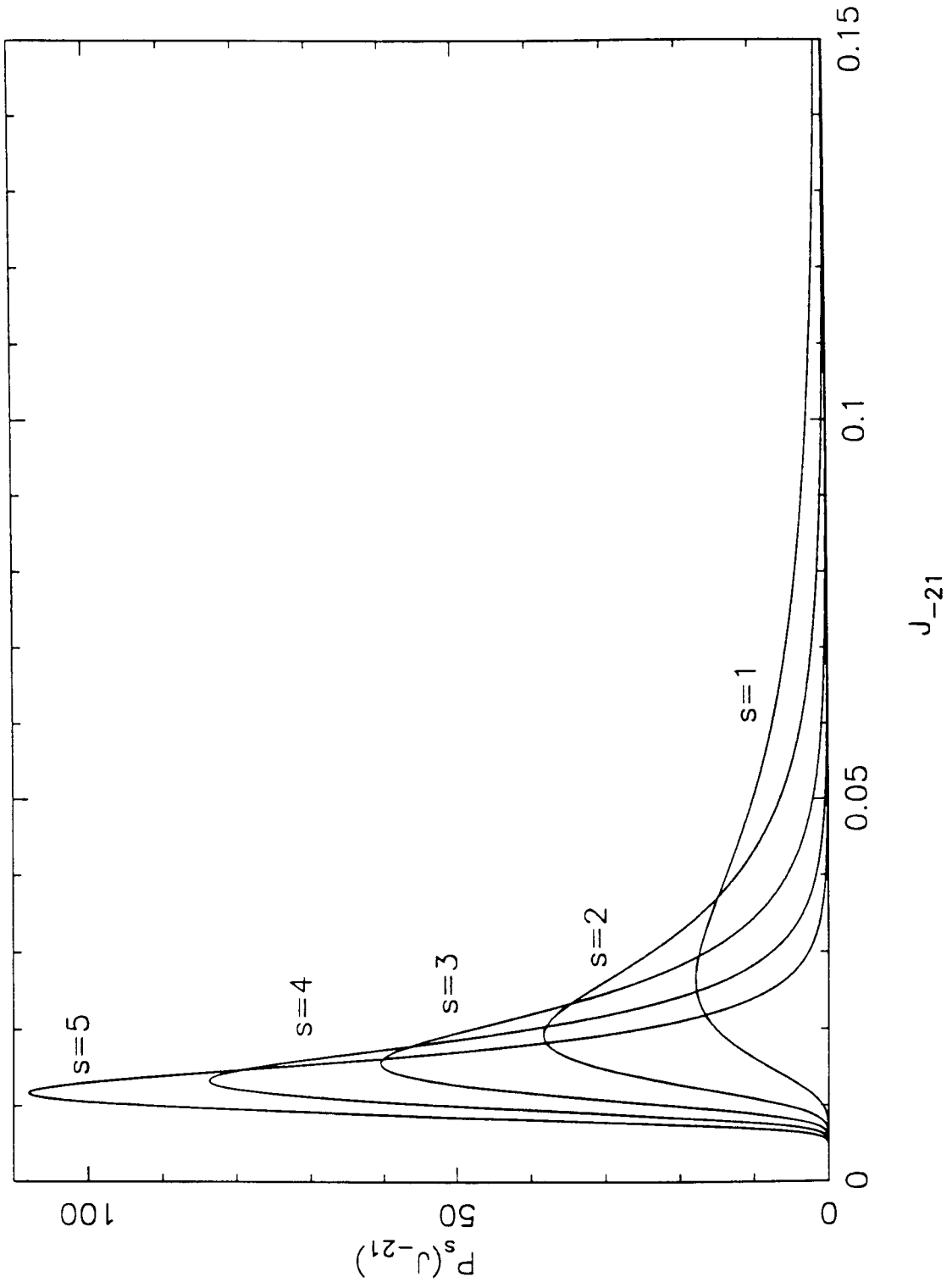

Figure 5

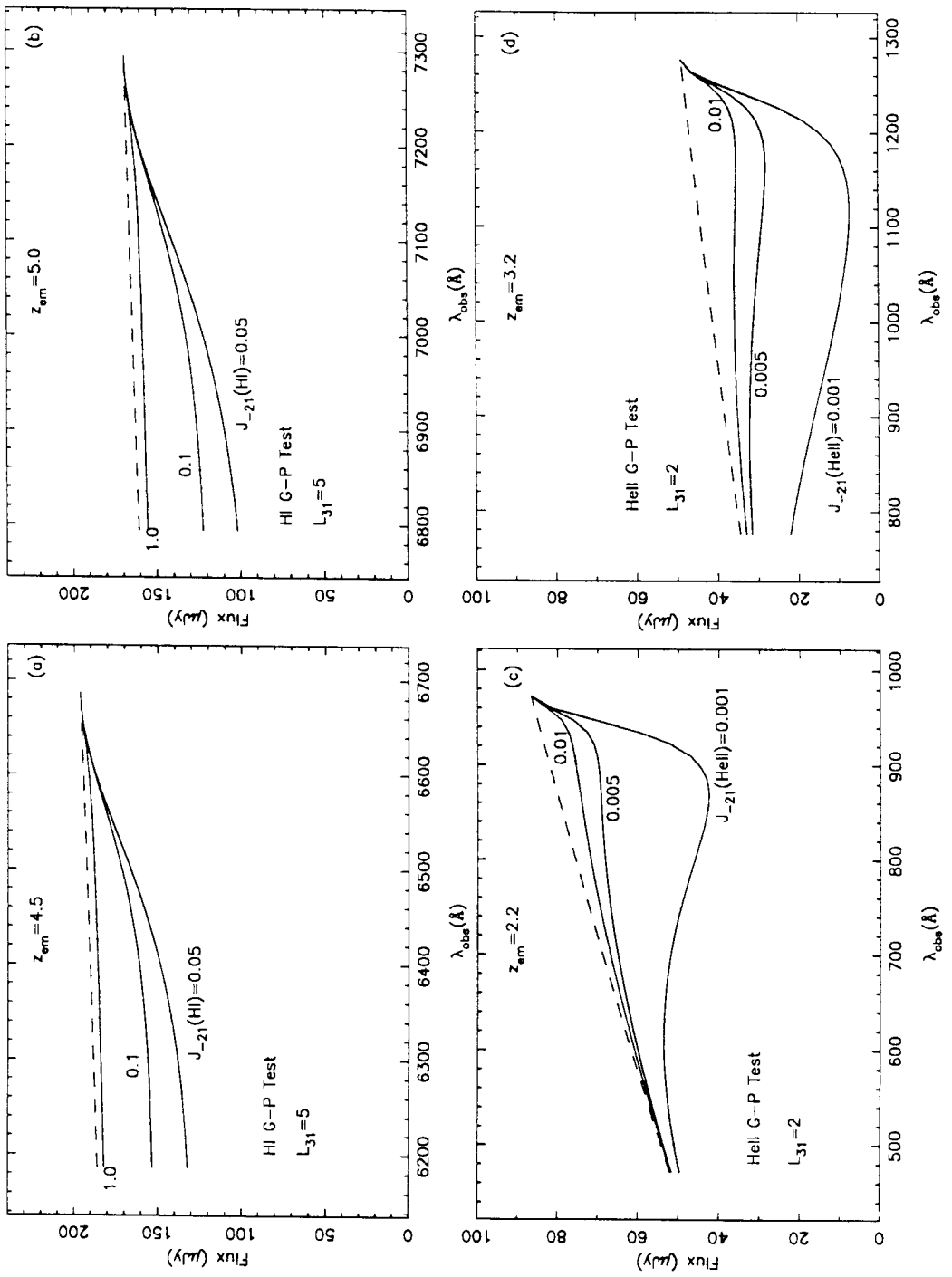
(a)
z_{em}=4.5
1.0
0.1
J_{-21}(HI)=0.05
HI G-P Test
L_{31}=5
(b)
z_{em}=5.0
1.0
0.1
J_{-21}(HI)=0.05
HI G-P Test
L_{31}=5
(c)
z_{em}=2.2
0.01
0.005
J_{-21}(HeII)=0.001
HeII G-P Test
L_{31}=2
(d)
z_{em}=3.2
0.01
0.005
J_{-21}(HeII)=0.001
HeII G-P Test
L_{31}=2
Flux (μJy)
λ_{obs}(Å)

Figure 6

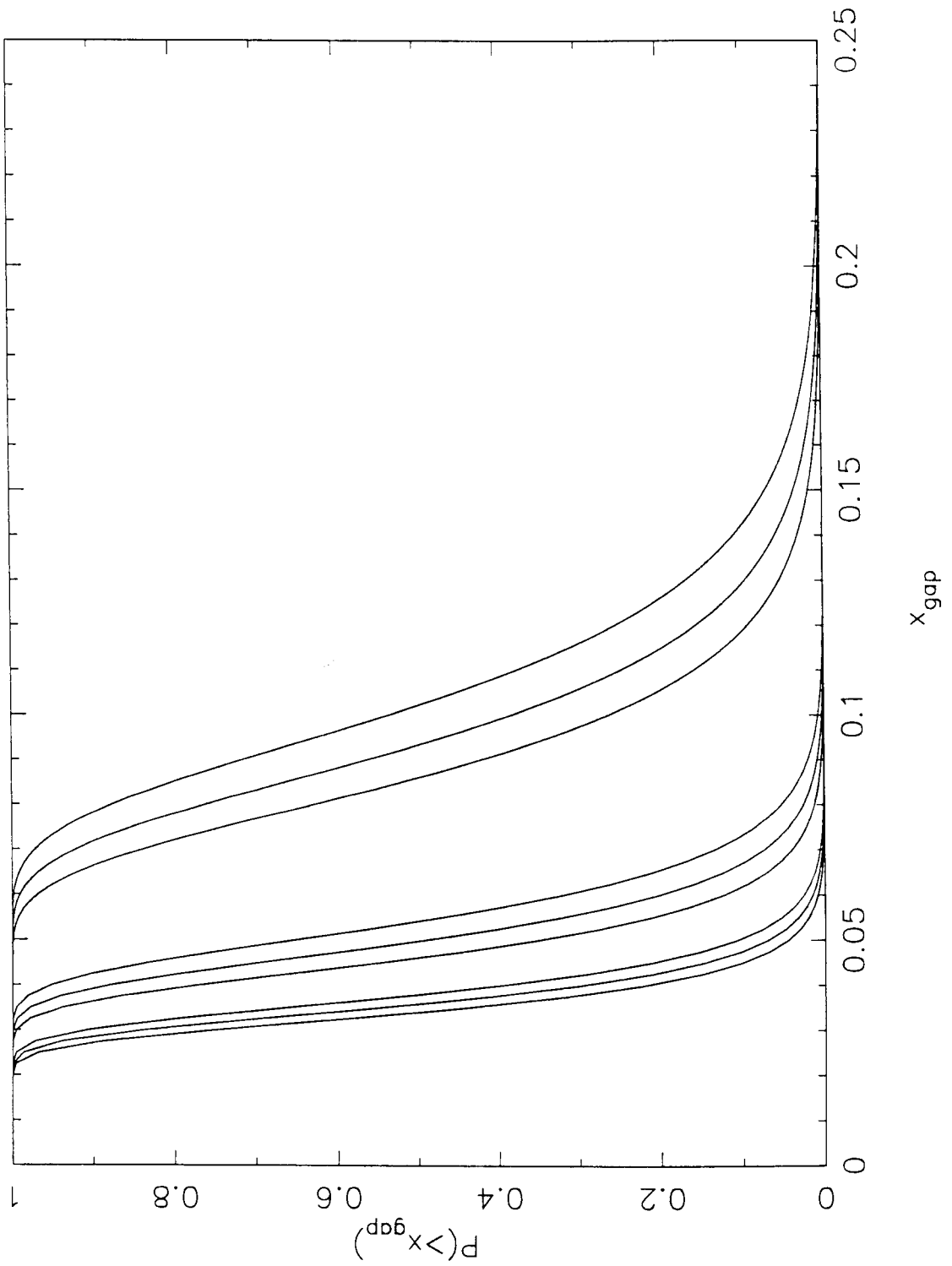

Figure B1

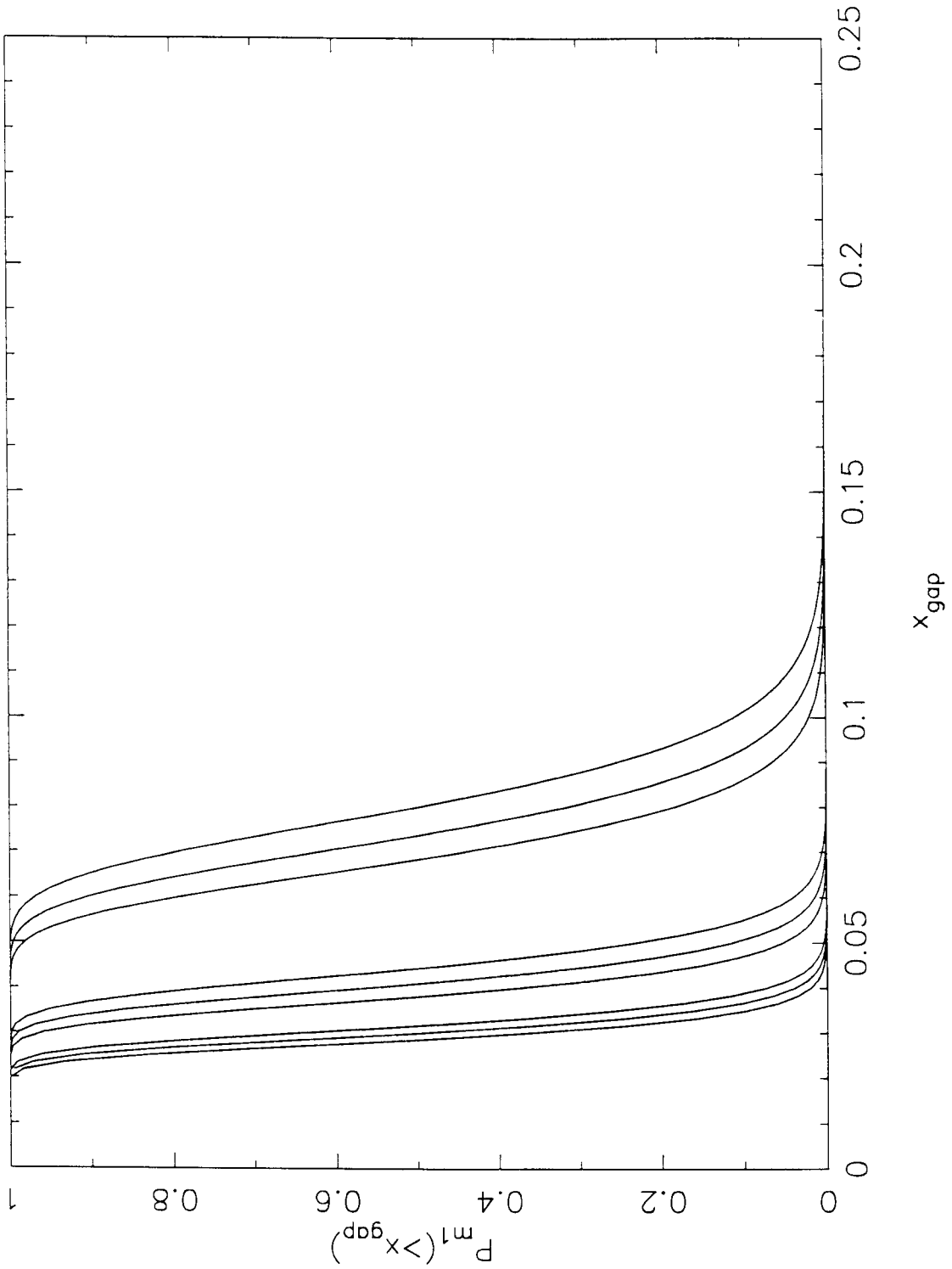

Figure B2

CHAPTER FOUR

INTENSITY CORRELATION OF IONIZING BACKGROUND AT HIGH REDSHIFTS

SUMMARY. We have derived the joint probability distribution of intensities of ionizing background at two different places. The intensity correlation function ξ_J has been calculated for randomly distributed QSOs as the main ionizing sources. The QSO Lyα clouds can be used as intensity indicators to reveal ξ_J at high z. We have measured the equivalent width correlation function $\xi_{1/W}$ for some selected QSOs and have found, in some cases, strong correlation signals at small separations. Careful examination shows that such signals are mainly produced by the lines near QSO emission redshifts. One explanation is that the high S/N near QSO emission redshifts enable us to detect very weak lines which result in the correlation signal. Another explanation is that the correlated intensities of ionizing field near luminous QSOs have caused the observed equivalent width correlation. If the latter explanation is correct, from the affected range by QSOs, we conclude that J_{ν_L} is less than 10^{-21}ergs s^{-1}cm^{-2}Hz^{-1}sr^{-1} at $z \sim 3.5$.

1 INTRODUCTION

In Chapter Three we have shown that absorptions produced by QSO absorption line systems reduce the total number of ionizing sources involved in generating the ionizing background and therefore enhance the J_{ν_L} fluctuations significantly, if QSOs are the main ionizing sources at early epochs. In this paper we discuss a related subject, the correlation of the ionizing field at high redshifts. We examine the relation between the intensity correlation and the equivalent width correlation of QSO Lyα forest lines and explore the possibility that the observable equivalent width correlation may be used to constrain the source space density.

2 DERIVATION OF INTENSITY CORRELATION FUNCTION ξ_J

2.1 Markoff's Method and the Joint Probability Distribution $W(J_0, J_1)$

Suppose there are N ionizing sources which are randomly distributed in a region of volume V. Here we only consider for Euclidean space. At high redshifts the absorption produced by QSO absorption line systems can effectively block away ionizing flux from the far away sources and the ionizing field at the Lyman limit frequency ν_L is a local phenomenon (see §3.2). So it is good enough to use results derived for a Euclidean space at high redshifts. We assume that the occurrence of ionizing sources with a Lyman limit frequency luminosity L at the position $\vec{r}$ is governed by the probability distribution function $f(\vec{r}, L)$. Given two positions $\vec{r} = 0$ and $\vec{r}_1$ we want to know the probability $w_N(J_0, J_1)dJ_0dJ_1$ that the mean

Lyman limit frequency intensity at $\vec{r} = 0$ is between $J_0 \rightarrow J_0 + dJ_0$ and at the same time the mean Lyman limit frequency intensity at $\vec{r}_1$ is between $J_1 \rightarrow J_1 + dJ_1$. Using Markoff's method (see Chandrasekhar 1943) we can easily write down the probability distribution:

$$w_N(J_0, J_1) = \frac{1}{(2\pi)^2} \int_{-\infty}^{\infty} d\rho \int_{-\infty}^{\infty} d\sigma e^{-i\rho J_0} e^{-i\sigma J_1} A_N(\rho, \sigma), \tag{2.1}$$

where $A_N(\rho, \sigma) = I^N$ and

$$I = \int dL \int_V e^{i\rho j_0} e^{i\sigma j_1} f(\vec{r}, L) d^3\vec{r}. \tag{2.2}$$

In the above expression

$$j_0 = \frac{1}{4\pi} \frac{L}{4\pi r^2} e^{-\tau(r)} \tag{2.3}$$

and

$$j_1 = \frac{1}{4\pi} \frac{L}{4\pi |\vec{r} - \vec{r}_1|^2} e^{-\tau(|\vec{r} - \vec{r}_1|)} \tag{2.4}$$

are the mean Lyman limit frequency intensities at $\vec{r} = 0$ and $\vec{r}_1$, respectively, produced by a source of luminosity L at the position $\vec{r}$. Here we assume that the optical depth τ at ν_L between $\vec{r}_1$ and $\vec{r}_2$ depends only on the distance between the two points. Actually the absorption along various lines of sight can be different because of the fluctuations in the number of absorbing clouds involved. But as we will see in §3.2 that there are many optically thick absorbing clouds contained in a volume of a radius one absorption length scale at high z, so the fluctuations in the number of clouds can be neglected.

Now consider that the total number of sources in the volume V is not a fixed number but obeys Poisson distribution with a mean total number $\langle N \rangle$, that is,

$$P(N, \langle N \rangle) = \frac{\langle N \rangle^N}{N!} e^{-\langle N \rangle}. \tag{2.5}$$

In this case the probability distribution becomes

$$\begin{aligned} W(J_0, J_1) &= \sum_{N=0}^{\infty} P(N, \langle N \rangle) w_N(J_0, J_1) \\ &= \frac{1}{(2\pi)^2} \int_{-\infty}^{\infty} d\rho \int_{-\infty}^{\infty} d\sigma e^{-i\rho J_0} e^{-i\sigma J_1} A(\rho, \sigma), \end{aligned} \tag{2.6}$$

where $A(\rho, \sigma) = e^{-C_1(\rho) - C_2(\rho, \sigma)}$ with

$$C_1(\rho) = \int dL \int_V \left(1 - e^{i\rho j_0}\right) \Phi(L, \vec{r}) d^3\vec{r}, \tag{2.7}$$

and

$$C_2(\rho, \sigma) = \int dL \int_V e^{i\rho j_0} \left(1 - e^{i\sigma j_1}\right) \Phi(L, \vec{r}) d^3\vec{r}. \tag{2.8}$$

In the above expressions $\Phi(L, \vec{r}) \equiv \langle N \rangle f(\vec{r}, L)$ is the luminosity function. Since

$$\delta(s) = \frac{1}{2\pi} \int_{-\infty}^{\infty} dx e^{-isx} \tag{2.9}$$

and $A(\rho, \sigma = 0) = e^{-C_1(\rho)}$, one can easily get the probability density of J_0 at $\vec{r} = 0$:

$$P(J_0) = \int_0^{\infty} W(J_0, J_1) dJ_1 = \frac{1}{2\pi} \int_{-\infty}^{\infty} d\rho e^{-i\rho J_0 - C_1(\rho)}. \tag{2.10}$$

A detailed discussion of $P(J_0)$ produced by randomly distributed sources at high z can be found in Chapter Three. Using the relation

$$\delta'(s) = \frac{-i}{2\pi} \int_{-\infty}^{\infty} x\, e^{-isx} dx \tag{2.11}$$

and integrating by parts we get the mean intensity at $\vec{r} = 0$:

$$\langle J_0 \rangle = \int_0^\infty J_0 P(J_0) dJ_0 = \int dL \int_V j_0 \Phi(L, \vec{r}) d^3\vec{r}. \tag{2.12}$$

It is also not difficult to calculate two more lower moments of $W(J_0, J_1)$. We have

$$\int_0^\infty J_1 W(J_0, J_1) dJ_1 = \frac{1}{2\pi} \int_{-\infty}^\infty d\rho e^{-i\rho J_0 - C_1(\rho)} \int dL \int_V e^{i\rho j_0} j_1 \Phi(L, \vec{r}) d^3\vec{r} \tag{2.13}$$

and

$$\langle J_0 J_1 \rangle \equiv \int_0^\infty dJ_0 \int_0^\infty J_0 J_1 W(J_0, J_1) dJ_1 = \int dL \int_V j_0 j_1 \Phi(L, \vec{r}) d^3\vec{r} + \langle J_0 \rangle \langle J_1 \rangle. \tag{2.14}$$

2.2 The Intensity Correlation Function ξ_J

In the following discussions we make some further approximations. We assume that the ionizing sources are uniformly distributed in the volume V and the luminosity of an ionizing source is independent of its position, so that $\Phi(L, \vec{r}) = n\phi(L)$, where $n = \langle N \rangle / V$ is the mean number density of sources and $\int \phi(L) dL = 1$. Since the absorption produced by QSO absorption line systems is significant, especially at high redshifts (see §3.2), we can extend the integration to the whole space. We thus get

$$\langle J_1 \rangle = \langle J_0 \rangle = \langle J \rangle \equiv \frac{n\langle L \rangle}{4\pi} \int_0^\infty e^{-\tau(r)} dr, \tag{2.15}$$

where $\langle L \rangle = \int L\phi(L) dL$ is the mean luminosity of the ionizing sources. We define the Lyman limit frequency intensity correlation function as

$$\xi_J(r_1) = \frac{\langle J_0 J_1 \rangle}{\langle J_0 \rangle^2} - 1. \tag{2.16}$$

Using the above approximations and introducing the new variable $l = |\vec{r} - \vec{r}_1|$, we get

$$\xi_J(r_1) = \frac{1}{8\pi n \left[\int_0^\infty e^{-\tau(r)} dr\right]^2} \frac{\langle L^2 \rangle}{\langle L \rangle^2} \frac{1}{r_1} I_J(r_1), \tag{2.17}$$

where

$$I_J(r_1) = \int_0^\infty \frac{e^{-\tau(r)}}{r} dr \int_{|r-r_1|}^{r+r_1} \frac{e^{-\tau(l)}}{l} dl. \tag{2.18}$$

The integration area in I_J is the shaded region in Fig. 1. We can choose a new co-ordinate systems (x, y) to simplify the integration (see Fig. 1). With

$$x = \frac{1}{\sqrt{2}}(r - l + r_1), \tag{2.19a}$$

$$y = \frac{1}{\sqrt{2}}(r + l - r_1), \tag{2.19b}$$

we get

$$I_J(r_1) = \int_0^{\sqrt{2}r_1} dx \int_0^\infty dy \frac{e^{-\tau(r)-\tau(l)}}{\left(\frac{1}{\sqrt{2}}y + \frac{r_1}{2}\right)^2 - \left(\frac{1}{\sqrt{2}}x - \frac{r_1}{2}\right)^2}. \tag{2.20}$$

To proceed further a particular form of $\tau(r)$ must be known. Here we assume that the optical depth takes the form: $\tau(r) = r/r_0$, where r_0 is the distance at which the effective optical depth at ν_L is unity. With this expression for the absorption we have $\tau(r) + \tau(l) = (\sqrt{2}y + r_1)/r_0$. This leads to

$$I_J(u_1) = 2 \int_{u_1}^\infty \frac{1}{u} \ln\left(\frac{u + u_1}{u - u_1}\right) e^{-u} du, \tag{2.21}$$

where $u_1 = r_1/r_0$. By introducing another new variable

$$v = \ln\left(\frac{u + u_1}{u - u_1}\right), \tag{2.22}$$

the I_J integration becomes

$$I_J(u_1) = 2\int_0^\infty \frac{v}{\mathrm{sh}v} e^{-u_1 \frac{1+e^{-v}}{1-e^{-v}}} dv. \tag{2.23}$$

For the mean intensity we have

$$\langle J_0 \rangle = \frac{n\langle L \rangle}{4\pi} r_0. \tag{2.24}$$

And the intensity correlation function is given by

$$\xi_J(r_1) = \frac{1}{8\pi r_0^3} \frac{1}{n} \frac{\langle L^2 \rangle}{\langle L \rangle^2} \frac{1}{u_1} I_J(u_1). \tag{2.25}$$

We show in Fig. 2 the numerical calculations of $I_J(u_1)/u_1$ as a function of u_1. Since $I_J(u_1 = 0) = \pi^2/2$, $\xi_J(r_1) \propto 1/r_1$ when r_1 approaches zero.

3 SOURCE LUMINOSITY FUNCTION, ABSORPTION AND $\xi_J(r_1)$

3.1 Ionizing Source Luminosity Functions and $\xi_J(r_1)$

To understand the effects produced by source luminosity functions we first consider a simple situation. Suppose that there are only two kinds of sources, one with a higher luminosity L_h and a space density n_h and another with a lower luminosity L_l and a space density n_l. In this case the total number density of sources is $n = n_h + n_l$ and the luminosity distribution is

$$\phi(L) = \frac{n_h \delta(L - L_h) + n_l \delta(L - L_l)}{n}. \tag{3.1}$$

From $\phi(L)$ we can easily get

$$\langle L \rangle = \frac{n_h L_h + n_l L_l}{n}, \tag{3.2}$$

and

$$\frac{1}{n}\frac{\langle L^2 \rangle}{\langle L \rangle^2} = \frac{n_h L_h^2 + n_l L_l^2}{(n_h L_h + n_l L_l)^2}. \tag{3.3}$$

We see that if the high luminosity objects dominate $\langle L \rangle$ thus they also dominate the mean intensity $\langle J \rangle$, then $\langle L^2 \rangle / (n \langle L \rangle^2) \simeq 1/n_h$; on the other hand if the low luminosity sources dominate $\langle L \rangle$ then $\langle L^2 \rangle / (n \langle L \rangle^2) \simeq (1/n_l)[1 + n_h L_h^2/(n_l L_l^2)]$. Roughly speaking the intensity correlation function ξ is inversely proportional to the mean number of dominating ionizing sources within a spherical region of radius r_0 (see Eq. 2.25).

At high redshifts, quasars are the only known ionizing sources which are observed in large quantity. We now examine how would their luminosity functions affect the intensity correlation function ξ. For definiteness we will adopt an Einstein-de Sitter universe ($q_0 = 0.5$) and use $H_0 = 50\text{km sec}^{-1}\text{Mpc}^{-1}$ in the following discussions and throughout the paper. According to Boyle, Shanks and Peterson (1988) the QSO luminosity function at $z < 2.2$ is most simply parameterised by two power laws, with $\Phi(L) \propto L^{-3.7\pm0.1}$ at high luminosities and $\Phi(L) \propto L^{-1.4\pm0.2}$ at low luminosities. The characteristic luminosity L^* evolves with redshift z. At higher redshifts the results for the QSO luminosity function are still controversial. For simplicity we assume here that at $z \geq 2.2$ quasars have a constant comoving space density and there was no luminosity evolution for individual sources. Thus

the proper QSO luminosity function at $z \geq 2.2$ can be expressed as

$$\Phi(L,z) = \begin{cases} \Phi(L^*)\left(\frac{L}{L^*}\right)^{-1.4}(1+z)^3 & \text{if } L \leq L^* \\ \Phi(L^*)\left(\frac{L}{L^*}\right)^{-3.7}(1+z)^3 & \text{if } L \geq L^*, \end{cases} \tag{3.4}$$

where L is the monochromatic luminosity at ν_L. Using the above expression we get

$$\frac{1}{n}\frac{\langle L^2\rangle}{\langle L\rangle^2} \simeq \frac{1}{2.5}\frac{1}{\Phi(L^*)L^*}\frac{1}{(1+z)^3}. \tag{3.5}$$

For the quasar spectrum we adopt $L_\nu \propto \nu^{-0.5}$ for $\lambda > 1216\mathring{A}$ and $L_\nu \propto \nu^{-1}$ for $\lambda < 1216\mathring{A}$. The Lyman limit frequency luminosity L and the absolute B magnitude M_B is then related by $L = 10^{-0.4M_B+20.33}$ergs sec^{-1}Hz^{-1}. From Boyle, Shanks and Peterson (1988) we know that at $z = 2.2$ the characteristic absolute B magnitude is $M_B^* \simeq -26.5$ and the corresponding comoving space density is about 10^{-6}Mpc^{-3}mag^{-1}. Using these figures we get $\langle L^2\rangle/(n\langle L\rangle^2) \simeq 0.4 \times 10^6(1+z)^{-3}$Mpc^3 for $z \geq 2.2$. A better estimate may be obtained by using Boyle, Shanks and Peterson (1988) model B QSO luminosity function. By adopting a lower luminosity cut-off $M_B = -20$ and a higher luminosity limit $M_B = -30$ we get, for $z \geq 2.2$, $\langle L^2\rangle/(n\langle L\rangle^2) \simeq 0.3 \times 10^6(1+z)^{-3}$Mpc^3, which makes only a slight modification. This result is not very sensitive to the assumed lower and higher cut-offs.

3.2 The Absorption Length Scale r_0

We now discuss the effects produced by QSO absorption line systems. It is known that the Lyman continuum absorption from quasar absorption line systems significantly attenuates the ionizing radiation background, especially at high redshifts (see Miralda-Escudé and Ostriker 1990). A useful description of absorption produced by

discrete clouds between z_{obs} and z_e at frequency ν_{obs} is the effective optical depth $\tau_{eff}(\nu_{obs}, z_{obs}, z_e)$ which is defined by $e^{-\tau_{eff}} \equiv \langle e^{-\tau} \rangle$, where the average is along various lines of sight. Let $\eta_z(N)dzdN$ be the mean number of absorbing clouds along various lines of sight in the redshift interval $z \rightarrow z + dz$ and with a neutral hydrogen column density in the range $N \rightarrow N + dN$, we have, for $\lambda_{obs} \leq 912\mathring{A}$,

$$\tau_{eff}(\nu_{obs}, z_{obs}, z_e) = \int_{z_{obs}}^{z_e} \int_{N_{min}}^{N_{max}} \eta_z(N)[1 - e^{-\tau_c(\nu_z, N)}]dNdz, \qquad (3.6)$$

where $\tau_c(\nu_z, N) = 6.3 \times 10^{-18} N[(1+z_{obs})/(1+z)]^3(\lambda_{obs}/912)^3$ is the optical depth of a single cloud, and N_{min} and N_{max} are the lower and upper column density limits, respectively. Observationally the distribution function $\eta_z(N)$ is not well determined. This is because at the high column density end the number of Lyman limit systems are not numerous enough, while at the low column density end the Lyα forest lines are badly blended together in usual intermediate-resolution spectra ($\sim 1\mathring{A}$). High signal-to-noise ratio, high spectral resolution observations are needed to improve our current knowledge about $\eta_z(N)$. For our purpose here we use a distribution function adopted by Miralda-Escudé and Ostriker (1990) in their Model A2:

$$\eta_z(N) = 5.6 \times 10^8 N^{-1.5} \left(\frac{1+z}{4}\right)^{2.4}, 10^{14}\mathrm{cm}^{-2} < N < 1.59 \times 10^{17}\mathrm{cm}^{-2}; \quad (3.7a)$$

$$\eta_z(N) = 4.6 \times 10^8 N^{-1.5} \left(\frac{1+z}{4}\right)^{0.5}, 1.59 \times 10^{17}\mathrm{cm}^{-2} < N < 10^{22}\mathrm{cm}^{-2}. \quad (3.7b)$$

Since $\eta_z(N) \propto N^{-1.5}$ and $\tau_c(\nu_z, N) \propto N$, the contributions to τ_{eff} from very small and very large column density clouds are negligible. We show in Fig. 3 our calculated $\tau_{eff}(\nu_L, z_{obs}, z)$ curves for $\nu_{obs} = \nu_L$. We see that $\tau_{eff}(\nu_L, z_{obs}, z)$ increases very rapidly with increasing z.

If we use Eq. (3.7b) and extrapolate it to both small and large column densities we can get an analytical approximation for τ_{eff}:

$$\tau_{eff}(\nu_{obs}, z_{obs}, z) \approx 2 \ln \left(\frac{1+z}{1+z_{obs}} \right) \left[\frac{(1+z_{obs})\lambda_{obs}}{912} \right]^{3/2} . \tag{3.8}$$

We also plot this approximation for ν_L in our Fig. 3 (the dashed lines). We see that this approximation is pretty good for $z_{obs} \simeq 2.5$ but underestimate the absorption at higher redshifts. Another approximation can be obtained by approximating in Eq. (3.6) $e^{-\tau_c} \simeq 1 - \tau_c$ for $\tau_c < 1$ and $e^{-\tau_c} \simeq 0$ for $\tau_c > 1$. This approximation is shown in dotted lines in Fig. 3 for ν_L. We see that this approximation always gives a higher τ_{eff} value.

In order to estimate the absorption length scale r_0 we introduce $z_c(z_{obs})$ by demanding $\tau_{eff}(\nu_L, z_{obs}, z_c(z_{obs}) \equiv 1$, i.e., at frequency ν_L the effective optical depth between z_{obs} and $z_c(z_{obs})$ is unity. Since at high redshifts the absorption is significant and $z_c(z_{obs}) - z_{obs}$ is small, we get

$$r_0(z_{obs}) \simeq 6 \times 10^3 (1+z_{obs})^{-2.5} [z_c(z_{obs}) - z_{obs}] \text{Mpc}. \tag{3.9}$$

Some calculated $z_c(z_{obs})$ and $r_0(z_{obs})$ are listed in Table 1. In this table we also list $J_{-22}(z_{obs})$, the mean Lyman limit intensity of ionizing field at redshift z_{obs}, expressed in unit of 10^{-22}ergs cm^{-2}sec^{-1}Hz^{-1}sr^{-1}. In this calculation we have used the Boyle, Shanks and Peterson (1988) model B QSO luminosity function at $z = 2.2$ and have assumed that for higher redshifts the comoving space density is fixed and there was no luminosity evolution for individual quasars. These assumptions are

also used to calculate $\langle L^2\rangle/(8\pi r_0^3 n\langle L\rangle^2)$ for various z_{obs}, which are listed in column 5 of Table 1. In the sixth column we give r_{corr}, the intensity correlation length scale at which the intensity correlation function ξ_J is unity. The last column of Table 1 lists $\Delta\lambda_{corr} \equiv \lambda_\alpha H_0(1+z)^{2.5} r_{corr}/c$, where $\lambda_\alpha = 1215.67\mathring{A}$. This is the separation of two Lyα lines at $z = 0$ produced by two clouds separated by a distance $r_{corr}(z_{obs})$ at z_{obs} along a line of sight. Using the Table 1 values we have calculated $1 + \xi_J(r)$ as a function of separation r at various redshifts. Our results are shown in Fig. 4. From these calculations we see that at high redshifts the ionizing field intensity correlation is significant and it may be detected by studying high resolution, high signal to noise ratio QSO absorption spectra.

We now give a rough estimate of N_c, the mean number of optically thick Lyman limit systems (LLS) in a spherical region of radius r_0. From Eq. (3.7b) we know that the mean number density of LLS along a line of sight is $dN/dz \approx 1.15(1+z)^{0.5}$. The definition of r_0 means that on average there is about one LLS within a distance r_0 along the line of sight. Let the absorption cross section of LLS be $\sigma_c = \pi r_c^2$, where r_c is the absorption radius of a LLS cloud, N_c can be estimated by $N_c \sim 4\pi r_0^2/(3\sigma_c)$. For $r_c = 5$kpc and $r_0 \simeq 18$Mpc at $z = 4$ we get $N_c \sim 10^7$. This means that there were many optically thick absorbing clouds contained in a spherical region of radius r_0 and the fluctuations in the number of clouds could be neglected in calculating the intensity of ionizing field. From the assumed QSO luminosity function we can also see that at $z = 4$ there are only about 3 QSOs, on average, with M_B bright than -26.5mag in a spherical region of radius r_0. More accurately we have

$4\pi r_0^3 n\langle L\rangle^2/(3\langle L^2\rangle) \simeq 10$ at $z = 4$. This is the reason why the fluctuations in the ionizing field are significant at high z.

Finally we should point out that the recent work by Lanzetta (1991) has shown that the LLS may evolve much faster than what we have assumed $dN/dz \propto (1+z)^{0.5}$ at high z. And Schmidt, Schneider and Gunn (1991) have recently shown that bright QSOs are endangered species at early epochs and their comoving space density decline steeply for redshifts larger than 3. So we may have considerably underestimated the fluctuations and intensity correlations in the ionizing field at high z, if bright QSOs are the dominating sources.

4 QSO ABSORPTION LINES AND $\xi_J(r)$

4.1 Lyα Forest Line Clouds as Intensity Indicators

In the previous section we have shown that if the "observed" quasars dominate the ionizing field then the small scale correlation of the background intensity is significant, especially at high redshifts. According to standard models the Lyα forest lines observed in quasar absorption spectra are produced by intervening clouds which are highly ionized by the ionizing background. Therefore these clouds may serve as intensity indicators at high z and help us to determine the intensity correlation function observationally. When this is done we can compare the results with our theoretical calculations to get important information about the luminosity function of the ionizing sources. We now discuss how this could be done in practice.

Assume the majority of Lyα forest lines are on the linear part of the curve of growth and the rest equivalent width W of an absorption line is proportional to the Lyman limit frequency intensity J of the ionizing field. We may write $W = A/J$, where A depends on the intrinsic properties of an absorbing cloud. Let the probability distribution of A be $f(A)$, we then get

$$\langle \frac{1}{W} \rangle = \int\int \frac{J}{A} f(A) P(J) dA dJ = \langle \frac{1}{A} \rangle \langle J \rangle, \tag{4.1}$$

and

$$\begin{aligned} \langle \frac{1}{W_1} \frac{1}{W_2} \rangle &= \int\int\int\int \frac{J_1}{A_1} \frac{J_2}{A_2} f(A_1) f(A_2) W(J_1, J_2) dA_1 dA_2 dJ_1 dJ_2 \\ &= \langle \frac{1}{A} \rangle^2 \langle J_1 J_2 \rangle, \end{aligned} \tag{4.2}$$

where the two subscripts represent two different positions 1 and 2, separated by a distance r. We see that

$$\frac{\langle \frac{1}{W_1} \frac{1}{W_2} \rangle}{\langle \frac{1}{W} \rangle^2} \equiv 1 + \xi_{1/W}(r) = \frac{\langle J_1 J_2 \rangle}{\langle J \rangle^2} \equiv 1 + \xi_J(r). \tag{4.3}$$

This indicates that we may get the intensity correlation function $\xi(r)$ by simply measuring the $1/W$ correlation of QSO Lyα forest lines. Unfortunately this is not quite true. In the above equations we have assumed that we are able to detect all lines, including very weak lines, and the integration is over the whole range of J and A. Observationally only those absorption lines with W larger than some limiting or cut-off value W_c can be positively detected. In this case the integration region at a given spacial place is the shaded area shown in Fig. 5. And the above equations

need to be modified. Let A_{min} and A_{max} be the lower and upper limits of A and denote $J_A = A_{min}/W_c$ and $J_{max} = A_{max}/W_c$, we then get

$$\langle \frac{1}{W} \rangle = \frac{C}{C_b}, \tag{4.4}$$

where

$$C = \int_0^{J_A} J\,P(J)dJ\langle \frac{1}{A} \rangle + \int_{J_A}^{J_{max}} J\,P(J)dJ \int_{JW_c}^{A_{max}} \frac{f(A)}{A} dA, \tag{4.5}$$

and

$$C_b = \int_0^{J_A} P(J)dJ + \int_{J_A}^{J_{max}} P(J)dJ \int_{JW_c}^{A_{max}} f(A)dA. \tag{4.6}$$

We also have

$$\langle \frac{1}{W_1}\frac{1}{W_2} \rangle = \frac{D}{D_b}, \tag{4.7}$$

where

$$\begin{aligned} D = & \int_0^{J_A} dJ_1 \int_0^{J_A} W(J_1,J_2)J_1J_2dJ_2\langle \frac{1}{A} \rangle^2 + \\ & \int_{J_A}^{J_{max}} dJ_1 \int_{J_A}^{J_{max}} W(J_1,J_2)J_1J_2dJ_2 \int_{J_1W_c}^{A_{max}} \frac{f(A_1)}{A_1} dA_1 \int_{J_2W_c}^{A_{max}} \frac{f(A_2)}{A_2} dA_2 + \\ & 2 \times \int_0^{J_A} dJ_1 \int_{J_A}^{J_{max}} W(J_1,J_2)J_1J_2dJ_2 \int_{J_2W_c}^{A_{max}} \frac{f(A_2)}{A_2} dA_2 \langle \frac{1}{A} \rangle, \end{aligned} \tag{4.8}$$

and

$$\begin{aligned} D_b = & \int_0^{J_A} dJ_1 \int_0^{J_A} W(J_1,J_2)dJ_2 + \\ & \int_{J_A}^{J_{max}} dJ_1 \int_{J_A}^{J_{max}} W(J_1,J_2)dJ_2 \int_{J_1W_c}^{A_{max}} f(A_1)dA_1 \int_{J_2W_c}^{A_{max}} f(A_2)dA_2 + \\ & 2 \times \int_0^{J_A} dJ_1 \int_{J_A}^{J_{max}} W(J_1,J_2)dJ_2 \int_{J_2W_c}^{A_{max}} f(A_2)dA_2. \end{aligned} \tag{4.9}$$

It is clear that the measured $1+\xi_{1/W} \equiv \langle 1/(W_1 W_2)\rangle / \langle 1/W\rangle^2$ also depends on W_c and $f(A)$.

4.2 Equivalent Width Cut-off Effect—A Top-hat Toy Model

To investigate the cut-off effect we consider a simple one-dimensional toy model here. Suppose some identical "ionizing sources" are randomly distributed in a straight line. The mean source number per unit length is n. Assume the "intensity" produced by such a source is of the top-hat shape with an affection range $2l$, that is the intensity at x produced by a source located at x_s is given by

$$j = \begin{cases} j_c & \text{for } x_s - l < x < x_s + l, \\ 0 & \text{otherwise.} \end{cases} \tag{4.10}$$

The mean intensity is clearly $\langle J\rangle = \langle N_t\rangle j_c$, where $\langle N_t\rangle \equiv 2ln$ is the mean total source number within a length $2l$. Since the probability of finding N sources in a length $2l$ is $\langle N_t\rangle^N e^{-\langle N_t\rangle}/N!$, the intensity probability distribution $P(J)$ is

$$P(J) = e^{-\langle N_t\rangle} \sum_{N=0}^{\infty} \frac{\langle N_t\rangle^N}{N!} \delta(J - Nj_c). \tag{4.11}$$

The intensities at two points 1 and 2, separated by a distance $r > 2l$, are not correlated, and we have $W(J_1, J_2) = P(J_1)P(J_2)$ in this case. But for separation $r < 2l$, the intensities are indeed correlated. The correlation is generated because the sources falling within the length $2l - r$ near the positions 1 and 2 can affect the intensities at both points. With this physical picture in mind the joint probability distribution $W(J_1, J_2)$ can be written down directly:

$$W(J_1, J_2) = e^{-(nr+\langle N_t\rangle)} \sum_{M=0}^{\infty} \sum_{N=0}^{\infty} \sum_{K=0}^{\infty} \frac{(nr)^{N+K}(\langle N_t\rangle - nr)^M}{N!M!K!} \times$$

$$\delta\left[J_1-(N+M)j_c\right]\delta\left[J_2-(K+M)j_c\right]. \tag{4.12}$$

Using the above equation the intensity correlation function $\xi(r)$ can be shown to be

$$\xi_J(r)=\begin{cases}\frac{1}{\langle N_t\rangle}\left[1-\frac{nr}{\langle N_t\rangle}\right] & \text{for } 0\le r\le 2l,\\ 0 & \text{for } r\ge 2l.\end{cases} \tag{4.13}$$

We can also show that Marcoff's method applied to the one-dimensional problem leads to the same results.

In our Fig. 6 the calculated intensity correlation function $\xi_J(r)$ is shown in dashed lines as a function of r. In the calculations we have used $j_c = 1$, $2l = 1$ and $n = 10$. We have adopted different $f(A)$ distributions to investigate the cut-off effect. For clouds having an identical $A = A_0$ value, the condition $W > W_c$ means we can detect an absorption line only at places where $J < J_c \equiv A_0/W_c$. Fig. 6(a) shows the calculated $\xi_J(r)$ curves for various J_c values. We have also investigated the cut-off effect for uniform and power law $f(A)$ distributions. Our results are plotted in Fig. 6(b), (c) and (d). We see that when W_c increases the "observed" correlation $\xi_{1/W}$ usually decreases. But for different $f(A)$ distributions the fall off speed of $\xi_{1/W}$ is different. In Fig. 6(d) the small open circles are results of our Monte Carlo simulations for $W_c = 0$, $W_c = 0.08$ and $W_c = 0.15$. They agree well with the calculated results. In Fig. 7 we show a new model, which is similar to the model shown in Fig. 6(d) but with $A_{min} = 10$ and $n = 100$. The two models have the same $\langle 1/W\rangle$ but the intensity correlation is reduced in the new model. The intensity distribution $P(J)$ is more sharply peaked around $\langle J\rangle$ since n is larger in

the new model. This means $\xi_{1/W}$ drops more rapidly when W_c increases (see Fig. 7).

We point out that the one-dimensional top-hat toy model discussed above is not a good approximation to the real ionizing field. But the behavior of $\xi_{1/W}$ under an imposed W_c should be similar for real Lyα forest absorption lines. We also point out that in all the above discussions we have assumed that most Lyα forest lines are on the linear part of the curve of growth so that we have $W \propto 1/J$. Since weak lines dominate $\xi_{1/W}$ and since many, if not all, strong absorption lines which we will study later in §5 may in fact be blends of several weaker components (see Pettini *et al.* 1990), this may be a reasonable assumption. The future work should also examine the saturation effect.

5 ABSORPTION LINE EQUIVALENT WIDTH CORRELATION $\xi_{1/W}$

5.1 Measurement of $\xi_{1/W}$

To compare our calculations with the real observational data we have measured the equivalent width correlation functions for some selected quasars. There are $N(N-1)/2$ line pairs for a quasar with N observed Lyα forest absorption lines. For a high redshift QSO there are many Lyα forest lines between Lyβ and Lyα emission region and these lines sample a fairly large distance along the line of sight. So high z QSOs with high quality spectra observed are ideal objects for our

statistical studies. We calculate the proper separation between the two clouds with absorption redshifts z_1 and $z_2(> z_1)$ by

$$r(z_1, z_2) = \frac{2c}{H_0} \frac{1}{1+z} \left[(1+z_1)^{-1/2} - (1+z_2)^{-1/2} \right], \tag{5.1}$$

where $z = (z_1 + z_2)/2$. We then regroup the $N(N-1)/2$ line pairs into many bins, each with a size $\Delta\log(r)$=constant, and the equivalent width correlation $1+\xi_{1/W}$ is estimated for each bin. It is clear that the results thus obtained depend on the bin size. What we have done is to require that the first bin is large enough to contain about 15 line pairs.

We have carried out our measurements by using the published QSO absorption line lists. We have excluded all identified absorption systems and the lines shortward of Lyβ emission. Since different quasars are observed by different authors with different sensitivity to absorption features we have decided not to combine all quasars together to form a huge sample, rather, to do it individually. For each quasar we construct several line samples. These samples are described by three parameters. The first one is the rest equivalent width cut-off W_c, which means only those lines with a rest equivalent width $W > W_c$ are accepted in the sample. The second is r_L, which allows no lines with a distance from the quasar less than r_L be included in the sample. This is desired to avoid the inverse effect. The third parameter is the lower wavelength cut-off λ_{lc}, which excludes the lines with $\lambda_{obs} < \lambda_{lc}$. Our results for the four quasars with $z_{em} > 3.65$ are shown in Fig. 8. The results for four other quasars are plotted in Fig. 9. The sample parameters and the references to the

absorption line lists are given in Table 2.

5.2 Discussion of Individual QSOs

5.2.1 Q0000–263 ($z_{em} = 4.104$)

This QSO, discovered by Hazard and McMahon (1988), is the brightest QSO known with a redshift larger than 4.0. The extrapolation of the mean line density $dN/dz \approx 2.67(1+z)^{2.37}$ (Lu *et al.*, 1991) to $z \simeq 4$ predicts $\sim$ 84 Lyα forest lines with $W > 0.36\AA$ for this QSO. Actually 70 are observed between the Lyβ and Lyα emission region, slightly lower but not inconsistent with the extrapolation. Our results for the rest equivalent width correlation function are plotted in Fig. 8(a) for 7 different line samples. The samples 1, 2, 4 and 6 indeed produce a significant signal at the smallest separation. From the figure we also see that the signal is considerably reduced if we exclude those lines (about half of the total lines!) with a distance less than 30Mpc from the QSO (sample 3). Note that sample 6 satisfies the criteria which define sample 2 of Sargent *et al.* (1980), i.e., the signal-to-noise ratio in the spectrum is demanded to be larger than 10 to ensure that lines with rest equivalent widths greater than $0.16\AA$ will not be lost in the continuum noise.

If the strong correlation signal is due to the enhanced ionizing field near the QSO, we can estimate the intensity of the ionizing field at $z = 4.1$. From Sargent *et al.* (1989) Fig. 1 we know that the observed flux at $\lambda_{obs} = 7000\AA$ is about 380μJy. Longward of Lyα emission Sargent *et al.* measured a spectral index $\alpha \simeq 1$ ($f_\nu \propto$

$\nu^{-\alpha}$). According to Steidel and Sargent (1987) the true continuum in the Lyα forest region can be represented by the extrapolation of the continuum defined longward of Lyα emission, we thus estimate a Lyman limit luminosity $L \approx 7 \times 10^{31}$ergs $\sec^{-1}\mathrm{Hz}^{-1}$ for this QSO. The mean intensity of the ionizing field at ν_L can be obtained by using $J \approx L/(4\pi r_{eq})^2$, where r_{eq} is the distance from the QSO at which the intensity produced by the quasar is equal to the mean intensity. Adopting $r_{eq} > 20$Mpc, we get $J_{-22} < 1.2$ at $z = 4.1$. This is at least an order of magnitude smaller than the value $\log J \approx -21 \pm 0.5$ estimated by Bajtlik *et al.* (1988) and Lu *et al.* (1991) for $1.7 < z < 3.8$. Notice that since $L \propto H_0^{-2}$ and $r_{eq} \propto H_0^{-1}$ the estimated J does not depend on H_0. We also point out that if the QSO has a steeper spectrum shortward of Lyα emission then the estimated J will be even smaller.

5.2.2 Q1208+101 ($z_{em} = 3.811$)

The spectral resolution for this QSO is not high (1.6$\AA$). The sample 1, which includes all lines, does not show any significant correlation signal for $\log(r(\mathrm{kpc})) > 2.7$. The sample 2, which excludes several weakest lines, shows a signal in the first bin, and further exclusion of the lines within a distance 10Mpc from the QSO (the sample 4) reduces the correlation signal.

5.2.3 Q2000–330 ($z_{em} = 3.78$)

The absorption spectrum of this QSO has been fairly extensively discussed in the

literature. We notice that with a comparable resolution Steidel (1990) found 119 absorption lines between $\lambda_{obs} = 5000\AA$ and $\lambda_{obs} = 5805\AA$, while Hunstead *et al.* (1986) observed 145 in the same spectral range! We have used the line list compiled by Hunstead *et al.* to estimate the equivalent width correlation. According to Hunstead *et al.* the line list is highly reliable and essentially complete for $W_{obs} \geq 1.0\AA$, or $W > 0.25\AA$. As can be seen from Fig. 8(c) there is a significant correlation signal in the first separation bin for the samples 1, 2 and 4. Exclusion of the lines within a distance 30Mpc (the sample 5) from the QSO reduces the signal considerably.

From Sargent *et al.* (1989) Fig. 1 we see that the observed flux at $\lambda_{obs} = 7000\AA$ is about 350μJy. The spectral index longward of Lyα emission is given by Sargent *et al.* as $\alpha \simeq 0.75$ (corrected for Galactic reddening). These leads to $L \approx 6 \times 10^{31}$ergs $\sec^{-1}\mathrm{Hz}^{-1}$. Adopting $r_{eq} \approx 20$Mpc we get $J_{-22} \approx 0.9$ at $z = 3.8$.

5.2.4 Q0055–269 ($z_{em} = 3.653$)

Only 43 Lyα forest lines are listed by Steidel (1990). The sample 1 shows fairly large fluctuations in correlation and produces a strong signal for the first separation bin. The strong signal disappears when the seven weak lines (lines 42 t0 48) within a distance 5Mpc from the QSO are removed.

Sargent *et al.* (1989) Fig. 1 shows that the observed flux at $\lambda_{obs} = 7000\AA$ is about 170μJy. The spectral index longward of Lyα emission is given by Sargent *et al.* as $\alpha \simeq 0.47$. These lead to $L \approx 3 \times 10^{31}$ergs $\sec^{-1}\mathrm{Hz}^{-1}$. Adopting $r_{eq} \approx 5$Mpc

we get $J_{-22} \approx 8$ at $z = 3.65$, this is in agreement with the result obtained by Bajtlik *et al.* and Lu *et al.*.

5.2.5 Q1442+101 ($z_{em} = 3.544$) and Q1159+124 ($z_{em} = 3.502$)

These two QSOs both have a redshift $z_{em} > 3.5$. For Q1442+101 the line list by Morton *et al.* (1989) lists 83 Lyα forest lines. The spectral resolution for this quasar is low ($\sim 2\AA$). For Q1159+124 (res.=0.8, 1.5$\AA$) Sargent *et al.* (1988) list 98 Lyα forest lines. We have measured the equivalent width correlations for these two quasars. We did not find any significant correlation signal at a separation $\log(r(\text{kpc})) > 2.7$ (2.6) for Q1442 (for Q1159). The results for these two quasars are not plotted.

5.2.6 Q0837+109 ($z_{em} = 3.326$)

This QSO was selected because the high resolution (0.8$\AA$) spectrum by Sargent *et al.* (1988) reveals 88 Lyα forest lines. The samples 1, 4 and 5 display a significant correlation signal at the smallest separation. Careful examination shows that the signal is largely produced by the three very weak lines (16, 17 and 18) at $\lambda_{obs} \sim 4919\AA$ (see the sample 6 result). These three lines may not be real since all of them have $W < 0.1\AA$.

5.2.7 Q0142–100 ($z_{em} = 2.727$)

The high resolution spectrum (0.8Å) by Sargent *et al.* (1988) shows 115 Lyα forest lines between the Lyβ and Lyα emission region. We did not find any significant correlation at a scale $\log(r(\mathrm{kpc})) > 2.5$ (see Fig. 9(b)).

5.2.8 Q2206–199 ($z_{em} = 2.559$)

This QSO was selected for our correlation study because Pettini *et al.* (1990) observed it with an extremely high resolution ($\sim 0.09\AA$). There are 74 Lyα forest lines in the line list given by Pettini *et al.*. Although there are gaps in the spectrum which are not covered by the observation this should not affect the correlation measurement significantly. The extremely high resolution enables us to explore the correlation at very small separations. Marginal signals are detected at small separations, that are caused by very weak lines with $W < 0.1\AA$ (see Fig. 9(c)).

5.2.9 Q1247+267 ($z_{em} = 2.039$)

This QSO was selected because it has a relatively low redshift. Also this is a very bright quasar and the spectrum by Sargent *et al.* (1988) has a very high S/N ratio. There are 47 Lyα forest lines listed by Sargent *et al.*. The sample 1, which includes all these lines, shows a significant signal for the smallest separation bin (see Fig. 9(d)). After removing the 7 lines (lines 42 to 48) within a distance 20Mpc from the quasar the correlation signal disappears.

From Green *et al.* (1980) Fig. 9 we see that the observed flux at $\lambda_{obs} = 6000\AA$ is about 750μJy. The spectral index longward of Lyα emission is $\alpha \simeq 0.5$. We thus

have $L \approx 5 \times 10^{31}$ergs sec^{-1}Hz^{-1}. Adopting $r_{eq} \approx 20$Mpc we get $J_{-22} \approx 0.8$ at $z = 2$.

5.3 Summary and Discussion

We have measured the equivalent width correlation functions of the six highest redshift QSOs ($z_{em} > 3.5$) for which we could find the absorption line lists in the literature. We have also investigated four other QSOs which have high quality spectra and published absorption line lists. In four cases (Q0000–263, Q2000–330, Q0055–269 and Q1247+267) we have detected a positive correlation signal in the smallest separation bins, which seems to have been produced mainly by the lines near the QSO emission redshifts.

It is well known that there are many uncertainties involved in measuring equivalent widths of QSO absorption lines: (i) the noise due to counting statistics, sky-background and small-scale detector irregularities; (ii) the subjective decomposition of blended lines; and (iii) the uncertainty in the continuum level in the Lyα forest region. Our measurement of the equivalent width correlation relies critically on the quality of measurement of the weak lines, because of the uncertainties these lines are usually the least reliable, especially in the case of low resolution and low S/N ratio spectra. We also know that the measured redshift of an absorption line does not necessarily represent its position in space. At $z = 4$ a line of sight peculiar velocity 100km/sec corresponds to a separation of 180kpc. Such velocity dispersion, as well as poor spectral resolution, affect our correlation results at small separations.

But these uncertainties alone are not enough to explain why the correlation is produced by the lines near QSO emission redshifts. One possibility is that the spectral signal-to-noise ratio (S/N) systematically declines towards the blue end because of the observed wavelengths becoming closer to the ultra-violet atmosphere cutoff and because of instrumental throughput and detector sensitivities decrease at shorter wavelengths. Also a strong Lyα emission will enhance S/N near the emission redshift. This may allow more weak lines near QSO emission redshift to be accepted into the line list and thus generate a significant equivalent width correlation. In Fig. 10 we have plotted the S/N for some line samples of Q0000–263, Q0055–269 and Q1247+267. Notice that in Q1247 the S/N is the continuum signal-to-noise ratio while in Q0000 and Q0055 the S/N is calculated over the range of pixel values included in each absorption line; thus, for the weakest lines, the plotted value represent the actual continuum S/N, whereas for strong lines the plotted value is likely to be considerably less than the actual continuum S/N (Steidel 1990). The decline of the S/N towards the blue end can be clearly seen. To test this explanation simulated spectra with inhomogeneous continuum S/N should be measured to see if a significant correlation can be generated. Another explanation for the correlation signal is that the continuum level at the blue wing of the Lyα emission line has be underestimated, or the continuum level at the shorter wavelengths has been overestimated. This can also lead to more weak lines near the QSO emission redshift and thus an equivalent width correlation signal.

On the other hand if the above mentioned observational uncertainties are not

serious at least for some line samples, say, the sample 6 of Q0000–263, then the detected correlation signal needs a physical explanation. We have discussed in §5.2.1 the possibility that the signal may be produced by the enhanced ionizing field near QSOs. In the case of the Q0000–263 sample 6, the affected range is large and the inferred J at $z = 4.1$ is considerably smaller than the value estimated by Bajtlik *et al.* (1988) and Lu *et al.* (1991) for lower redshifts. But it may still be consistent with what we have computed for QSO contribution (see Table 1). It is interesting to note that very recently Dobrzycki and Bechtold (1991) have discovered a large ($\sim$ 10Mpc) void in the spectrum of QSO 0302-003. From the assumption that the void is due to the proximity effect generated by the observed nearby quasar, they derived $J_{-21} = 0.1$ at $z \approx 3.2$. But this result can be further complicated by the possible quasar anisotropic emission and luminosity variation in the time scale of a few times 10^7 years.

After removing the enhanced ionization effect the residual small (or even zero) equivalent correlation may be explained by invoking the cut-off effect which we have discussed in §4.

At present epoch the mean space density of L^* galaxies is roughly $10^{-2}\mathrm{Mpc}^{-3}$, while for QSOs we have assumed that the comoving space density is $n\langle L\rangle^2/\langle L^2\rangle \simeq 3 \times 10^{-6}\mathrm{Mpc}^{-3}$ at $z \geq 2.2$ (see §3.1). Since ξ_J is inversely proportional to source space density, we are not expected to see any detectable $\xi_{1/W}$ if galaxies dominate the ionizing field, unless we include those lines near a powerful QSO.

6 CONCLUSIONS

By using Markoff's method we have derived the joint probability distribution of intensities of ionizing field at two different places. The intensity correlation function ξ_J has been calculated for randomly distributed QSOs as the main ionizing sources, including the absorption produced by QSO absorption line systems. We have shown that the Lyα forest line clouds can be used as intensity indicators to reveal ξ_J at high z. The equivalent width cutoff effect, which is introduced because spectroscopic observations cannot detect very weak lines, has been examined by constructing a top-hat toy model. It is shown that such effect usually leads to a smaller equivalent width correlation $\xi_{1/W}$, compared with ξ_J. We have measured $\xi_{1/W}$ for some selected QSOs and have found, in some cases, strong correlation signals at small separations. Careful examination has shown that such signals are mainly produced by the lines near the QSO emission redshifts. One possible explanation to the detected correlation is that the spectral S/N is not uniform, it declines at shorter wavelengths. This means that more weak lines can be detected near the QSO emission redshifts which leads to the measured equivalent width correlation. Another explanation is that the correlation is produced by the enhanced ionizing field near QSOs. If this latter explanation is true, from the affected range by QSOs we conclude that J_{ν_L} is less than 10^{-21}ergs cm^{-2}s^{-1}Hz^{-1}sr^{-1} at $z \sim 3.5$. More works are needed to determine the nature of the detected correlation.

ACKNOWLEDGMENTS

This work was supported in part by NSF Grant AST84-51725. We thank Drs. Wal Sargent and Chuck Steidel for useful discussion.

REFERENCES

Bajtlik, S., Duncon, R. C. & Ostriker, J. P., 1988. *Astrophys. J.*, **327**, 570.

Boyle, B. J., Shanks, T. & Peterson, B. A., 1988. *Mon. Not. R. astr. Soc.*, **235**, 935.

Chandrasekhar, S., 1943. *Rev. Mod. Phys.*, **15**, 1.

Dobrzycki, A. & Bechtold, J., 1991. *Astrophys. J. Lett.*, **377**, L69.

Green, R. F., Pier, J. R., Schmidt, M., Estabrook, F. B., Lane, A. L. & Wahlquist, H. D., 1980. *Astrophys. J.*, **239**, 483.

Hazard, C. & McMahon, R. G., 1988. unpublished.

Hunstead, R. W., Murdoch, H. S., Peterson, B. A., Blades, J. C., Jauncey, D. L., Wright, A. E., Pettini, M. & Savage, A., 1986. *Astrophys. J.*, **305**, 496.

Lanzetta, K. M., 1991. *Astrophys. J.*, **375**, 1.

Lu, L., Wolfe, A. M. & Turnshek, D. A., 1991. *Astrophys. J.*, **367**, 19.

Miralda-Escudé, J. & Ostriker, J. P., 1990. *Astrophys. J.*, **350**, 1.

Morton, D. C., Peterson, B. A., Chen, J-S., Wright, A. E. & Jauncey, D. L., 1989. *Mon. Not. R. astr. Soc.*, **241**, 595.

Pettini, M., Hunstead, R. W., Smith, L. J. & Mar, D. P., 1990. *Mon. Not. R. astr. Soc.*, **246**, 545.

Sargent, W. L. W., Boksenberg, A. & Steidel, C. C., 1988. *Astrophys. J. Suppl. Ser.*, **68**, 539.

Sargent, W. L. W., Steidel, C. C. & Boksenberg, A., 1989. *Astrophys. J. Suppl. Ser.*, **69**, 703.

Sargent, W. L. W., Young, P. J., Boksenberg, A. & Tytler, D., 1980. *Astrophys. J. Suppl. Ser.*, **42**, 41.

Schmidt, M., Schneider, D. P. & Gunn, J. E., 1991. To appear in: *Space Distribution of Quasars*, ed. D. Crampton (Astron. Soc. of the Pacific, San Francisco), in press.

Steidel, C. C., 1990. *Astrophys. J. Suppl. Ser.*, **72**, 1.

Steidel, C. C. & Sargent, W. L. W., 1987. *Astrophys. J.*, **313**, 171.

Table 1. Some calculated results.

z_{obs}	$z_c(z_{obs})$	$r_0(z_{obs})$(Mpc)	$J_{-22}(z_{obs})$	$\frac{\langle L^2\rangle}{8\pi r_0^3 n\langle L\rangle^2}$	r_{corr}(kpc)	$\Delta\lambda_{corr}(\mathring{A}\ )$
2.2	2.52	104.8	5.0	3.2×10^{-4}	163.5	0.61
2.5	2.79	75.9	4.8	6.4×10^{-4}	236.0	1.10
3.0	3.24	45.0	4.2	2.1×10^{-3}	446.4	2.90
3.5	3.70	27.9	3.7	6.1×10^{-3}	758.9	6.62
4.0	4.17	18.2	3.3	1.6×10^{-2}	1175.7	13.34
4.2	4.36	15.6	3.2	2.2×10^{-2}	1319.8	16.52

Table 2. Absorption line samples for measuring $\xi_{1/W}$.

Object	Sample	W_c (Å)	r_L (Mpc)	λ_{lc} (Å)	# of lines	Pair # in bin 1, 2	Refs.
Q0000–263	S1				140	17, 40	1
$z_{em} = 4.104$	S2		20		96	16, 41	
res.=1.2Å	S3		30		73	16, 38	
	S4	0.16			124	15, 38	
	S5	0.2			112	20, 36	
	S6	0.16	20	5515	62	20, 33	
	S7	0.2	20		77	17, 37	
Q1208+101	S1				62	15, 44	1
$z_{em} = 3.811$	S2	0.2			55	19, 32	
res.=1.6Å	S3		10		47	16, 27	
	S4	0.2	10		44	16, 32	
Q2000–330	S1				126	19, 35	2
$z_{em} = 3.78$	S2	0.16			111	16, 34	
res.=1.5Å	S3	0.25			84	12, 41	
	S4		20		93	17, 29	
	S5		30		74	19, 45	
	S6	0.16	20		81	18, 53	
	S7	0.25	20		63	18, 40	
Q0055–269	S1				43	19, 35	1
$z_{em} = 3.653$	S2	0.16			36	16, 25	
res.=1.1Å	S3		5		36	18, 28	
Q0837+109	S1				88	19, 34	3
$z_{em} = 3.326$	S2	0.1			80	15, 30	
res.=0.8Å	S3	0.2			55	15, 21	
	S4		20		57	16, 31	
	S5			4880	81	15, 35	
	S6			4925	70	16, 35	
Q0142–100	S1				115	18, 30	3
$z_{em} = 2.727$	S2	0.1			91	16, 30	
res.=0.8Å	S3		10		106	14, 41	
Q2206–199	S1				74	14, 37	4
$z_{em} = 2.559$	S2	0.05			63	18, 28	
res.=0.09Å	S3	0.10			47	17, 62	
	S4		10		69	14, 32	

Table 2. (*continued*)

Object	Sample	W_c (Å)	r_L (Mpc)	λ_{lc} (Å)	# of lines	Pair # in bin 1, 2	Refs.
Q1247+267	S1				47	16, 47	3
$z_{em} = 2.039$	S2	0.1			39	17, 29	
res.=0.8Å	S3		20		40	16, 37	

References: 1. Steidel 1990; 2. Hunstead *et al.* 1986; 3. Sargent *et al.* 1988; 4. Pettini *et al.* 1990.

FIGURE CAPTIONS

Figure 1. The coordinate systems (r, l) and (x, y); and the integration area (shaded area) for calculating $I_J(r_1)$.

Figure 2. $I_J(u_1)/u_1$ as a function of u_1.

Figure 3. The effective optical depth $\tau_{eff}(\nu_L, z_{obs}, z)$ as a function of z for various z_{obs}. The dashed and dotted lines are the two approximations (see the text).

Figure 4. Calculated intensity correlation function $1 + \xi_J(r)$ at various epoch z.

Figure 5. The integration region (shaded) for calculating Eqs. (4.1) and (4.2) when a cut-off W_c is imposed.

Figure 6. Calculated equivalent width correlation function $\xi_{1/W}$ for the top-hat toy model. Various cut-offs are labeled beside the curves. (a) $f(A) \propto \delta(A - A_0)$; (b) uniform $f(A)$ distribution; (c) $f(A) \propto A^{-1.7}$ with a high A cut-off; (d) $f(A) \propto A^{-1.7}$ without a high A cut-off, the open circles are the Monte Carlo simulation results for $W_c = 0.0$, 0.08 and 0.15.

Figure 7. Calculated equivalent width correlation function $\xi_{1/W}$ for the top-hat toy model. Various cut-offs are labeled beside the curves. $f(A) \propto A^{-1.7}$ without a high A cut-off, similar to the model in Fig. 6(d) but with $A_{min} = 10$ and $n = 100$.

Figure 8. Measured equivalent width correlation functions for four QSOs with $z_{em} > 3.65$. (a) Q0000–263; (b) Q1208+101; (c) Q2000–330; (d) 0055–269. Definitions of various samples can be found in Table 2.

Figure 9. Measured $\xi_{1/W}$ for some selected QSOs. (a) Q0837+109; (b) Q0142–100; (c) Q2206–199; (d) 1247+267. Definitions of various samples can be found in Table 2.

Figure 10. (a) The signal-to-noise ratio S/N calculated over the range of pixel values included in each absorption line for the Q0000–263 sample 1 lines (from Steidel 1990); (b) same as (a) but for the Q0000–263 sample 6 lines; (c) same as (a) but for the Q0055–269 sample 1 lines; (d) the continuum S/N for the Q1247+267 sample 1 lines (from Sargent *et al.* 1988).

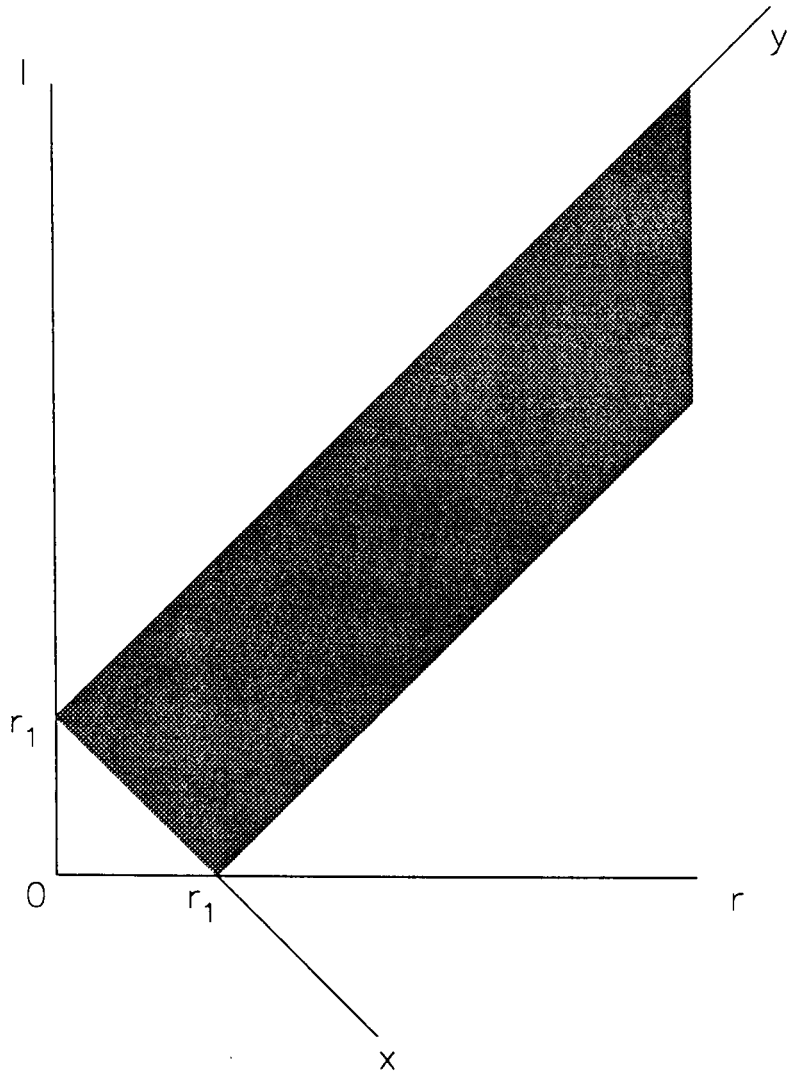

Figure 1

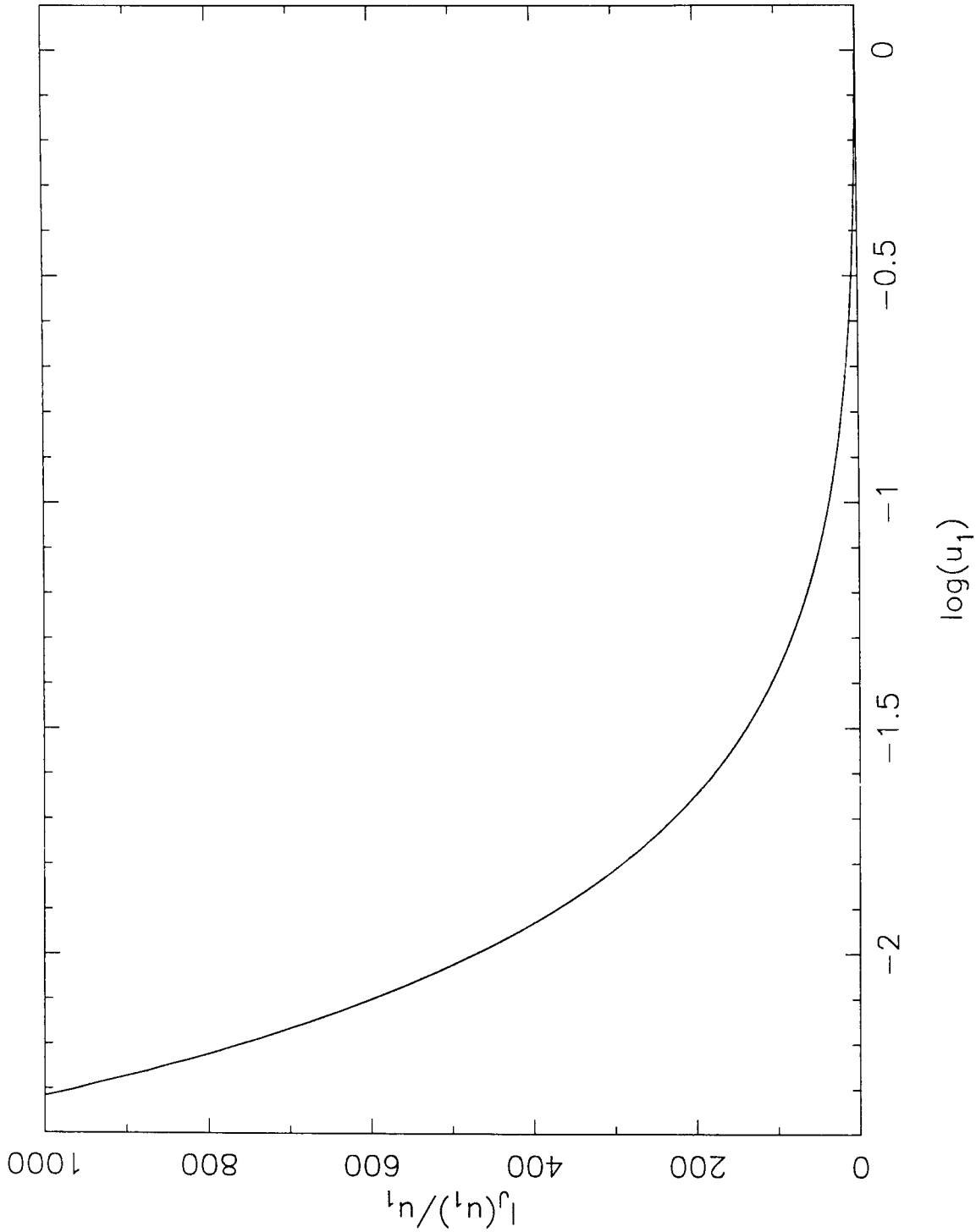

Figure 2

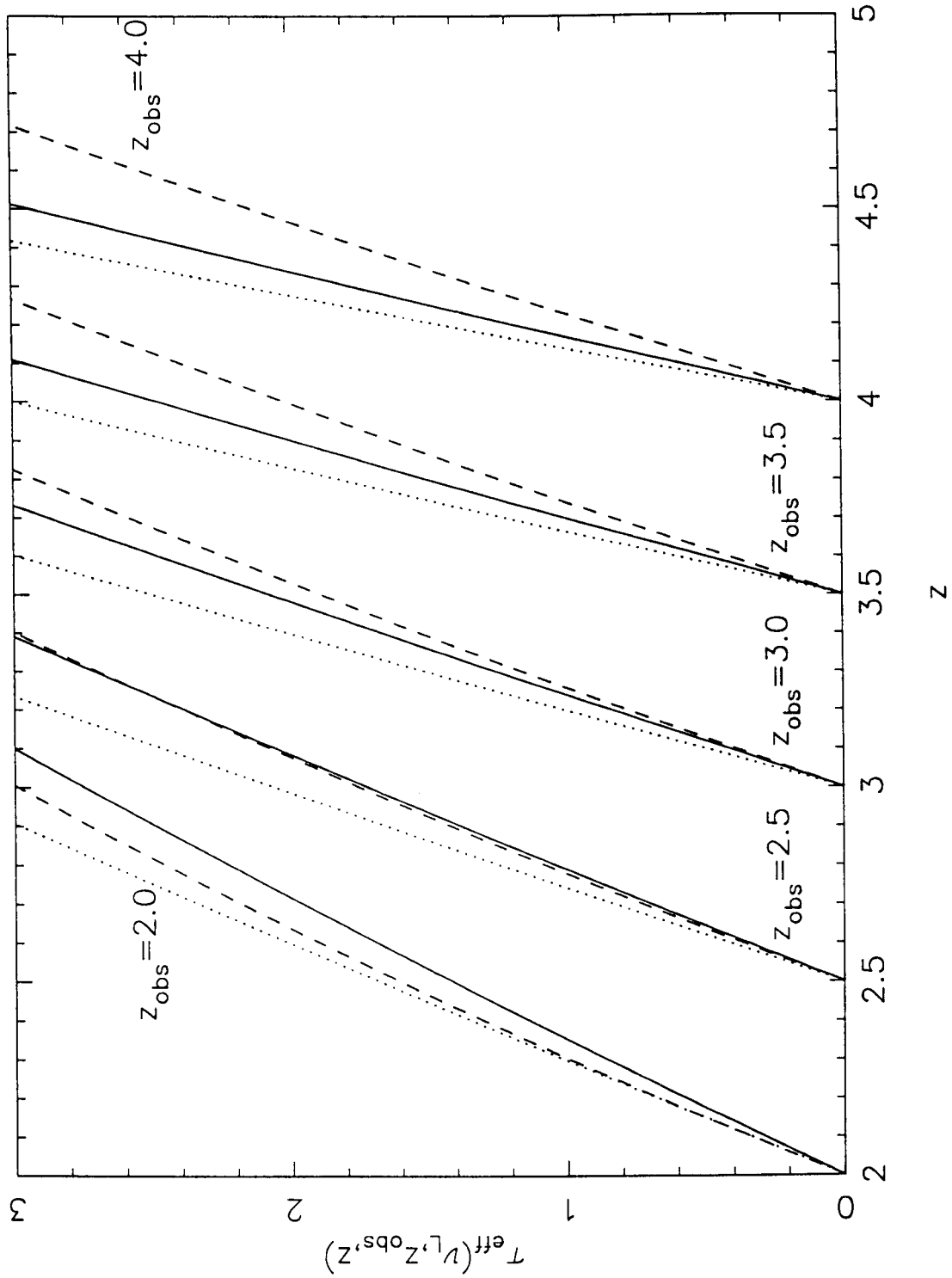
z_{obs}=4.0
z_{obs}=3.5
z_{obs}=3.0
z_{obs}=2.5
z_{obs}=2.0
$\tau_{eff}(\nu_L, z_{obs}, z)$
z
0
1
2
3
2
2.5
3
3.5
4
4.5
5

Figure 3

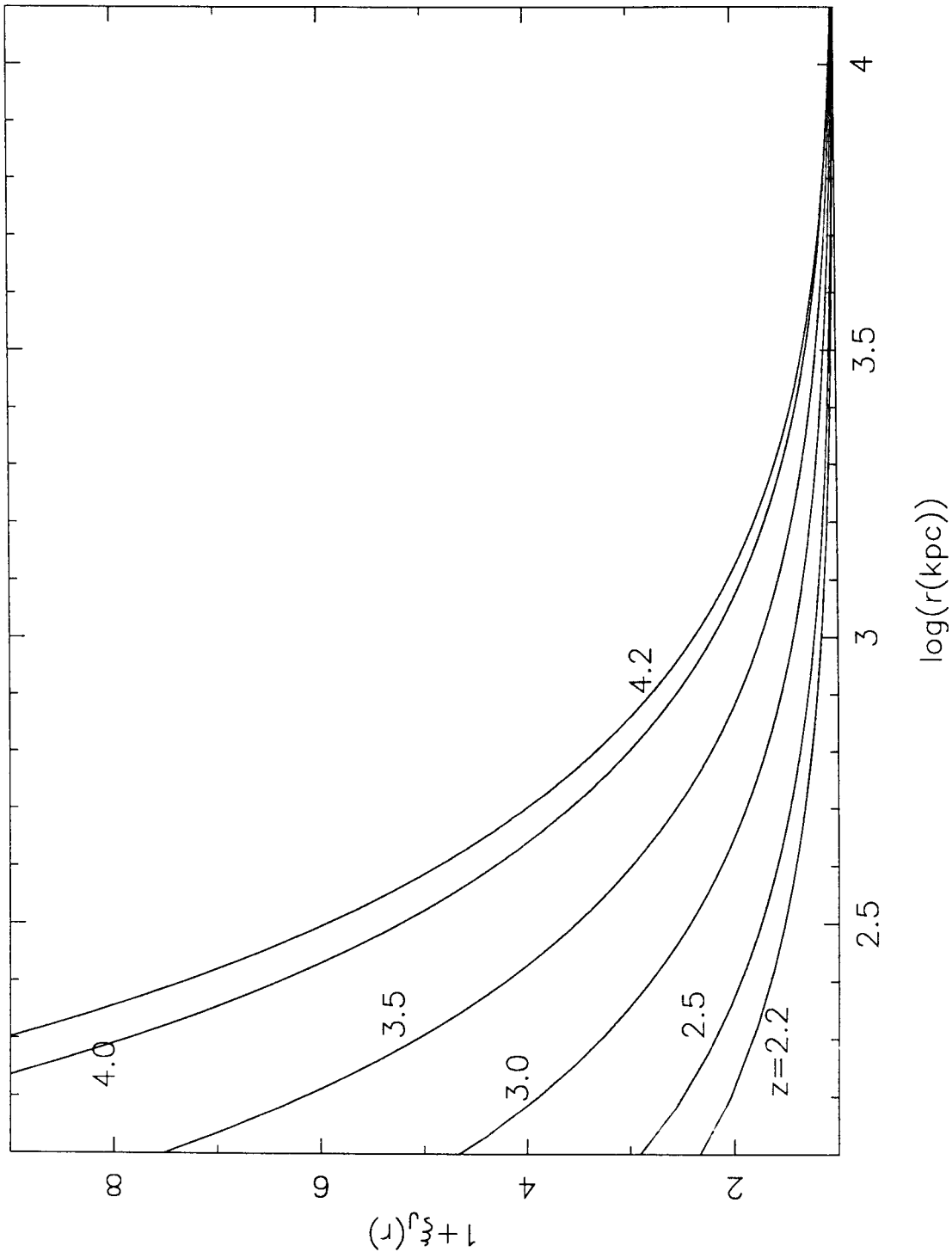

Figure 4

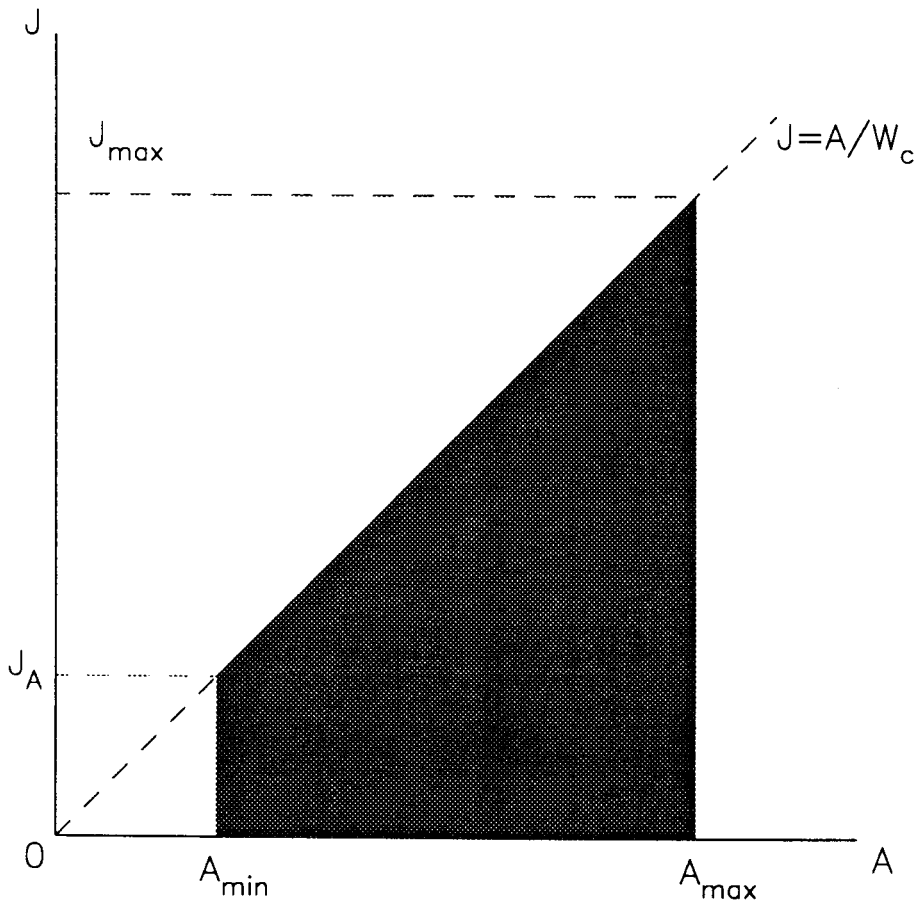

Figure 5

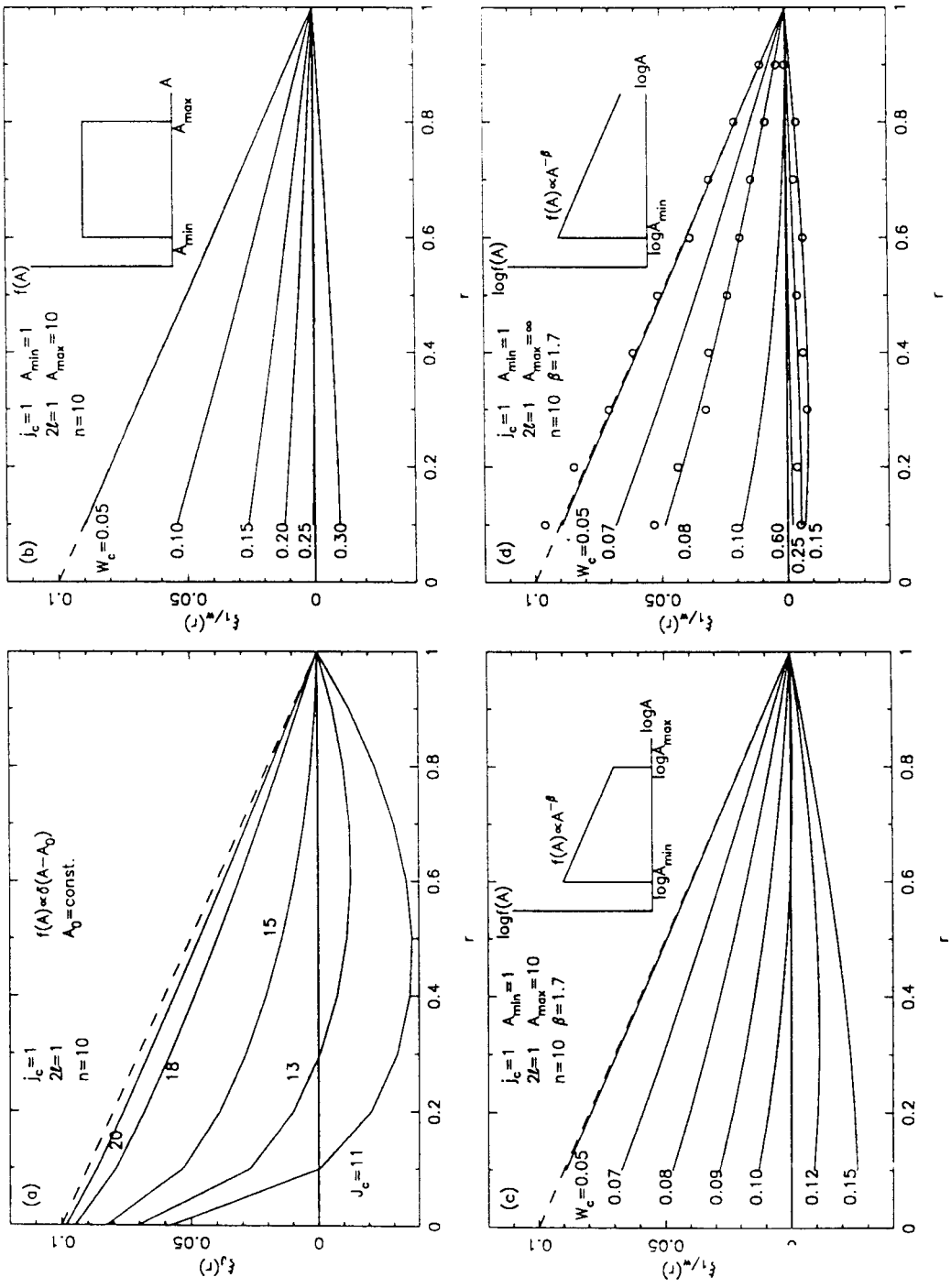
(a)
$j_c=1$ $2t=1$ $n=10$
$f(A)\propto\delta(A-A_0)$
A_0=const.
20
18
15
13
$J_c=11$
$\xi_J(r)$
(b)
$j_c=1$ $A_{min}=1$ $2t=1$ $A_{max}=10$ $n=10$
f(A)
A_{min}
A_{max}
A
W_c=0.05
0.10
0.15
0.20
0.25
0.30
$\xi_{1/e}(r)$
(c)
$j_c=1$ $A_{min}=1$ $2t=1$ $A_{max}=10$ $n=10$ $\beta=1.7$
logf(A)
$f(A)\propto A^{-\beta}$
$\log A_{min}$
$\log A_{max}$
logA
W_c=0.05
0.07
0.08
0.09
0.10
0.12
0.15
$\xi_{1/e}(r)$
(d)
$j_c=1$ $A_{min}=1$ $2t=1$ $A_{max}=\infty$ $n=10$ $\beta=1.7$
logf(A)
$f(A)\propto A^{-\beta}$
$\log A_{min}$
logA
W_c=0.05
0.07
0.08
0.10
0.60
0.25
0.15
$\xi_{1/e}(r)$
r

Figure 6

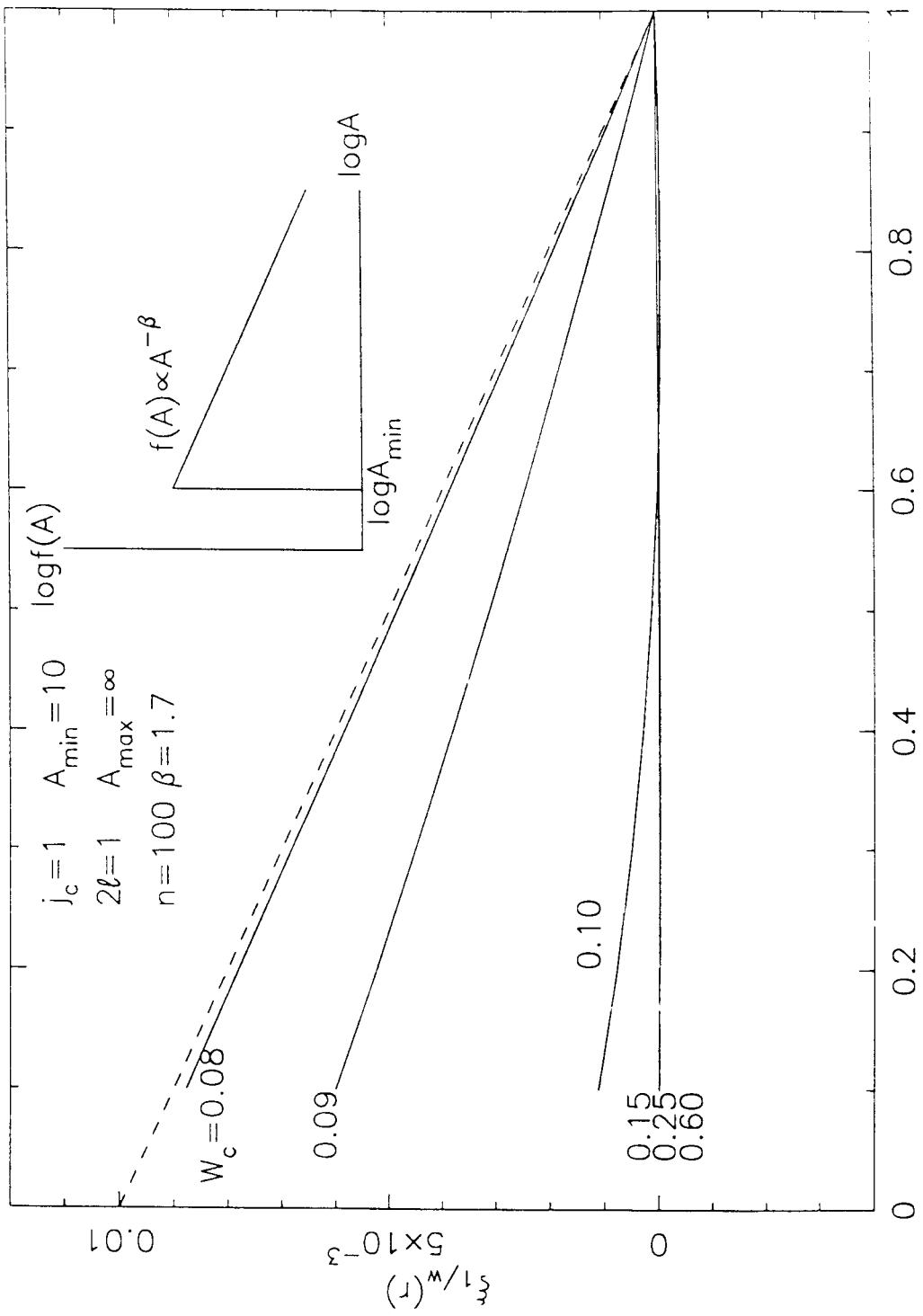
$\xi_{1/w}(r)$
0.01
5×10^{-3}
0
0
0.2
0.4
0.6
0.8
1
r
W_c=0.08
0.09
0.10
0.15
0.25
0.60
j_c=1 A_{min}=10 logf(A)
2ℓ=1 A_{max}=∞
n=100 β=1.7
$f(A)\propto A^{-\beta}$
logA
$logA_{min}$

Figure 7

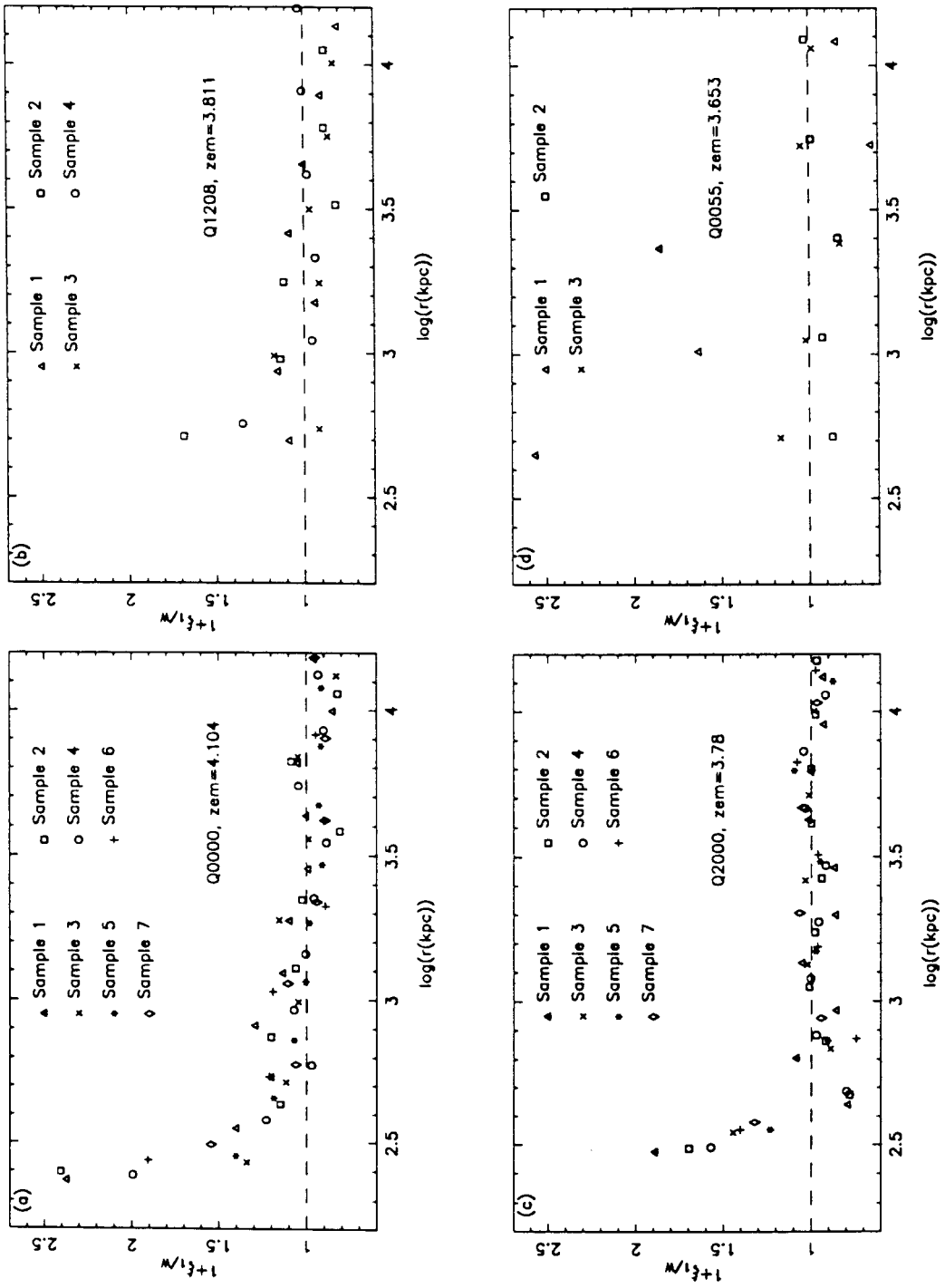
(a)
Q0000, zem=4.104
(b)
Q1208, zem=3.811
(c)
Q2000, zem=3.78
(d)
Q0055, zem=3.653
Sample 1
Sample 2
Sample 3
Sample 4
Sample 5
Sample 6
Sample 7
1+ξ1/W
log(r(kpc))

Figure 8

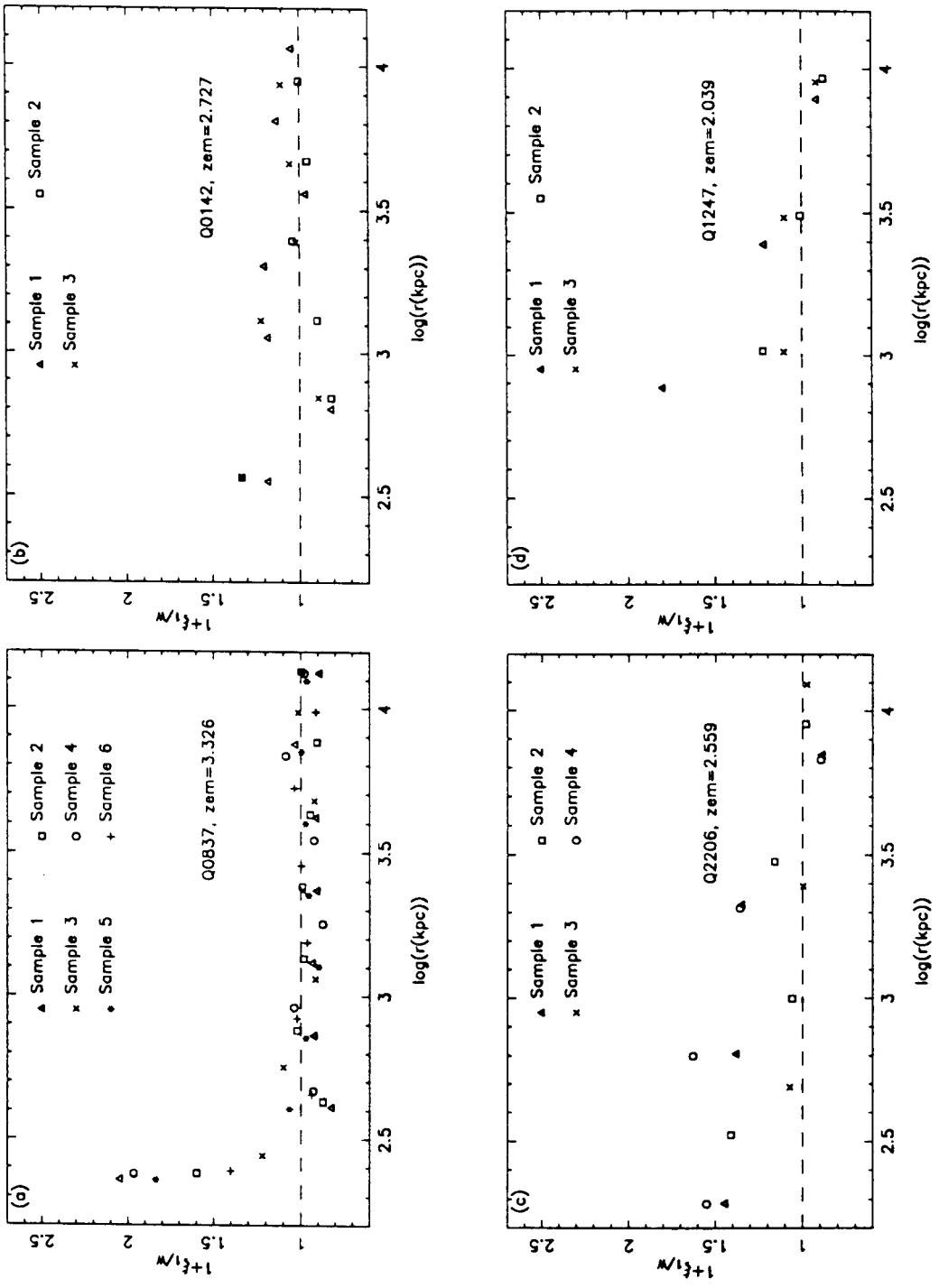
(a)
Sample 1
Sample 2
Sample 3
Sample 4
Sample 5
Sample 6
Q0837, zem=3.326
(b)
Sample 1
Sample 2
Sample 3
Q0142, zem=2.727
(c)
Sample 1
Sample 2
Sample 3
Sample 4
Q2206, zem=2.559
(d)
Sample 1
Sample 2
Sample 3
Q1247, zem=2.039
1+ξ1/W
log(r(kpc))

Figure 9

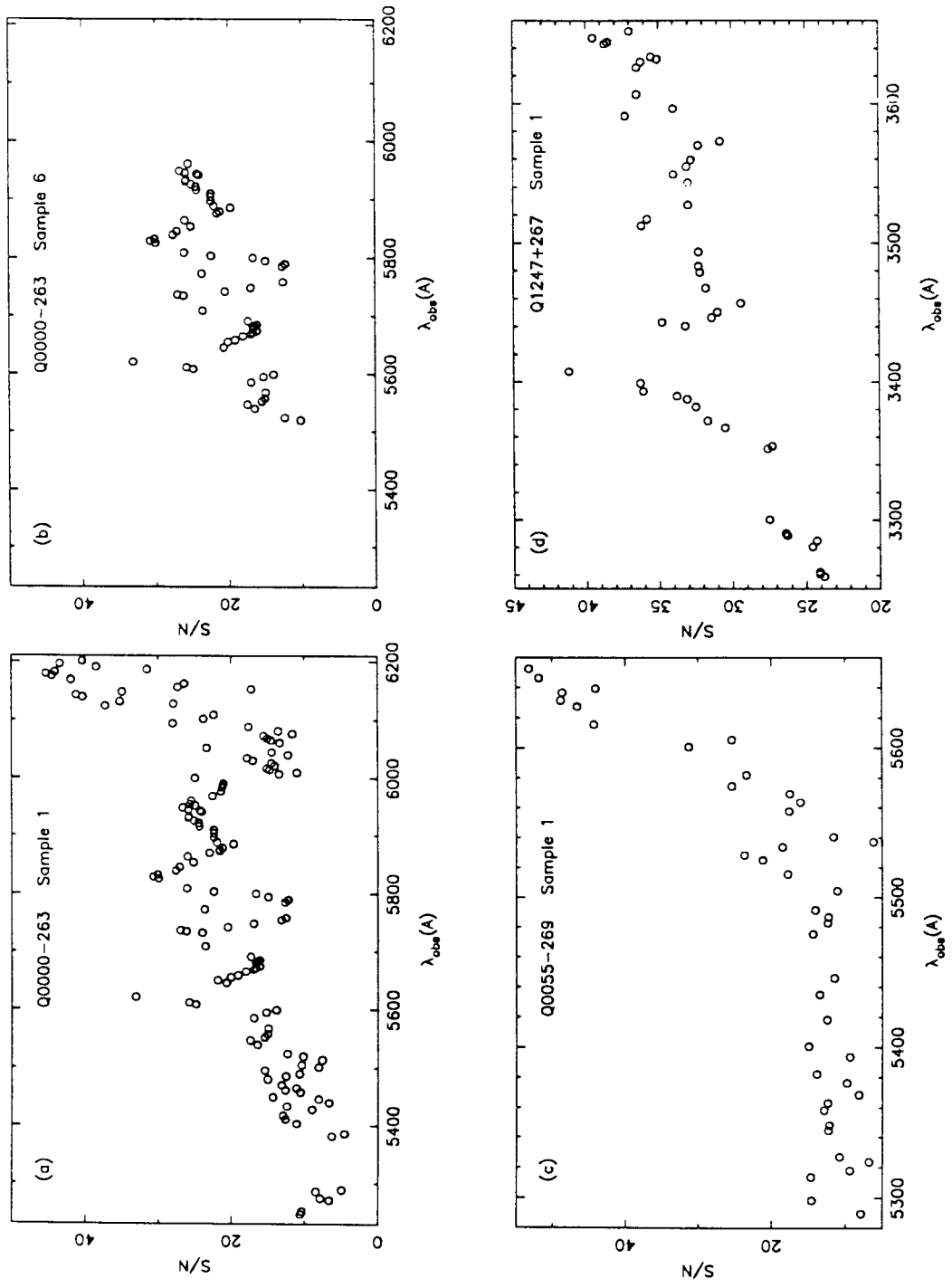
(a)
Q0000-263 Sample 1
(b)
Q0000-263 Sample 6
(c)
Q0055-269 Sample 1
(d)
Q1247+267 Sample 1
S/N
λ_{obs}(A)

Figure 10

CHAPTER FIVE

ON THE HI COLUMN DENSITY DISTRIBUTION OF QSO ABSORPTION LINE SYSTEMS

SUMMARY. We present a simple explanation for the observed neutral hydrogen column density distribution of QSO absorption line systems. We model a "typical" absorption system as a non-uniform spherical hydrogen cloud exposed to an isotropic ionizing background. We solve the coupled ionization balance and radiation transfer problem (the "inverse HII region" problem) for the absorbing clouds and calculate the column density distribution $f(N)$. We show that with an appropriate density gradient in the clouds we can reproduce the observed overall power law distribution and the apparent excess of absorption systems with $N \geq 2 \times 10^{20}\mathrm{cm}^{-2}$, which is recently discovered by Lanzetta *et al.* (1991). The calculated $f(N)$ curve is not sensitive to the input ionizing spectra and is a generic feature of the assumed density distribution. In our model all QSO absorption lines have the same origin, the ionized outer envelopes produce the weak Lyα forest lines while the neutral cores result in the damped Lyα systems. We discuss the consequences of such models and propose star-forming dwarf galaxies as primary candidates for QSO absorption line systems. Our calculations also showed that the uniform cloud models are highly unlikely.

1 INTRODUCTION

High resolution spectroscopy observations of bright quasars have revealed a very impressive feature of neutral hydrogen column density distribution of QSO absorption line systems. From $\log N(\mathrm{HI}) \sim 13$ for the weak Lyα forest line systems to $\log N(\mathrm{HI}) \sim 22$ for the damped Lyα systems, the distribution function $f(N)$ can roughly be represented by a single power law: $f(N) \propto N^{-\beta}$ with $\beta \sim 1.5$ (Tytler 1987, Sargent *et al.* 1989). This remarkable observational fact sets very stringent constraints to the possible models of QSO absorption line systems. For example, if QSO absorption line systems are produced by randomly distributed and randomly oriented identical sheets, then the resulting column density distribution would be $f(N) \propto N^{-3}$ (notice that for a tilted sheet the projected cross section along a line of sight is reduced), too steep to explain the observed distribution. Another example concerns the pressure confined model of Lyα forest line systems (Sargent *et al.* 1980; Ostriker and Ikeuchi 1983; Ikeuchi and Ostriker 1986). In this model the optically thin ($\log N < 17$) clouds are confined by a hotter and more rarefied intergalactic medium. But as pointed out by Rees (1987), since the model requires the same density for all clouds at a certain epoch, column density N scales only with the cube root of mass, and for $10^{13}\mathrm{cm}^{-2} < N < 10^{17}\mathrm{cm}^{-2}$ a resulting range of 10^{12} in cloud masses is too large to be accommodated.

The observed smooth connection of the optically thin and the optically thick parts around $N \sim 10^{17}\mathrm{cm}^{-2}$ in the observed $f(N)$ curve is a surprising result.

People had expected that for those clouds with $N \gtrsim 10^{17}\mathrm{cm}^{-2}$, where self-shielding occurs, the distribution would look very different. Duncan and Ostriker (1988) had constructed models in which a "step-down" in $f(N)$ at $N \sim 10^{17}\mathrm{cm}^{-2}$ does appear. They claimed their result is in agreement with the observations by Bechtold (1987). We now know that better data from Sargent *et al.* (1989) have failed to show such a "step down" at the claimed place. However, very recently Lanzetta *et al.* (1991) have measured a large sample of damped Lyα systems and discovered an apparent excess of absorption systems with $N \geq 2 \times 10^{20}\mathrm{cm}^{-2}$ compared with what is expected based on an extrapolation of the column density distribution for systems with $N < 2 \times 10^{20}\mathrm{cm}^{-2}$. In this paper we demonstrate that non-uniform spherical clouds with an appropriate radial density distribution can reproduce the observed column density distribution. We solve the coupled ionization equilibrium and radiation transfer problem in such clouds and discuss the implications of this model.

2 MODEL CALCULATIONS

2.1 Model Description

We develop a simple model for Lyα clouds below. We model a "typical" absorption system as a spherical hydrogen cloud with a non-uniform density distribution

$$n_H(r) = n_H(0)/(1 + (r/r_c)^2)^p, \tag{2.1}$$

where $n_H(0)$ is the central number density, r_c is the core radius and p is a constant. Since we are only interested in the neutral hydrogen content of a cloud here, the neglect of helium introduces little error (the results including helium will be given in a separate paper).

We adopt the widely held belief that Lyα clouds are photoionized by an isotropic ionizing background produced by integrated UV flux from quasars and young galaxies at high redshifts. Since the optically thin outer envelope of a cloud has little effect on the radiation transfer, we have done our calculations by using a cut-off radius R_{cut} for an absorbing cloud. R_{cut} is smaller than the real cloud size R_c, but we make sure that R_{cut} is big enough so that the final results will not be affected. The geometry of such non-uniform spherical clouds is shown in Fig. 1.

We solve the ionization equilibrium in a cloud:

$$n_{HI} \int_{\nu_L}^{\infty} \frac{4\pi J_\nu \sigma_\nu}{h\nu} d\nu = \alpha_B(HI,T)(n_H - n_{HI})^2, \tag{2.2}$$

where ν_L is the Lyman limit frequency, $\alpha_B(HI,T)$ is the hydrogen recombination coefficient to all excited states, and $\sigma_\nu = \sigma_0(\nu/\nu_L)^{-3}$ with $\sigma_0 = 6.3 \times 10^{-18}\text{cm}^2$ is the hydrogen photoionization cross section. In our calculations we have assumed $\alpha_B(HI,T)$ is a constant throughout the cloud, i.e., the cloud is isothermal. Since $\alpha_B(HI,T)$ varies only slowly with temperature T, this is a fairly good approximation at the optically thin outer parts. At the optically thick parts of an absorbing cloud, hydrogen is mostly neutral and the neutral fraction is independent of the

adopted recombination coefficient. Since the transition region between the optically thin and the optically thick parts is quite narrow, as we will see below, this assumption should not affect our results seriously.

The mean intensity J_ν at radius r is given by

$$4\pi J_\nu = 2\pi J_\nu^0 \int_{-1}^{1} e^{-\tau_\mu(\nu/\nu_L)^{-3}} d\mu, \tag{2.3}$$

where J_ν^0 is the mean intensity of the isotropic ionizing background and $\mu = \cos\theta$ (see Fig. 1). For $\mu < 0$ we have

$$\tau_\mu(r) = \sigma_0 \int_r^{R_{cut}} \frac{n_{HI}(r')dr'}{\sqrt{1-(r/r')^2(1-\mu^2)}}; \tag{2.4a}$$

and for $\mu > 0$ we get

$$\tau_\mu(r) = \sigma_0 \int_{r_{min}}^{r} \frac{n_{HI}(r')dr'}{\sqrt{1-(r/r')^2(1-\mu^2)}} + \sigma_0 \int_{r_{min}}^{R_{cut}} \frac{n_{HI}(r')dr'}{\sqrt{1-(r/r')^2(1-\mu^2)}}, \tag{2.4b}$$

where $r_{min} = r\sqrt{1-\mu^2}$. Let $t^2 = (r'/r_{min}) - 1$, the above two equations can be rewritten as

$$\tau_\mu(r) = 2\,\sigma_0 r\sqrt{1-\mu^2} \int_{\sqrt{1/\sqrt{1-\mu^2}-1}}^{\sqrt{R_{cut}/r_{min}-1}} \frac{1+t^2}{\sqrt{2+t^2}} n_{HI}[r_{min}(1+t^2)]dt \tag{2.5a}$$

for $\mu < 0$, and

$$\begin{aligned}\tau_\mu(r) =& 2\,\sigma_0 r\sqrt{1-\mu^2} \int_0^{\sqrt{1/\sqrt{1-\mu^2}-1}} \frac{1+t^2}{\sqrt{2+t^2}} n_{HI}[r_{min}(1+t^2)]dt \\ &+ 2\,\sigma_0 r\sqrt{1-\mu^2} \int_0^{\sqrt{R_{cut}/r_{min}-1}} \frac{1+t^2}{\sqrt{2+t^2}} n_{HI}[r_{min}(1+t^2)]dt\end{aligned} \tag{2.5b}$$

for $\mu > 0$. Eqs. (2.5a) and (2.5b) have been used in our numerical calculations.

Define A as

$$A = \frac{\int_{\nu_L}^{\infty} \frac{4\pi J_\nu \sigma_\nu}{h\nu} d\nu}{\alpha_B(HI, T)}, \tag{2.6}$$

we get

$$n_{HI} = \frac{n_H}{\left(1 + \frac{A}{2n_H}\right) + \sqrt{\left(1 + \frac{A}{2n_H}\right)^2 - 1}}. \tag{2.7}$$

It is clear that when A decreases n_{HI} increases, and a larger n_{HI} leads to a smaller A value. So we can use an iteration scheme to solve the above ionization equilibrium. For the starting step we simply neglect absorption and A is easily calculated. From Eq. (2.7) n_{HI} is calculated and τ_μ is calculated from Eqs. (2.5a) and (2.5b). Then a better A is evaluated, and a better n_{HI} calculated, and so on. In our practice this scheme is quite stable and the solution converges quickly after 10—20 iterations.

After n_{HI} has been obtained, we calculate the neutral fraction $\log(n_{HI}/n_H)$, the radial optical depth $\tau_r(r)$, and the optical depth at an impact distance b, $\tau_b(b)$. These two optical depths are given by

$$\tau_r(r) = \sigma_0 \int_r^{R_{cut}} n_{HI}(r\prime) dr\prime, \tag{2.8}$$

and

$$\tau_b(b) = 2\sigma_0 \int_0^{(R_{cut}^2 - b^2)^{1/2}} n_{HI}(z) dz. \tag{2.9}$$

Since the probability of obtaining a column density in the range N—$N + dN$ is proportional to the projected area corresponding to b—$b + db$, the neutral column density distribution function can be written as

$$f(N)dN = -Bbdb, \tag{2.10}$$

where B is a normalization constant. This expression implicitly assumes that all absorbing clouds are identical.

2.2 Density Gradient in a Cloud

We first examine the number density distribution $n_H(r)$. At radius $r \gg r_c$, $n_H(r) \propto r^{-2p}$. Since the outer envelope of a cloud is almost completely ionized and $n_{HI} \propto n_H^2$ we have for low column densities $f(N) \propto N^{-\beta}$, where $\beta = (4p+1)/(4p-1)$ (see Rees 1987 and Milgrom 1988). Observationally, Hunstead (1987) found that at $\langle z \rangle$=3.6, $\beta = 1.57 \pm 0.05$ for $\log N > 13.25$; while Carswell (1987) claimed $\beta \sim 1.75$ for $13.5 < \log N < 15.5$. We adopt $\beta = 5/3$ and thus use $p = 1$ in our model calculations.

We are still left with two free parameters, $n_H(0)$ and r_c, in the $n_H(r)$ distribution. We now try to "determine" very roughly the values of these two parameters for our model clouds. Firstly, we observe that the central hydrogen column density, i.e., the maximum neutral hydrogen column density in optically thick case, is given by $N_H(0) \simeq 10^{22} n_H(0)(r_c/\mathrm{kpc})\mathrm{cm}^{-2}$. If we require $N_H(0) \simeq 10^{22}\mathrm{cm}^{-2}$, which is about the maximum observed neutral hydrogen column density in QSO absorption line systems, we get $n_H(0)(r_c/\mathrm{kpc}) \simeq 1$. Secondly we notice that for a small core radius and an input ionizing background $J_\nu^0 = J_0(\nu/\nu_L)^{-s}$, the neutral column density as a function of the impact parameter b is given by

$$N(b) \simeq 2 \times 10^{20} n_H^2(0) \left(\frac{b}{\mathrm{kpc}}\right)^{-3} \left(\frac{r_c}{\mathrm{kpc}}\right)^4 \left(\frac{3+s}{3}\right) \times$$

$$\left(\frac{\alpha_B(HI,T)}{2\times10^{-13}}\right)\left(\frac{J_0}{10^{-21}}\right)^{-1}\mathrm{cm}^{-2} \qquad (2.11)$$

for the optically thin outer envelope. Spectroscopic observations of the gravitationally lensed QSO pair Q2345+007 A, B by Foltz *et al.* (1984) showed that the two lines of sight contained a number of common Lyα absorber at $z_{abs} \simeq 2$. New analyses by McGill (1990), Duncan (1991) and Steidel and Sargent (1991) have shown that the characteristic size of Lyα clouds is not well constrained by the observations and it could be considerably larger than the previously quoted $\sim$ 10kpc. This is further supported by the very recent work of Smette *et al.* (1991) for the Lyα forest in the gravitational lens system UM 673 A, B (z_{em}=2.727, separation 2.″2). They found that all 68 lines present at 5σ in B are present in A; there are only two anti-coincidences (present in A, not in B at 3σ), and these could be a MgII doublet. They also found that the equivalent widths are strongly correlated in the two spectra, essentially proving that the two lines of sight intersect the same clouds. The inferred cloud diameters are in the range $12 < d < 160h_{50}^{-1}$kpc (2σ limits). If we take $J_0 \sim 10^{-21}$ergs sec^{-1}cm^{-2}Hz^{-1}sr^{-1}, a value suggested by studying the so called "proximity effect" in Lyα forest line distribution near quasar emission redshifts (Bajtlik *et al.* 1987 and Lu *et al.* 1991), and require $N(b) = 10^{15}$cm^{-2} at b = 20kpc, we get very roughly, using $n_H(0)(r_c/\mathrm{kpc}) \simeq 1$, $n_H(0) \sim 5\mathrm{cm}^{-3}$ and $r_c \sim 0.2$kpc. We will use these values in most of our models. And we will also do some calculations with different input $n_H(0)$ and r_c values.

2.3 Input Ionizing Spectra and Models

At present we don't know what kind of objects dominated the ionizing background at high redshifts. So we don't know the spectral shape of ionizing field. We do know that absorption produced by QSO absorption line systems is significant, especially at high redshifts. Because of such absorption the resulting integrated spectrum of ionizing background will be quite different from the intrinsic source spectrum (see Chapter Two and Chapter Three). It is then clear that the absorption and the resulting background are coupled together. This makes it very difficult to determine the ionizing spectrum at high frequencies, because we have to model the helium absorption in absorbing clouds to get a self-consistent solution. Fortunately the hydrogen content of a cloud is not very sensitive to the number of high energy photons because of the small ionization cross section of HI at high frequencies. We will try various ionizing spectra below and examine the resulting neutral hydrogen column density distributions.

2.3.1 Power Law Spectra

Quasars have a power law intrinsic spectrum. Here we consider an input power law ionizing background:

$$J_\nu^0 = J_0(\nu/\nu_L)^{-s}. \tag{2.12}$$

We choose $s = 1.5$ for simplicity and call these P15 models. One P15 model, P15-I, is shown in Fig. 2. The input model parameters can be found in Table 1. Notice that the result depends on the ratio $J_0/\alpha_B(HI,T)$, not J_0 or $\alpha_B(HI,T)$ individually. For $J_0/\alpha_B(HI,T) = 5\times10^{-9}\mathrm{ergs\ cm^{-5}Sr^{-1}Hz^{-1}}$, $\alpha_B(HI,T) = 2\times10^{-13}\mathrm{cm^3s^{-1}}$ means

$J_0 = 10^{-21}$ergs s^{-1}cm^{-2}Sr^{-1}Hz^{-1}. The observed data points are from Lanzetta *et al.* (1991). For comparison we have normalized our results to the observations at log$N$=17.6, simply because this column density bin has a small vertical error bar. We see that our simple model fits the observations quite well. And it even reproduces the apparent excess at $N \geq 2 \times 10^{22}$cm^{-2}. We see that a significant deviation from the power law distribution begins at log$N \gtrsim 19.5$ and a "shoulder" is formed around log$N \sim 20.5$.

2.3.2 Black Body Spectra

Spectra of young galaxies, in which there are still many massive main sequence stars, may be approximated by black body radiation. We now consider a black body ionizing field:

$$J_\nu^0 = J_B \frac{2h\nu^3}{c^2} \frac{1}{e^{\frac{h\nu}{kT}} - 1}, \tag{2.13}$$

where T is the black body temperature and J_B is a normalization constant. We calculate for T=3,000K and T=5,000K and call these BB models. Two such BB models, BB-I and BB-II, have been calculated and the results are shown again in Fig. 2. The input parameters are listed in Table 1. The normalization is done by assuming that the total ionizing photons are the same as in the above P15-I model. This leads to $J_B = 887.66 \times 10^{-21}$ for T=3,000K and $J_B = 50.68 \times 10^{-21}$ for T=5,000K. It is equivalent to say that $J_{\nu_L} = 2.4 \times 10^{-21}$ergs s^{-1}cm^{-2}Sr^{-1}Hz^{-1} for T=3,000K and $J_{\nu_L} = 1.2 \times 10^{-21}$ergs s^{-1}cm^{-2}Sr^{-1}Hz^{-1} for T=5,000K. Because of the lack of hard photons the low T model produces a steeper transition from the

ionized region to the neutral core. This results in a slightly larger bump in $f(N)$ distribution around $\log N$=20.5 for the low T model. We see that these two models still fit the observations quite well. This means that the neutral hydrogen column density distribution is not sensitive to the spectral shape of the input ionizing field.

2.3.3 Flat Spectra with a Cut-off

It has been shown in Chapter Two and Chapter Three that for ionizing sources with an intrinsic power law spectrum $L_\nu \propto \nu^{-s}$, because of the Lyman continuum absorptions produced by QSO absorption line systems, the resulting spectral index of ionizing background is tilted from s to $s - 1.5$ near the Lyman limit frequency. So it is of great interest to consider an input flat spectrum with a cut-off at ν_c:

$$J_\nu^0 = \begin{cases} J_0 & \text{if } \nu_L < \nu < \nu_c; \\ 0 & \text{if } \nu > \nu_c. \end{cases} \tag{2.14}$$

We choose the HeI (504$\AA$) or HeII edge (228$\AA$) as the cut-off frequency in our calculations and call these P0C models. Such cut-offs may be relevant if the helium absorption is important and/or if young galaxies dominate the ionizing background (see Miralda-Escudé and Ostriker 1990). Results of five P0C models are shown in Fig. 3. The corresponding input parameters are given in Table 1. We see that for $\lambda_c = 504\AA$ (model P0C-IV) the transition from the optically thin region to the optically thick core is sharp and a sizable bump in $f(N)$ distribution near $\log N$=20.5 results in. We also see from our models P0C-I, P0C-II and P0C-III that increasing the amplitude of the ionizing field at the Lyman limit frequency reduces

the size of the neutral core, but the shape of $f(N)$ curve is almost unaffected. All these three models fit the observations fairly well. In the model P0C-V we have used $n_H(0) = 0.5\text{cm}^{-3}$ and the central hydrogen column density is thus lowered by a factor of 10, we see again that the $f(N)$ curve is similar to the other models. We conclude that the shape of the $f(N)$ curve is a generic feature of the assumed density profile in the absorbing clouds and is not affected significantly by the input ionizing spectra. So the observed $f(N)$ distribution may be used as a diagnostic to determine the density distribution within absorbing clouds.

2.3.4 δ-function Spectra

We have seen from the above that different input ionizing spectra produce somewhat different features near $\log N$=20. Generally the transition from the optically thin region to the optically thick region is sharper and the bump feature is more significant when there are very few high energy photons. Here we consider an extreme case in which all the ionizing photons have the same frequency ν_L, i.e., the ionizing spectrum is a δ-function:

$$J_\nu^0 = J_0 \delta(\nu - \nu_L), \tag{2.15}$$

where J_0 is a normalization constant. Again we choose to normalize to the total ionizing photons of our model P15-I. This normalization leads to $J_0 = 2.2 \times 10^{-6}$ergs $\text{s}^{-1}\text{cm}^{-2}\text{Sr}^{-1}$. We call these D models. One such model, D-I, is shown in Fig. 2. The input parameters are given in Table 1. As expected the bump feature is quite remarkable and the fit to the observations is poor at $\log N \sim 19.5$.

2.4 Uniform Clouds

If we let r_c be very large in our density distribution $n_H(r)$, we get a uniform cloud. To understand the $f(N)$ distribution for uniform clouds we first consider the case in which all clouds are neutral. The neutral column density corresponding to an impact distance b is $N = 2n_{HI}(R_c^2 - b^2)^{1/2}$ for a uniform neutral cloud, where R_c is the radius of a cloud. If all clouds are the same we get

$$f(N) \propto \begin{cases} N & \text{for } N < N_{max}; \\ 0 & \text{for } N > N_{max}. \end{cases} \tag{2.16}$$

In the above expression $N_{max} = 2R_c n_{HI}$ is the maximum neutral column density. Therefore we expect that the neutral cores of optically thick clouds will produce a $f(N) \propto N$ at high N end and the ionized outer parts will also lead to a $f(N) \propto N$ for low column densities. To see how the transition region joins the high and low N parts on the $f(N)$ curve we have calculated four uniform models. We call these U models. In all these models we have used a flat spectrum with a cut-off at λ_c for the input ionizing field. Our results are shown in Fig. 4. The input parameters can be found in Table 1. All our four models have the same normalization constant B. These curves confirm our speculation about the slop at both high and low N ends. We see that the calculated shape of $f(N)$ curves for uniform clouds is very different from what is observed. Thus many kinds of clouds with different sizes and densities are needed, and their relative space densities have to be fine-tuned in order to reproduce the observations. We feel that such uniform cloud model is highly unlikely.

3 DISCUSSION

We have seen from §2 that our simple models fit the observations quite well. But we want to point out that in the above calculations we have assumed that all absorbing clouds are the same. This certainly is an oversimplification. There may exist many kinds of clouds with different masses and diameters. But as long as these clouds are optically thick at the center and have an appropriate density profile, they all produce a similar column density distribution, and the shape of the resulting $f(N)$ distribution will not be very different. Deviation from a single power law distribution does occur because the central parts of a cloud are neutral while the outer parts are ionized. But we see that the "bump" appears at $\log N \sim 20.5$, instead of at $\log N \sim 17$ as some people had claimed. Our simple model thus explains the overall power law shape of $f(N)$ and the apparent excess at $N \geq 2 \times 10^{20}\mathrm{cm}^{-2}$ quite naturally. Our results also support the speculation made a few years ago by Tytler (1987) that all QSO absorption lines have the same origin and belong to a single population. In this new picture the Lyα forest lines are produced when going through ionized outer envelopes of absorbing clouds, while the damped Lyα systems arise from neutral cores. Similar conclusions have also been reached by Murakami and Ikeuchi (1990) in a recent paper.

We now turn to discuss the consequences implied by our model. First we notice that the hydrogen mass of a cloud is given by

$$M_H \simeq 3 \times 10^8 n_H(0) \left(\frac{r_c}{\mathrm{kpc}}\right)^2 \left(\frac{R_c}{\mathrm{kpc}}\right) M_\odot, \tag{3.1}$$

for $p = 1$ and $R_c \gg r_c$. For $n_H(0) = 5\text{cm}^{-3}$, $r_c = 0.2\text{kpc}$ and $R_c = 50\text{kpc}$ we get $M_H \simeq 3 \times 10^9 M_\odot$, similar to that of the present day dwarf galaxies.

We then estimate Ω_0^c, the contribution of such clouds to the present day cosmological density parameter. To do this we first evaluate the comoving space density of absorbing clouds at redshift z, $n_{com}(z)$. For simplicity we again assume all clouds are identical. Let dn/dz be the number of systems with neutral column density larger than some criterion value N_c in unit redshift interval, and let σ be the absorption cross section for producing $N \geq N_c$, we then get

$$n_{com}(z) = \frac{dn/dz}{\sigma(dl/dz)} \frac{1}{(1+z)^3}, \tag{3.2}$$

where dl is the proper length interval corresponding to dz. dl/dz depends on the cosmological models used. For the standard Friedmann cosmology ($\Lambda = 0$) with a density parameter Ω_0, we have

$$\frac{dl}{dz} = \frac{c}{H_0}(1+z)^{-2}(1+\Omega_0 z)^{-1/2}. \tag{3.3}$$

In a flat inflation model with a non-zero cosmological constant, we get

$$\frac{dl}{dz} = \frac{c}{H_0}\Omega_0^{-1/2}(1+z)^{-1}\left[(1+z)^3 + \Omega_0^{-1} - 1\right]^{-1/2}. \tag{3.4}$$

The above expression can be obtained by differentiating Peebles' (1984) Eq. (7) relative to z. According to Sargent *et al.* (1989) the number of clouds per unit redshift interval, with Lyman limit optical depth $\tau \geq 1.5$, is ~ 2 at redshift $z \simeq 3$. Let $r_{1.5}$ be the impact distance corresponding to a $\tau = 1.5$, we have $\sigma = \pi r_{1.5}^2$. For

our model P0C-I $r_{1.5} \simeq 4$kpc. Adopting this value we get, at $z = 3$, $n_{com}(z) \simeq 7h\mathrm{Mpc}^{-3}$ and $4h\mathrm{Mpc}^{-3}$ for $\Omega_0 = 1$ and 0.2, respectively, in the standard Friedmann model; $n_{com}(z) \simeq 3h\mathrm{Mpc}^{-3}$ for $\Omega_0 = 0.2$ in a flat inflation model with a non-zero cosmological constant. In these expressions $h = H_0/(100\mathrm{km\ sec}^{-1}\mathrm{Mpc}^{-1})$. These values can be compared with the local number density of dwarf galaxies. In the above three cases we thus have $\Omega_0^c h \sim 0.023$, 0.013, and $0.010(M_H/10^9\mathrm{M}_\odot)$ from QSO absorption line systems at $z = 3$. For comparison the theory of Big Bang nucleosynthesis predicts $\Omega_b h^2 \lesssim 2.2 \times 10^{-2}$, where Ω_b is the baryon density in units of the critical density (Kawano *et al.* 1988). We see that at $z = 3$ it is possible that most baryons took the form of QSO absorption line systems.

We can also estimate the volume filling fraction, f_c, for our model clouds. We have, at redshift z,

$$f_c = \frac{4\pi}{3} R_c^3 n_{com}(z)(1+z)^3. \tag{3.5}$$

For the three cases considered above we get $f_c \sim 0.23$, 0.13 and $0.10h(R_c/50\mathrm{kpc})^3$ at $z = 3$. We see that at $z = 3$ our model clouds filled a large fraction of the universe.

We must point out that due to the simplifications used in this paper the above estimates are necessarily very crude. Although it has been demonstrated that our results are compatible with current observations and theories, the adopted model parameters are by no means unique. Different sets of parameters might lead to very different conclusions about M_H, Ω_0^c and f_c. A complete model should also address

the effects due to a distribution of cloud masses and sizes which we currently don't know. Future observations are needed especially to get better determination of the sizes of absorbing clouds.

We also point out that since cloud mass M_H is small in our models, its gravity cannot confine the hot outer envelope. These clouds may be confined by cold dark matter minihalos as suggested by Rees (1986) and Ikeuchi (1986) or they may be undergoing free expansion when the ionization of the universe occurred (Bond *et al.* 1988). Whether such mechanisms can produce the right density profile across an absorbing cloud remains to be investigated. In such investigations it is necessary to include thermodynamics and hydrodynamics.

We notice that the Lyα forest lines and the stronger metal containing Lyman limit systems evolve quite differently (Hunstead 1987; Sargent *et al.* 1989). This cannot be due to the evolution of ionizing background alone. It is true that the decrease of J_ν^0 at low redshift (see Bechtold *et al.* 1987) increases the neutral core radius and thus we would expect to see more high N systems than predicted by a non-evolving model. But at the same time the absorption cross sections for producing low column density lines also increase and the resulting $f(N)$ distribution will not be changed significantly. This point has already been demonstrated by our model calculations in §2. Thus the low N systems and the stronger lines would evolve in a similar way, inconsistent with the observations. Clearly we need some other mechanisms to produce different evolution laws for low N and high N systems.

One possibility is that because of the increase of neutral core radius at low redshift, an absorbing cloud might become more vulnerable to gravitational instability, as pointed out by Murakami and Ikeuchi (1990). The central parts of a cloud may collapse, fragment, and form stars. In this way the observed clustering of strong line systems can be explained and there are metal lines associated with these strong lines. It is also possible that the absorbing clouds may merge together to form larger systems at later times. They could evolve into dwarf galaxies, or/and even normal galaxies which we observe today. Still another possibility is that the ionized outer envelope is undergoing free expansion, as we have mentioned before. This reduces n_H within the envelope and leads to a decrease of detectable absorption systems along a line of sight at low redshift. There is one more piece of evidence which favors this freely expanding envelope picture (actually it is not that free since the expansion is against gravity of a cloud). Recent observations by Pettini *et al.* (1990) indicate that very low-N Lyα forest lines have small velocity widths (but see Peacock 1991 and Carswell *et al.* 1991). The temperatures implied by these lines are less than 10^4K and cannot be reconciled with photoionization. But Duncan *et al.* (1991) have shown that these observations can be understood as the result of expansion cooling against some confining agent (gravity or external pression).

ACKNOWLEDGMENTS

This work was partly supported by NSF Grant AST84-51725. L. Z. thanks a Li Ming scholarship award.

REFERENCES

Bajtlik, S., Duncan, R. C. & Ostriker, J. P., 1987. *Astrophys. J.*, **327**, 570.

Bechtold, J., 1987. In: *High Redshift and Primeval Galaxies*, eds. J. Bergeron, D. Kunth, B. Rocca-Volmerange, and J. Tran Thanh Van (France: Editions Frontières), p397.

Bechtold, J., Weymann, R. J., Lin, Z. & Malkan, M. A., 1987. *Astrophys. J.*, **315**, 180.

Bond, J. R., Szalay, A. S. & Silk, J., 1988. *Astrophys. J.*, **324**, 627.

Carswell, R. F., 1987. In: *Quasar Absorption Lines*, p91, eds. Blades, C. *et al.*, Cambridge University Press.

Carswell, R. F., Lanzetta, K. M., Parnell, H. C. & Webb, J. K., 1991. *Astrophys. J.*, **371**, 36.

Duncan, R. C., 1991. *Astrophys. J. Lett.*, **375**, L41.

Duncan, R. C. & Ostriker, J. P., 1988. unpublished preprint.

Duncan, R. C., Vishniac, E. T. & Ostriker, J. P., 1991. *Astrophys. J. Lett.*, **368**, L1.

Foltz, C. B., Weymann, R. J., Roser, H. J. & Chaffee, F. H., 1984. *Astrophys. J. Lett.*, **281**, L1.

Hunstead, R. W., 1987. In: *Quasar Absorption Lines*, p71, eds. Blades, C. *et al.*, Cambridge University Press.

Ikeuchi, S., 1986. *Astrophs. Space Sci.*, **118**, 509.

Ikeuchi, S. & Ostriker, J. P., 1986. *Astrophys. J.*, **301**, 522.

Kawano, L., Schramm, D. & Steigman, G., 1988. *Astrophys. J.*, **327**, 750.

Lanzetta, K. M., Wolfe, A. M., Turnshek, D. A., Lu, L., McMahon, R. G. & Harzard, C., 1991. *Astrophys. J. Suppl. Ser.*, **77**, in press.

Lu, L., Wolfe, A. M. & Turnshek, D. A., 1991. *Astrophys. J.*, **367**, 19.

McGill, C., 1990. *Mon. Not. R. astr. Soc.*, **242**, 544.

Milgrom, M., 1988. *Astron. Astrophys.*, **202**, L9.

Miralda-Escudé, J. & Ostriker, J. P., 1990. *Astrophys. J.*, **350**, 1.

Murakami, I. & Ikeuchi, S., 1990. *Publ. Astron. Soc. Japan*, **42**, L11.

Ostriker, P. J. & Ikeuchi, S., 1983. *Astrophys. J. Lett.*, **268**, L63.

Peacock, J., 1991. *Nature*, **349**, 190.

Peebles, P. J. E., 1984. *Astrophys. J.*, **284**, 439.

Pettini, M., Hunstead, R. W., Smith, L. J. & Mar, D. P., 1990. *Mon. Not. R. astr. Soc.*, **246**, 545.

Rees, M. J., 1986. *Mon. Not. R. astr. Soc.*, **218**, 25p.

Rees, M. J., 1987. In: *Quasar Absorption Lines*, p107, eds. Blades, C. *et al.*, Cambridge University Press.

Sargent, W. L. W., Steidel, C. C. & Boksenberg, A., 1989. *Astrophys. J. Suppl. Ser.*, **69**, 703.

Sargent, W. L. W., Young, P. J., Boksenberg, A. & Tytler, D., 1980. *Astrophys. J. Suppl. Ser.*, **42**, 41.

Smette, A., Surdej, J., Shaver, P., Foltz, C. B., Chaffee, F. H., Weymann, R. J., Williams, R. E. & Magain, P., 1991. In: *Proceedings of the ESO Mini-Workshop on Quasar Absorption Lines*, ESO scientific Report #9.

Steidel, C. C. & Sargent, W. L. W., 1991. *Astron. J.*, in press.

Tytler, D., 1987. *Astrophys. J.*, **321**, 49.

Table 1. Model parameters.

Models	$n_H(0)$ (cm^{-3})	r_c (kpc)	R_{cut} (kpc)	$J_{\nu_L}/\alpha_B(HI,T)$ (ergs cm^{-5} Sr^{-1} Hz^{-1})	T (K)	$\lambda_c(\AA)$
P15-I	5	0.2	23	5.0×10^{-9}		
BB-I	5	0.2	23	1.2×10^{-8}	3×10^4	
BB-II	5	0.2	23	6.0×10^{-9}	5×10^4	
D-I	5	0.2	20			
P0C-I	5	0.2	23	5×10^{-9}		228
P0C-II	5	0.2	15	2.5×10^{-8}		228
P0C-III	5	0.2	30	1×10^{-9}		228
P0C-IV	5	0.2	23	5×10^{-9}		504
P0C-V	0.5	0.2	4	5×10^{-9}		228
U-I	0.05		5	5×10^{-9}		228
U-II	0.05		5	5×10^{-9}		504
U-III	0.05		3	5×10^{-9}		228
U-IV	0.03		5	5×10^{-9}		228

FIGURE CAPTIONS

Figure 1. Geometry of non-uniform spherical models.

Figure 2. (a) $\log(n_{HI}/n_H)$ *vs.* r for models P0C-I (solid line), P15-I (dashed line), BB-I (dot-dash-dot-dash line), BB-II (dotted line) and D-I (dash-dot-dot-dot line); (b) $\log(\tau_r(r))$ *vs.* r; (c) $\log(\tau_b(b))$ *vs.* b; (d) $\log(f(N))$ *vs.* $\log(N)$, the observed data points are from Lanzetta *et al.* (1991).

Figure 3. (a) $\log(n_{HI}/n_H)$ *vs.* r for models P0C-I (solid line), P0C-II (dashed line), P0C-III (dot-dash-dot-dash line), P0C-IV (dotted line) and P0C-V (dash-dot-dot-dot line); (b) $\log(\tau_r(r))$ *vs.* r; (c) $\log(\tau_b(b))$ *vs.* b; (d) $\log(f(N))$ *vs.* $\log(N)$, the observed data points are from Lanzetta *et al.* (1991).

Figure 4. (a) $\log(n_{HI}/n_H)$ *vs.* r for models U-I (solid line), U-II (dashed line), U-III (dot-dash-dot-dash line) and U-IV (dotted line); (b) $\log(\tau_r(r))$ *vs.* r; (c) $\log(\tau_b(b))$ *vs.* b; (d) $\log(f(N))$ *vs.* $\log(N)$.

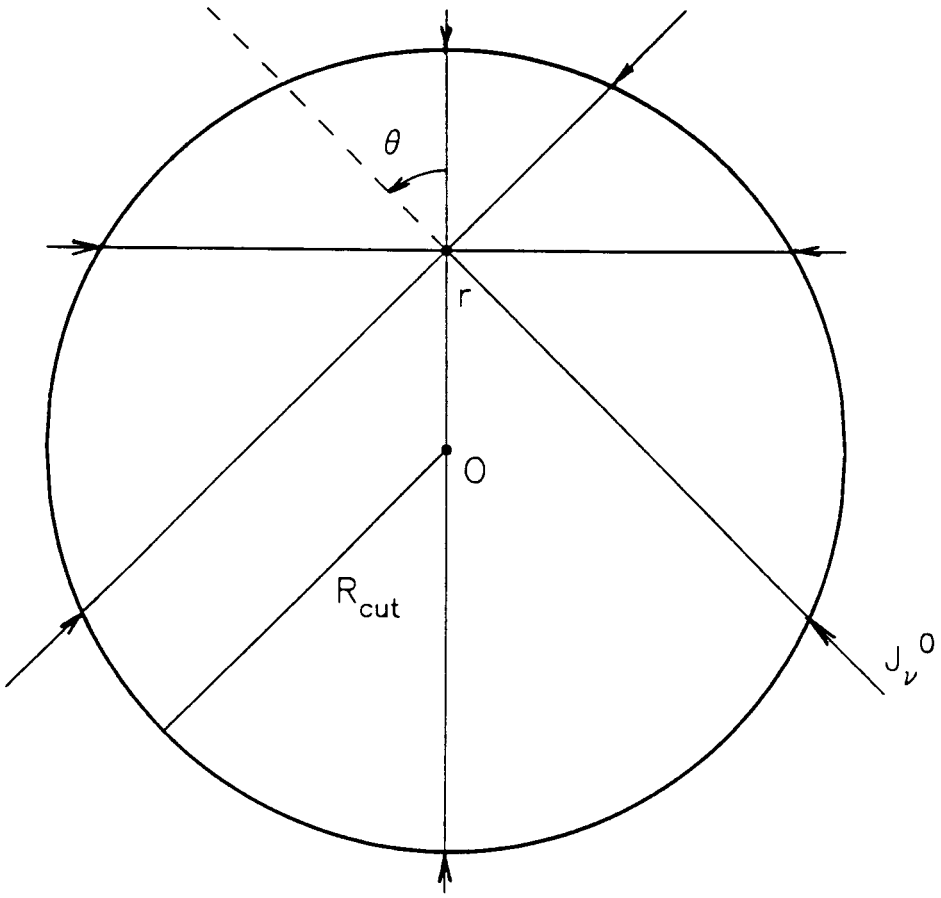

Figure 1

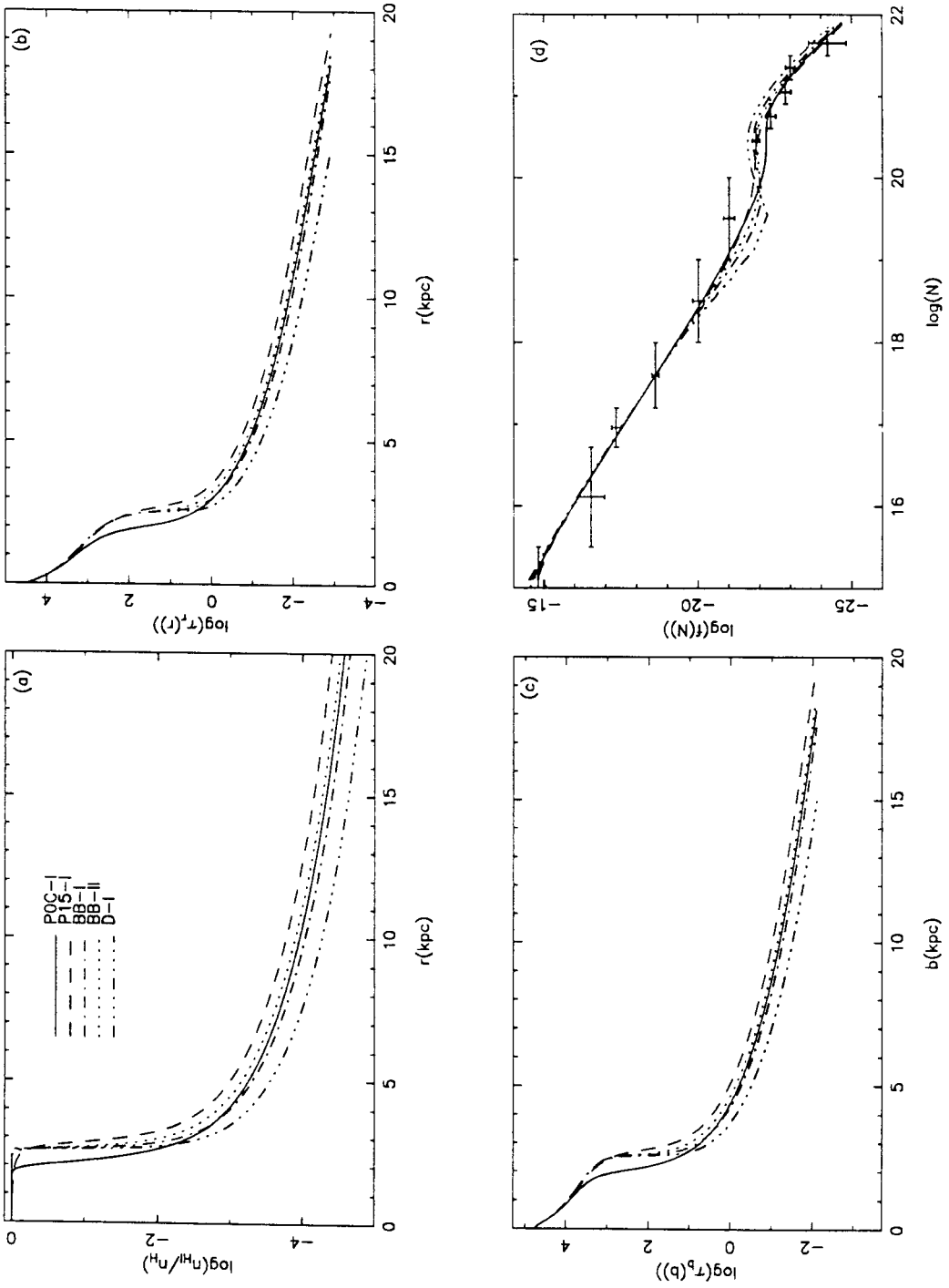
(a)
(b)
(c)
(d)
POC
P15
BB-I
BB-II
D-I
log(n_HI/n_H)
log(τ_r(r))
log(τ_b(b))
log(f(N))
r(kpc)
b(kpc)
log(N)

Figure 2

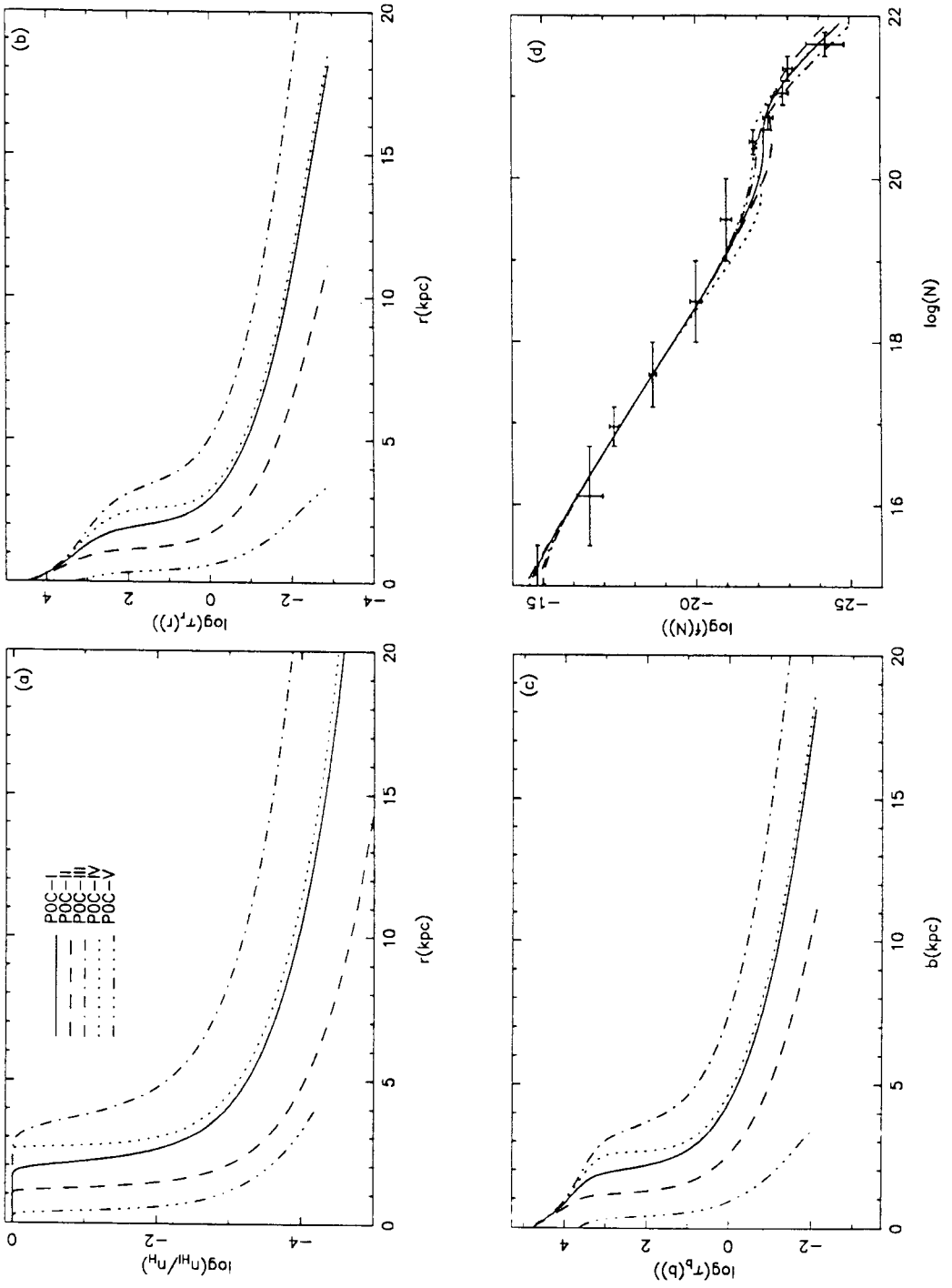
(a)
(b)
(c)
(d)
POC−I
POC−II
POC−III
POC−IV
POC−V
log(n_HI/n_H)
log(τ_r(r))
log(τ_b(b))
log(f(N))
r(kpc)
b(kpc)
log(N)

Figure 3

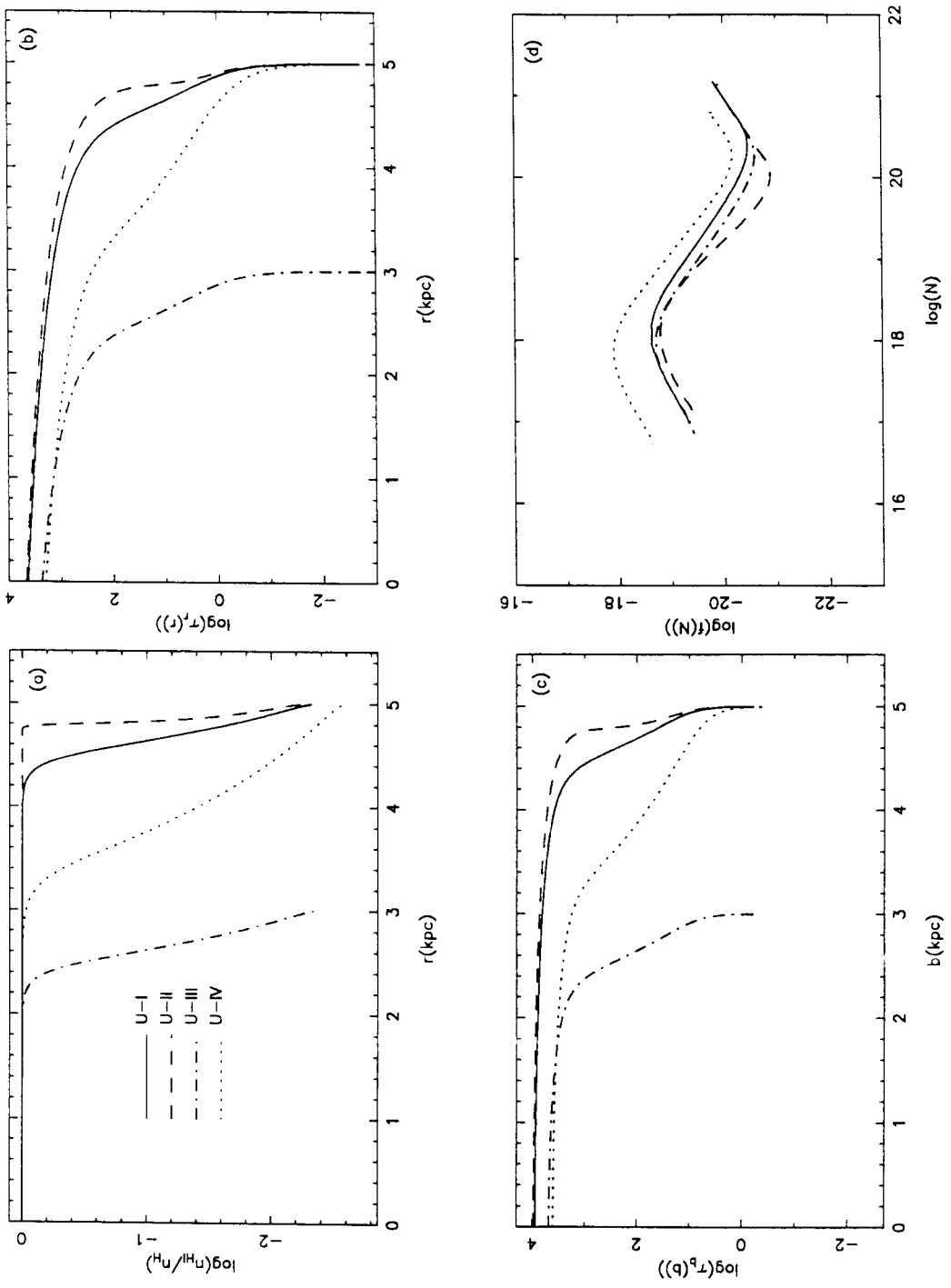
(a)
(b)
(c)
(d)
log(n_HI/n_H)
log(τ_r(r))
log(τ_b(b))
log(f(N))
r(kpc)
r(kpc)
b(kpc)
log(N)
U–I
U–II
U–III
U–IV

Figure 4

CHAPTER SIX

THE IONIZATION STRUCTURE OF QSO Lyα CLOUDS

SUMMARY. In this paper we present an iteration scheme to solve the coupled ionization balance and radiation transfer problem (the "inverse HII region" problem) for a non-uniform spherical cloud, which contains both hydrogen and helium and is exposed to an isotropic ionizing field. We calculate the HI, HeI and HeII abundances as a function of radius r. We explore the variation of the ionization structure under different input ionizing field spectra. As expected the HeI and HeII abundances are sensitive to the input ionizing flux at short wavelengths. We apply this model to the QSO Lyα clouds and discuss how to get a self-consistent spectral shape for the ionizing background.

1 INTRODUCTION

The HI continuum absorption produced by the QSO absorption line systems is significant, especially for high redshift objects and for the ionizing field at early epochs (Chapter Two). It significantly reduces the magnitude of the Lyman limit frequency intensity of the ionizing field and at the same time tilts the intrinsic source radiation spectrum (Chapter Two). Such absorption effect is easily calculated since we know from spectroscopic observations the HI column density distribution and the line number density evolution of QSO absorption line systems with cosmic time. The situation is very different for the absorptions produced by HeI and HeII in the same absorption systems, because these ionic species have not yet been directly observed.

There are at least two reasons why we should bother to model HeI and HeII absorptions. The first one is that with the launch of the *Hubble Space Telescope* we can now probe distant ($z_{em} \geq 3.1$) quasars at wavelengths shortward of the HeII Lyα emissions. This will enable us to carry out the HeII Gunn-Peterson test and to study the HeII Lyα forest lines (Møller and Jakobsen 1990). In order to predict how significant the HeII Lyα line blanketing is, we need the knowledge of the ionizing field at short wavelengths, i.e., the intensities at frequencies larger than the threshold energy $h\nu = 54.4$eV. Even if we have detected the HeII Gunn-Peterson absorption produced by smoothly distributed intergalactic medium (IGM) in the future, we also need this knowledge to translate the observed IGM n_{HeII} to the

IGM mass density.

The second reason for modeling the HeI and HeII absorptions in QSO absorption line systems is to explain the observed relative ionic column densities in QSO metal absorption line systems. In some models these systems are assumed to have been photoionized by the intergalactic ionizing background. Steidel and Sargent (1989) and Steidel (1990) have used photoionization models to show that the resulting relative column densities of the most abundant ions are very sensitive to the input spectral shape of ionizing radiation. They have demonstrated that the "soft" spectra such as those expected for young, star-forming galaxies will lead to the result that metal line systems are dominated by low-ionization species, in clear contrary with the observations. Thus, the observed relative ionic column densities in QSO metal line systems may be used to set some constraints for the dominating ionizing sources at high redshifts. To achieve this goal, however, we must first understand the frequency dependent absorptions to the ionizing flux produced by HI, HeI and HeII in QSO absorption line systems. Given the facts that the threshold energy for ionizing CIII is 47.9eV and the ionization potential of SiIII is 33.5eV, it is very important to get a good estimate for the HeII continuum absorption.

There are some simplified calculations which relate the HeI and HeII column densities to the observed HI column density by assuming the absorbing clouds are either fully neutral or highly photoionized. In some cases the clouds are also assumed to be uniform (Miralda-Escudé and Ostriker 1990, 1991; Giroux and Shapiro 1991;

Madau 1991). We have seen from Chapter Five that our non-uniform spherical cloud model reproduces the observed HI column density distribution quite well. So it is of great interest to see how this model predicts for the corresponding HeI and HeII column density distributions when helium is added in. In this paper we develop an iteration scheme to solve for the ionization structure within our model absorbing clouds and explore its variation under different input ionizing field spectra.

2 MODEL DESCRIPTION

2.1 Physical Processes and the Ionization Equilibrium

We develop a simple model for Lyα clouds below. We model a "typical" absorption system as a spherical hydrogen and helium gas cloud with a non-uniform total H density distribution

$$n_H(r) = \frac{n_H(0)}{\left[1 + \left(\frac{r}{r_c}\right)^2\right]^p}, \tag{2.1}$$

where $n_H(0)$ is the central number density, r_c is the core radius and p is a constant. From Chapter Five we see that the observed HI column density distribution of the QSO Lyα clouds requires $p \simeq 1$, so we use $p = 1$ in our calculations. The total helium number density is assumed here to be $n_{He} = n_H/12$.

We adopt the widely held belief that Lyα clouds are photoionized by an isotropic ionizing background produced by integrated UV flux from quasars and young galaxies at high redshifts. Since the optically thin outer envelope of a cloud

has little effect on the radiation transfer, we have done our calculations by using a cut-off radius R_{cut} for an absorbing cloud. R_{cut} is smaller than the real cloud size R_c, but we make sure that R_{cut} is big enough so that the final results will not be affected. The geometry of such non-uniform spherical clouds is shown in Fig. 1.

The ionization equations for H and He are straightforward to write down in the on-the-spot approximation, though complicated in detail. We have

$$\begin{aligned} & n_{HI}J_{HI} + y\, n_{HeII}n_e\alpha_1(HeI) + 0.96n_{HeII}n_e\alpha_B(HeI) + \\ & \quad 0.26\alpha_B(HeII)n_e n_{HeIII} + \frac{n_{HI}\alpha_1(HeII)n_e n_{HeIII}}{n_{HI}+16.2n_{HeI}+16n_{HeII}} + \\ & \quad \frac{[1-X(HeII)]n_{HI}\alpha_B(HeII)n_e n_{HeIII}}{n_{HI}+12.2n_{HeI}} + \\ & \quad 0.68X(HeII)\alpha_B(HeII)n_e n_{HeIII} + \\ & \quad \frac{0.74n_{HI}X(HeII)\alpha_B(HeII)n_e n_{HeIII}}{n_{HI}+8.7n_{HeI}} = n_p n_e \alpha_B(HI), \end{aligned} \tag{2.2a}$$

$$\begin{aligned} & n_{HeI}J_{HeI} + (1-y)n_{HeII}n_e\alpha_1(HeI) + \frac{16.2n_{HeI}\alpha_1(HeII)n_e n_{HeIII}}{n_{HI}+16.2n_{HeI}+16n_{HeII}} + \\ & \quad \frac{12.2[1-X(HeII)]n_{HeI}\alpha_B(HeII)n_e n_{HeIII}}{n_{HI}+12.2n_{HeI}} + \\ & \quad \frac{6.47n_{HeI}X(HeII)\alpha_B(HeII)n_e n_{HeIII}}{n_{HI}+8.7n_{HeI}} = n_e n_{HeII}\alpha_A(HeI), \end{aligned} \tag{2.2b}$$

and

$$n_{HeII}J_{HeII} + \frac{16n_{HeII}\alpha_1(HeII)n_e n_{HeIII}}{n_{HI}+16.2n_{HeI}+16n_{HeII}} = n_e n_{HeIII}\alpha_A(HeII). \tag{2.2c}$$

In the above equations

$$J_{HI} = \int_{\nu_L}^{\infty} \frac{4\pi J_\nu \sigma_\nu(HI)}{h\nu} d\nu, \tag{2.3a}$$

$$J_{HeI} = \int_{\nu_2}^{\infty} \frac{4\pi J_\nu \sigma_\nu(HeI)}{h\nu} d\nu, \tag{2.3b}$$

and

$$J_{HeII} = \int_{4\nu_L}^{\infty} \frac{4\pi J_\nu \sigma_\nu(HeII)}{h\nu} d\nu. \tag{2.3c}$$

The Lyman limit frequency has been denoted as ν_L. $h\nu_2 = 24.6$eV is the threshold energy for ionizing HeI. The mean intensity $J_\nu(r)$ at radius r is given by

$$4\pi J_\nu(r) = 2\pi J_\nu^0 \int_{-1}^{1} e^{-\tau_\nu(r,\mu)} d\mu, \tag{2.4}$$

where J_ν^0 is the intensity of the incident isotropic ionizing background and $\tau_\nu(r,\mu)$ is the optical depth at frequency ν measured from R_{cut} to r along the direction $\mu = \cos\theta$ (see Fig. 1). The optical depth per unit length is

$$\frac{d\tau_\nu}{dl} = \begin{cases} n_{HI}\sigma_\nu(HI) & \text{if } 13.6\text{eV} < h\nu < 24.6\text{eV}; \\ n_{HI}\sigma_\nu(HI) + n_{HeI}\sigma_\nu(HeI) & \text{if } 24.6\text{eV} < h\nu < 54.4\text{eV}; \\ n_{HI}\sigma_\nu(HI) + n_{HeI}\sigma_\nu(HeI) + & \\ \quad n_{HeII}\sigma_\nu(HeII) & \text{if } h\nu > 54.4\text{eV}. \end{cases} \tag{2.5}$$

The photoionization cross-sections for HI, HeI and HeII have been taken as (Osterbrock 1989) $\sigma_\nu(HI) = 6.3\times10^{-18}(\nu/\nu_L)^{-3}\text{cm}^2$, $\sigma_\nu(HeI) = 7.8\times10^{-18}(\nu/\nu_2)^{-2}\text{cm}^2$ and $\sigma_\nu(HeII) = 1.58\times10^{-18}(\nu/4\nu_L)^{-3}\text{cm}^2$. In our calculations we have assumed that the various recombination coefficients are constant throughout the cloud, i.e., the cloud is isothermal. The following values have been adopted which are accurate for cloud temperature $T = 2\times10^4$K: $\alpha_B(HI) = 1.43\times10^{-13}$, $\alpha_A(HeI) = 2.69\times10^{-13}$, $\alpha_B(HeI) = 1.55\times10^{-13}$, $\alpha_1(HeI) = 1.14\times10^{-13}$, $\alpha_A(HeII) = 1.36\times10^{-12}$, $\alpha_B(HeII) = 9.08\times10^{-13}$, and $\alpha_1(HeII) = 4.56\times10^{-13}$, all in units of $\text{cm}^3\text{sec}^{-1}$. The electron number density is $n_e = n_p + n_{HeII} + 2n_{HeIII}$.

The detailed descriptions of the physical processes involved in this problem can be found in Hummer and Seaton (1964) and Osterbrock (1989). Here we only briefly explain the ionization terms due to the ionizing photons produced by the recombinations to form HeI and HeII. The second term in Eq. (2.2a) and the second term in Eq. (2.2b) are due to the photons emitted in recombinations to the ground level of HeI. These photons have energies just above $h\nu_2$ which can ionize both HI and HeI. The fraction absorbed by H is (Osterbrock 1989)

$$y = \frac{n_{HI}}{n_{HI} + 7.33 n_{HeI}}. \tag{2.6}$$

The third term in Eq. (2.2a) is due to the ionizing photons emitted in recombinations to the excited levels of HeI. The fifth term in Eq. (2.2a), the third term in Eq. (2.2b) and the second term in Eq. (2.2c) are due to the recombination to the ground level of HeII. The photons are emitted with energies just above 54.4eV, capable of ionizing HI, HeI and HeII. The fourth term in Eq. (2.2a) comes from the HeII Balmer continuum emission. In this process the recombination photons have energies concentrated just above $h\nu_L = 13.6$eV. The sixth term in Eq. (2.2a) and the fourth term in Eq. (2.2b) are due to the recombinations that lead to $2\ ^2P$, resulting in HeII Lyα emission with $h\nu = 40.8$eV. We have assumed that among the recombinations to all the excited levels a fraction of $1 - X(HeII)$ ends up populating $2\ ^2P$. The other $X(HeII)$ fraction leads to population of $2\ ^2S$, resulting in HeII $2\ ^2S \rightarrow 1\ ^2S$ two-photon emission for which $h\nu' + h\nu'' = 40.8$eV. For the two-photon emission process, the photons with energies between 13.6eV and 24.6eV can only ionize HI (the seventh term in Eq. (2.2a)), while those photons with $h\nu > 24.6$eV

can ionize both HI and HeI (the eighth term in Eq. (2.2a) and the fifth term in Eq. (2.2b)). In calculating the fractions absorbed by HI and HeII we have used the approximate form of the two-photon spectrum given by Hummer and Seaton (1964). In our calculation we have adopted $X(HII) = 0.31$ (Hummer and Seaton 1964; Osterbrock 1989).

2.2 Solving the Ionization Equations

We adopt the following broken power law form for the incident isotropic ionizing field:

$$J_\nu^0 = \begin{cases} J_1^0 \left(\frac{\nu}{\nu_L}\right)^{-s_1} & \text{for } \nu_L < \nu < \nu_2; \\ J_2^0 \left(\frac{\nu}{\nu_2}\right)^{-s_2} & \text{for } \nu_2 < \nu < 4\nu_L; \\ J_3^0 \left(\frac{\nu}{4\nu_L}\right)^{-s_3} & \text{for } 4\nu_L < \nu < \nu_c; \\ 0 & \text{for } \nu > \nu_c. \end{cases} \tag{2.7}$$

The ionizing spectrum is cut off at ν_c. Now the problem is well defined: we want to find out $n_{HI}(r)$, $n_{HeI}(r)$ and $n_{HeII}(r)$ as functions of radius r.

To solve the coupled ionizing equations we first make a few simplifications. We drop all the terms involving n_{HeIII} in Eqs. (2.2a) and (2.2b). We also drop the second term in Eq. (2.2c) and replace $\alpha_A(HeII)$ by $\alpha_B(HeII)$, i.e., we assume all photons emitted in recombinations to HeII ground level are absorbed by HeII "on the spot". We thus have the simplified set of the ionization equations:

$$n_{HI}J_{HI} + y\,n_{HeII}n_e\alpha_1(HeI) + 0.96n_{HeII}n_e\alpha_B(HeI) = n_p n_e \alpha_B(HI), \tag{2.8a}$$

$$n_{HeI}J_{HeI} + (1-y)n_{HeII}n_e\alpha_1(HeI) = n_e n_{HeII}\alpha_A(HeI), \tag{2.8b}$$

and

$$n_{HeII}J_{HeII} = n_e n_{HeIII}\alpha_B(HeII). \tag{2.8c}$$

The dropped terms may be added as small perturbations after the above equations have been solved.

The coupled ionization equations with the incident isotropic ionizing field as boundary condition at R_{cut} can be solved by using an iteration procedure. For the starting step we assume the cloud is highly ionized and take $n_e = 7n_H/6$. We neglect the optical depths at all frequencies and J_{HI}, J_{HeI} and J_{HeII} are thus easily obtained. We calculate the first step number densities by using the following expressions:

$$n_{HI} = \frac{n_H}{1 + J_{HI}/[n_e\alpha_B(HI)]}, \tag{2.9}$$

$$n_{HeI} = \frac{n_{He}}{1 + JJ0}, \tag{2.10}$$

and

$$n_{HeII} = \frac{JJ0}{1 + JJ0} \times \frac{n_{He}}{1 + J_{HeII}/[n_e\alpha_B(HeII)]}, \tag{2.11}$$

where

$$JJ0 \equiv \frac{J_{HeI}}{n_e\alpha_A(HeI)}\left[1 + \frac{J_{HeII}}{n_e\alpha_B(HeII)}\right]. \tag{2.12}$$

After this the electron number density $n_e = 7n_H/6 - (n_{HI} + 2n_{HeI} + n_{HeII})$ and y are calculated by using the first step n_{HI}, n_{HeI} and n_{HeII}. The optical depth $\tau_\nu(r, \mu)$ can be calculated by integrating Eq. (2.5) along the direction μ. Then the new J_{HI}, J_{HeI} and J_{HeII} can be obtained by integrating over ν and μ. In our practice the directional integration is performed using a twenty-point Gaussian quadrature

procedure. Finally from the ionization equations the new number densities are calculated. In this step we use the following equations:

$$n_{HI} = \frac{n_H}{1 + J_{HI}/[n_e \alpha_B(HI)]} \left[1 - \frac{n_{HeII}}{n_H \alpha_B(HI)} [y\alpha_1(HeI) + 0.96\alpha_B(HeI)]\right], \tag{2.13}$$

$$n_{HeI} = \frac{n_{He}}{1 + JJ1}, \tag{2.14}$$

and

$$n_{HeII} = \frac{JJ1}{1 + JJ1} \times \frac{n_{He}}{1 + J_{HeII}/[n_e \alpha_B(HeII)]}, \tag{2.15}$$

where

$$JJ1 = \frac{J_{HeI}}{n_e \alpha_A(HeI)} \times \frac{1 + J_{HeII}/[n_e \alpha_B(HeII)]}{1 - (1 - y)\alpha_1(HeI)/\alpha_A(HeI)}. \tag{2.16}$$

It is very important to use the above expressions since they guarantee $0 \leq n_{HI} \leq n_H$ and $0 \leq n_{HeI}, n_{HeII} \leq n_{He}$. This last step is repeated many times until the results converge. In practice this scheme is quite stable and the whole process needs about twenty iterations to finish.

3 SOME NUMERICAL RESULTS

3.1 Model Results

We have carried out numerical calculations for several models. In these calculations we have adopted $n_H(0) = 5\,\mathrm{cm}^{-3}$, $r_c = 0.2\,\mathrm{kpc}$ and $s_1 = s_2 = s_3 = 0$. The other input model parameters are given in Table 1. In this table $J_{-21}(HI)$ is the HI Lyman limit intensity of the input ionizing field expressed in units of 10^{-21}ergs

$\sec^{-1}\mathrm{cm}^{-2}\mathrm{Hz}^{-1}\mathrm{sr}^{-1}$. $J_{-21}(HeI)$ and $J_{-21}(HeII)$ are similarly defined. The adoption of $J_{-21}(HI) = 0.715$ makes $J^0_{\nu_L}/\alpha_B(HI) = 5\times10^{-9}$ergs $\mathrm{cm}^{-5}\mathrm{Hz}^{-1}\mathrm{sr}^{-1}$, which is the value used in most of our Chapter Five models for pure hydrogen clouds.

The calculated HI, HeI and HeII fractions, n_{HI}/n_H, n_{HeI}/n_{He} and n_{HeII}/n_{He}, and their logarithms, as a function of radius r are given in Figs. 2—7. Also shown in these figures are the radial optical depth $\tau_r(r)$, and the optical depth at an impact distance b, $\tau_b(b)$. For HI these two optical depths are defined by

$$\tau_r(r) = \sigma_{\nu_L}(HI)\int_r^{R_{cut}} n_{HI}(r')dr', \tag{3.1}$$

and

$$\tau_b(b) = 2\sigma_{\nu_L}(HI)\int_0^{(R^2_{cut}-b^2)^{1/2}} n_{HI}(z)dz. \tag{3.2}$$

These two optical depths are similarly defined for HeI and HeII. In Figs.2—7 results for HI are shown in solid lines, HeI results in dashed lines and HeII results in dot-dash-dot-dash lines.

3.2 Discussion

We now discuss briefly some of the results. Comparing Fig. 2(b) (Model 1) and Fig. 4(b) (Model 3) we can examine the effect due to the different cut-off frequencies. In Fig. 2(b) ν_c/ν_L=15 while in Fig. 4(b) this ratio is 30. As we have discussed in Chapter Five the high frequency cut-off has little effect on the HI distribution. But the very high energy photons can effectively ionize HeI to form more HeII deep into the cloud. The reason is that the HeI photoionization cross section $\sigma_\nu(HeI)$

goes like ν^{-2} while $\sigma_\nu(HeII) \propto \nu^{-3}$. Since HeII is not further ionized by these very high energy photons, there is a net increase in HeII abundance. Compare the other curves in Figs. 2 and 4 we see this high frequency cut-off effect is not very significant to the optical depths $\tau_r(r)$ and $\tau_b(b)$.

We now compare Model 1 (Fig. 2) and Model 4 (Fig. 5). In Model 4 the intensity at the HeII Lyman limit is further decreased by a factor of 10, compared with that in Model 1. This has little effect on HI and HeI distributions. But since HeII ionizing photons are decreased significantly the HeII abundance is drastically increased, as can be seen from Fig. 5(b). The outcome is that beyond radius $r \simeq$ 4kpc the HeII Lyman limit optical depth $\tau_b(HeII)$ (at $\nu = 4\nu_L$) is about $\lesssim 100$ times larger than the HI Lyman limit optical depth $\tau_b(HI)$ (at ν_L). Since $J^0_{\nu_L}/J^0_{4\nu_L} = 100$ in Model 4, assuming the cloud is fully ionized we get $\tau_b(HeII)/\tau_b(HI) \simeq 45$. The reason this estimate is a factor of 2 smaller than the model result is that in our numerical calculations we have included the ionizing photons produced in the HeII recombination processes to form HeI. Since HeI absorbs the high energy photons and re-emits them at lower frequencies where the ionization cross section for ionizing HI is larger, thus the HI is further ionized. It will be very interesting to include the HeIII recombination terms which we have dropped to see how the ration $\tau_b(HeII)/\tau_b(HI)$ changes.

Comparison of Model 4 and Model 5 (Fig. 6) shows that decreasing the intensity at ν_2 affects the HI content deep into the cloud and the ionization boundary

is moved out a little bit (about 0.7kpc; see Figs. 4(b) and 5(b)). Again the HI optical depth $\tau_b(HI)$ is not significantly altered (see Figs. 4(d) and 5(d)). But understandably the HeI optical depth $\tau_b(HeI)$ is significantly increased (see Figs. 4(d) and 5(d)).

Finally in Model 6 (Fig. 7) the intensity at ν_2 is decreased by a factor of 10 as compared with that in Model 1. The comparison of these two models is like comparing Model 4 and Model 5.

It is clear from our model calculations that the absorptions produced by QSO absorption line systems and the resulting background are coupled together: in order to know the absorptions we need to know the input ionizing radiation spectrum, which, in turn, is determined by both the ionizing sources and the intervening absorbers. The spectral shape just above the HI Lyman limit frequency can be readily calculated if we know the source luminosity function. In this case only HI Lyman continuum absorption is important and we know from observations the HI column density distribution and the line number density evolution with redshift. For higher frequencies, at which HeI and HeII continuum absorption is significant, an iteration scheme may have to be used to get a self-consistent spectral shape for the ionizing field (Madau 1991), even though we know the source luminosity function. This is the work we are going to do in the next step.

ACKNOWLEDGMENT

This work was partly supported by NSF Grant AST84-51725.

REFERENCES

Giroux, M. L., & Shapiro, P. R., 1991. In: *After the First Three Minutes*, eds. S. S. Holt, C. L. Bennet, & V. Trimble (AIP), p352.

Hummer, D. G. & Seaton, M. J., 1964. *Mon. Not. R. astr. Soc.*, **127**, 217.

Madau, P., 1991. *Astrophys. J. Lett.*, **376**, L33.

Miralda-Escudé, J. & Ostriker, J. P., 1991. *Astrophys. J.*, submitted.

Miralda-Escudé, J. & Ostriker, J. P., 1990. *Astrophys. J.*, **350**, 1.

Møller, P. & Jakobsen, P., 1990. *Astron. Astrophys.*, **228**, 299.

Osterbrock, D. E., 1989. *Astrophysics of Gaseous Nebulae and Active Galactic Nuclei*, University Science Book, California.

Steidel, C. C., 1990. *Astrophys. J. Suppl. Ser.*, **74**, 37.

Steidel, C. C. & Sargent, W. L. W., 1989. *Astrophys. J. Lett*, **343**, L33.

Table 1. Model parameters.

Models	R_{cut} (kpc)	$J_{-21}(HI)$	$J_{-21}(HeI)$	$J_{-21}(HeII)$	ν_c/ν_L
M1	23	0.715	0.715	0.0715	15
M2	23	0.715	0.715	0.0715	20
M3	23	0.715	0.715	0.0715	30
M4	45	0.715	0.715	0.00715	15
M5	45	0.715	0.0715	0.00715	15
M6	45	0.715	0.0715	0.0715	15

FIGURE CAPTIONS

Figure 1. Geometry of the non-uniform spherical cloud models.

Figure 2. For Model 1 parameters. (a) Fractional ionization log(frac) *vs.* r for HI (solid line), HeI (dashed line) and HeII (dot-dash-dot-dash line); (b) Fractional ionization frac *vs.* r; (c) $\log(\tau_r(r))$ *vs.* r; (d) $\log(\tau_b(b))$ *vs.* b.

Figure 3. Same as in Fig. 2, but for Model 2 parameters.

Figure 4. Same as in Fig. 2, but for Model 3 parameters.

Figure 5. Same as in Fig. 2, but for Model 4 parameters.

Figure 6. Same as in Fig. 2, but for Model 5 parameters.

Figure 7. Same as in Fig. 2, but for Model 6 parameters.

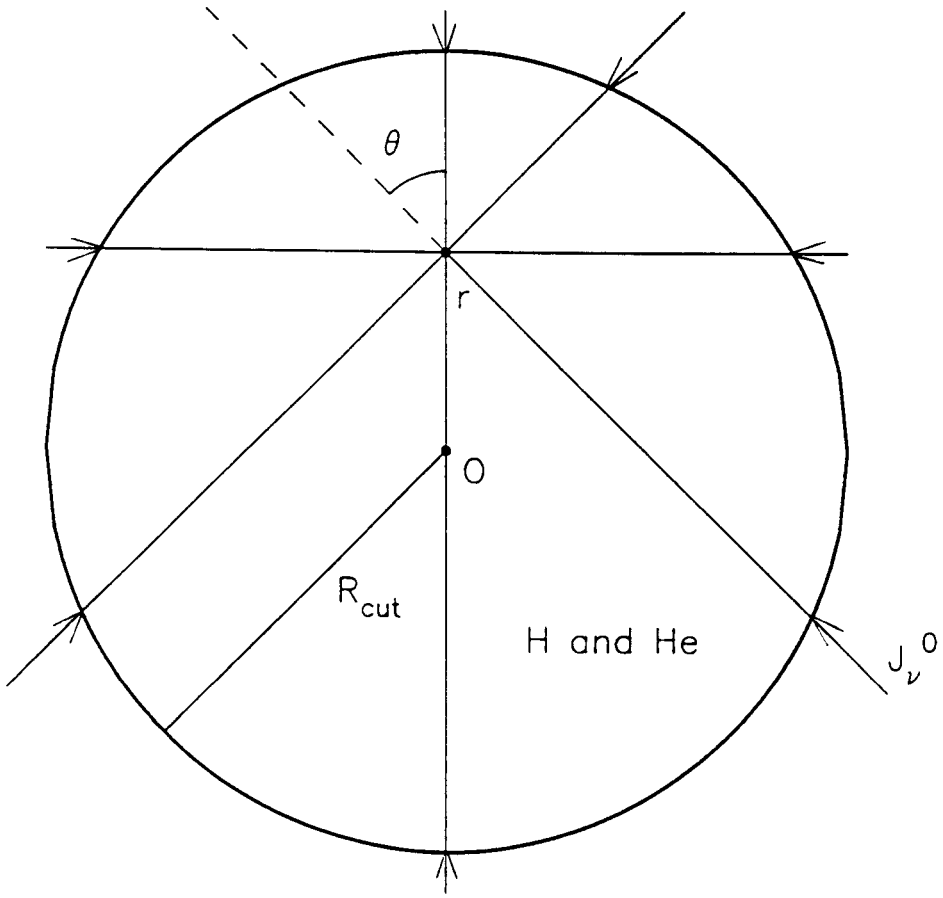

Figure 1

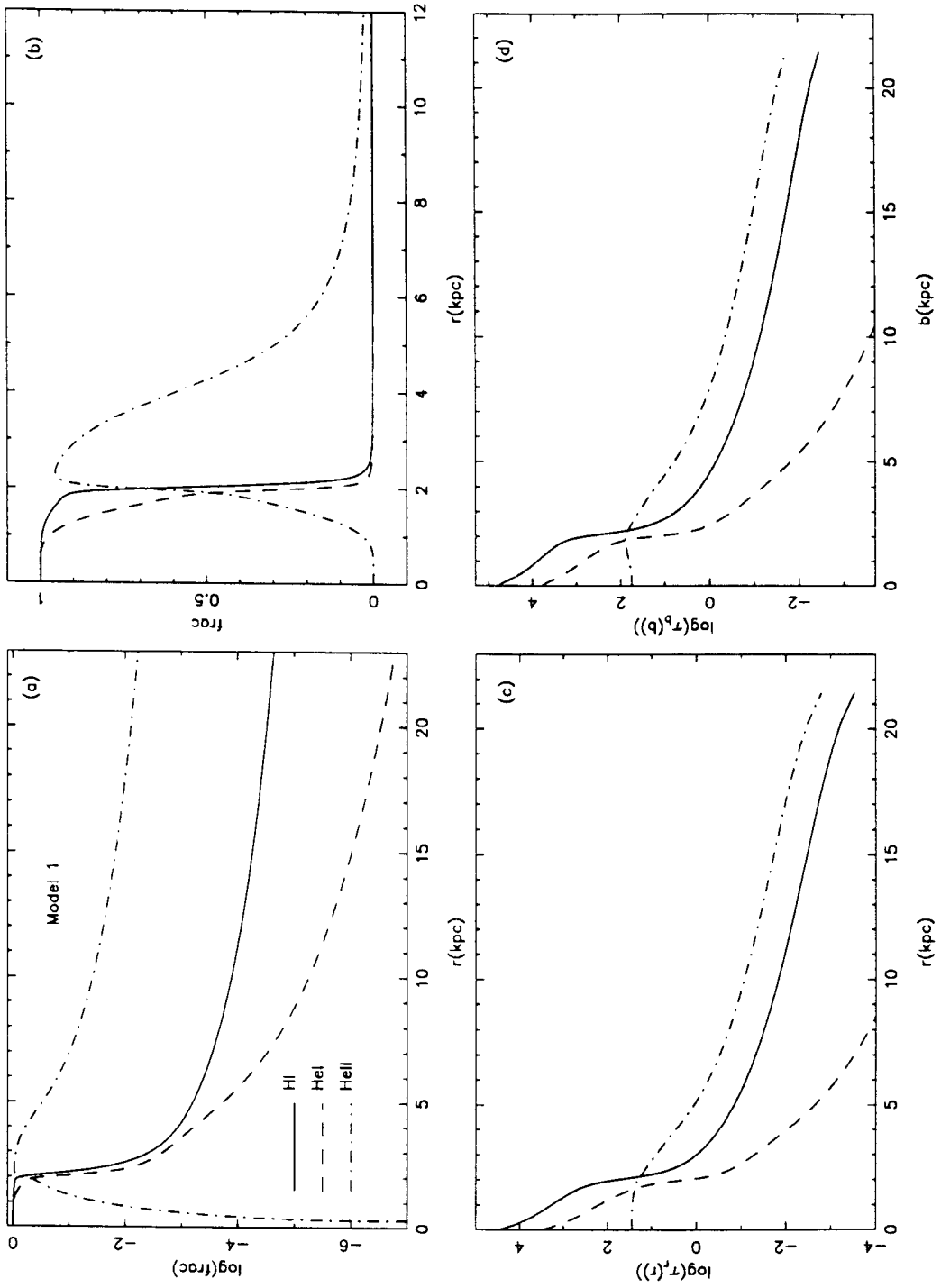
(a)
Model 1
HI
HeI
HeII
log(frac)
r(kpc)
(b)
frac
(c)
log(τ_r(r))
r(kpc)
(d)
log(τ_b(b))
b(kpc)

Figure 2

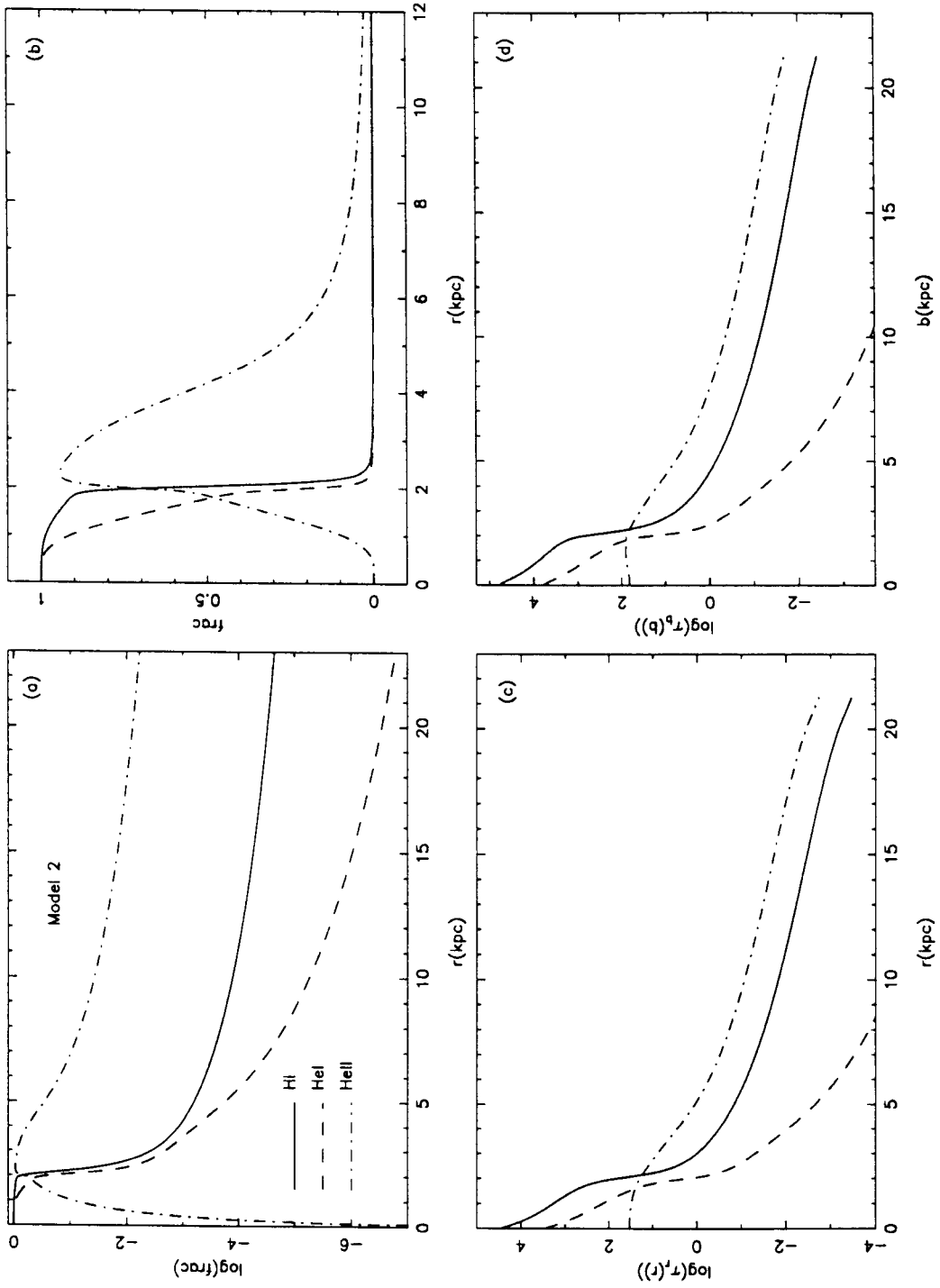
(a)
Model 2
HI
HeI
HeII
log(frac)
r(kpc)
(b)
frac
(c)
log(τ_r(r))
r(kpc)
(d)
log(τ_b(b))
b(kpc)

Figure 3

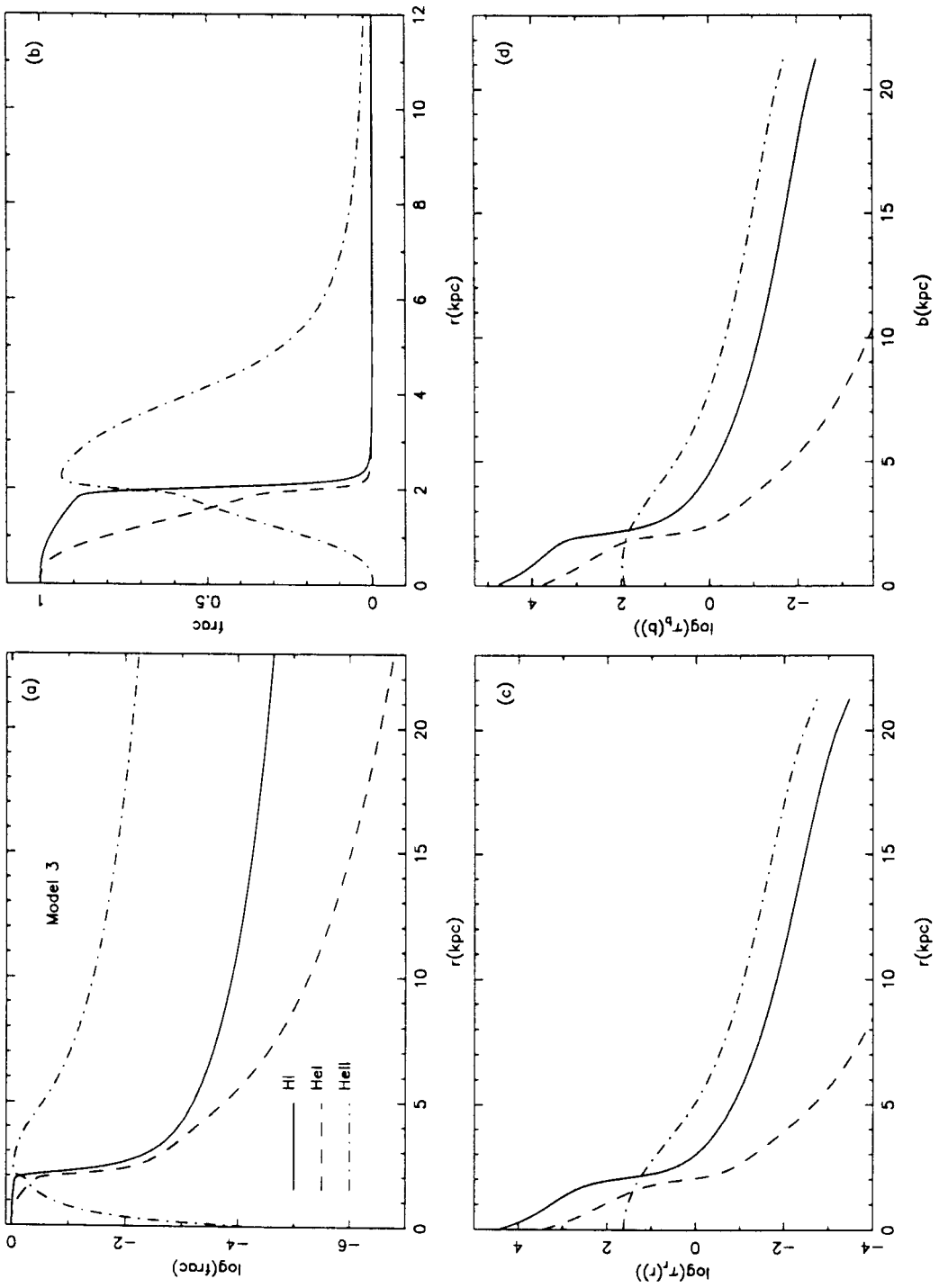
(a)
Model 3
HI
HeI
HeII
log(frac)
r(kpc)
(b)
frac
(c)
log(τ_r(r))
r(kpc)
(d)
log(τ_b(b))
b(kpc)

Figure 4

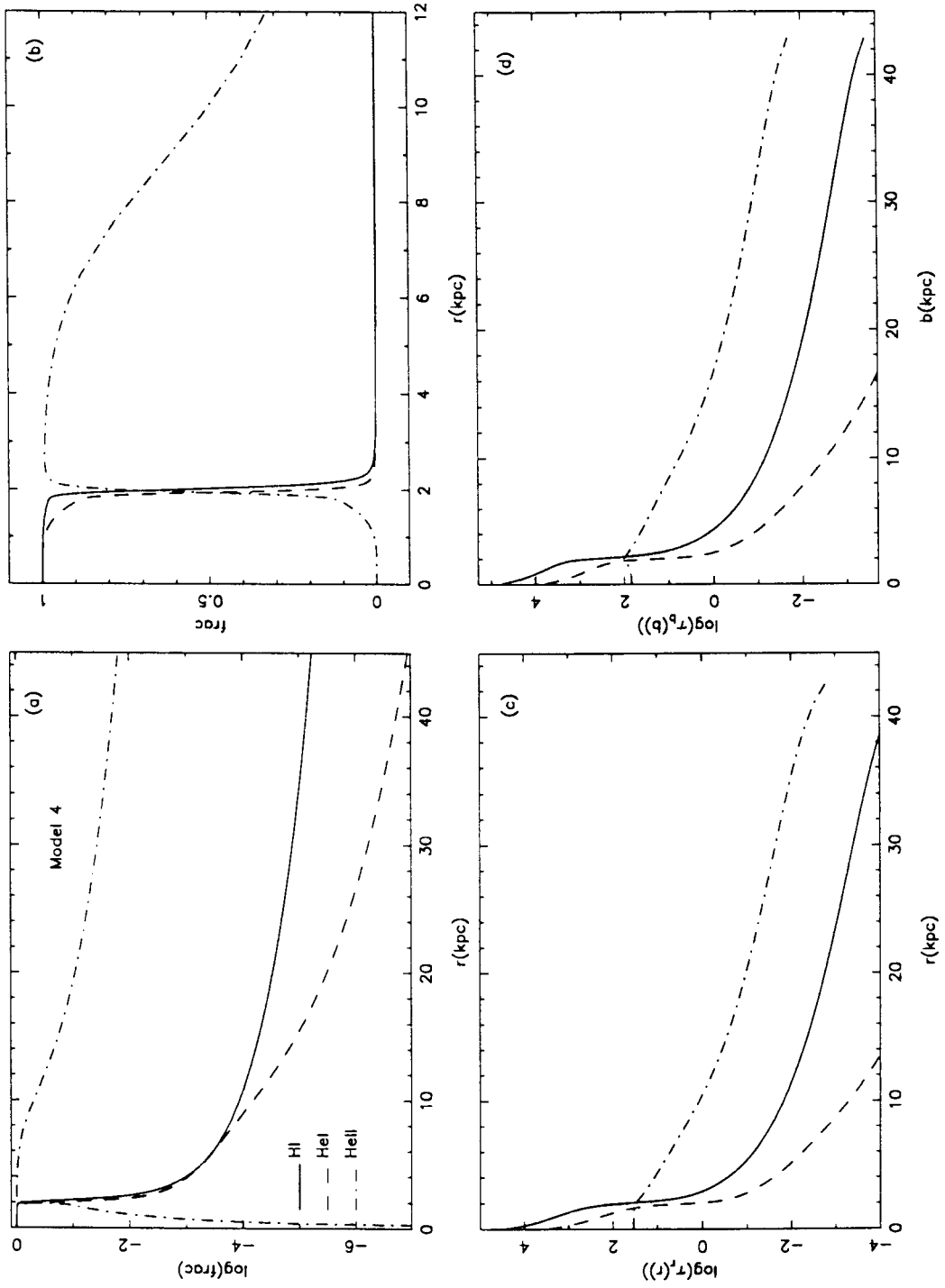
(a)
Model 4
HI
HeI
HeII
log(frac)
r(kpc)
(b)
frac
(c)
log(τ_r(r))
r(kpc)
(d)
log(τ_b(b))
b(kpc)

Figure 5

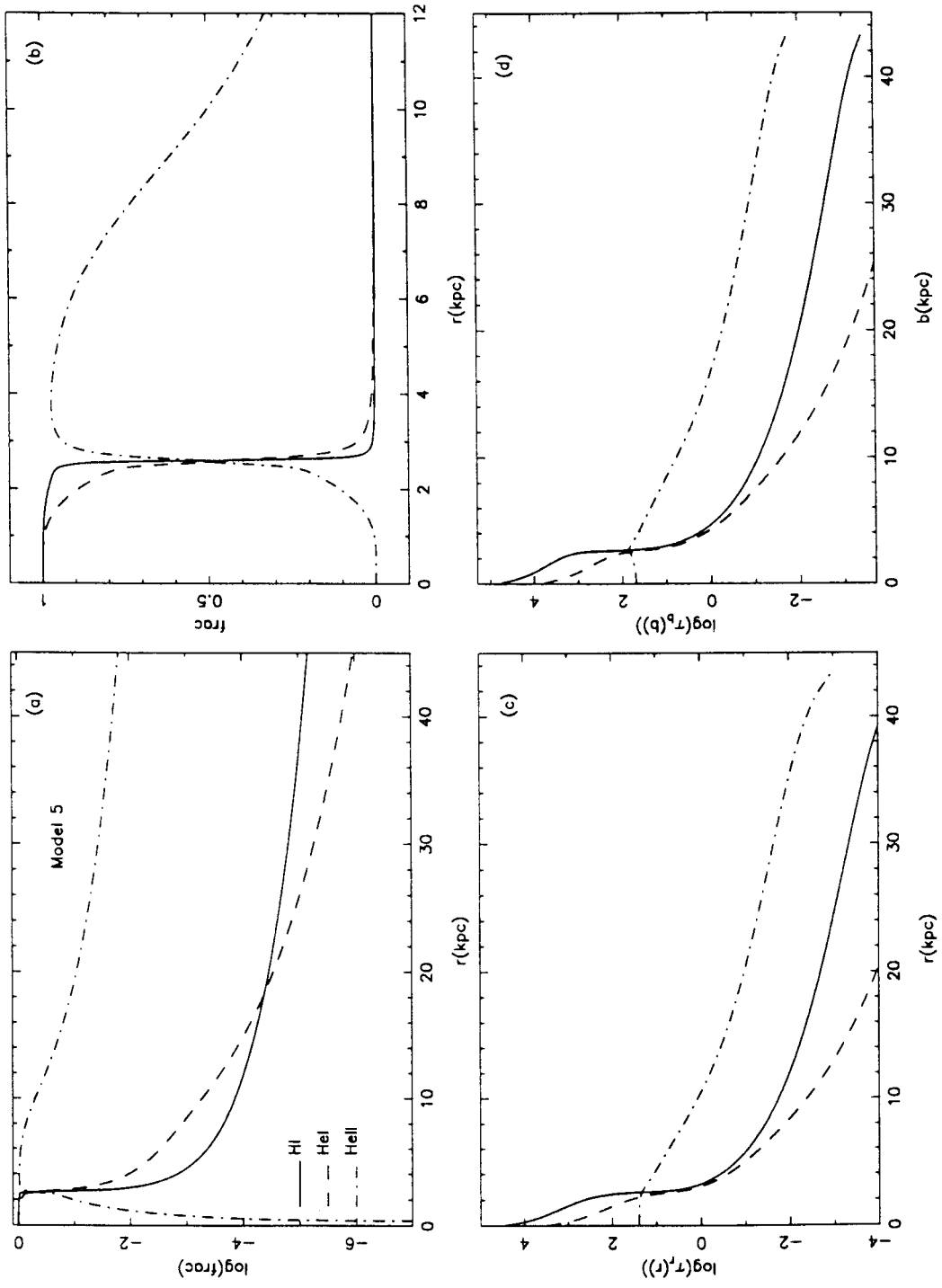
(a)
Model 5
HI
HeI
HeII
log(frac)
r(kpc)
(b)
frac
(c)
log(τ_r(r))
r(kpc)
(d)
log(τ_b(b))
b(kpc)

Figure 6

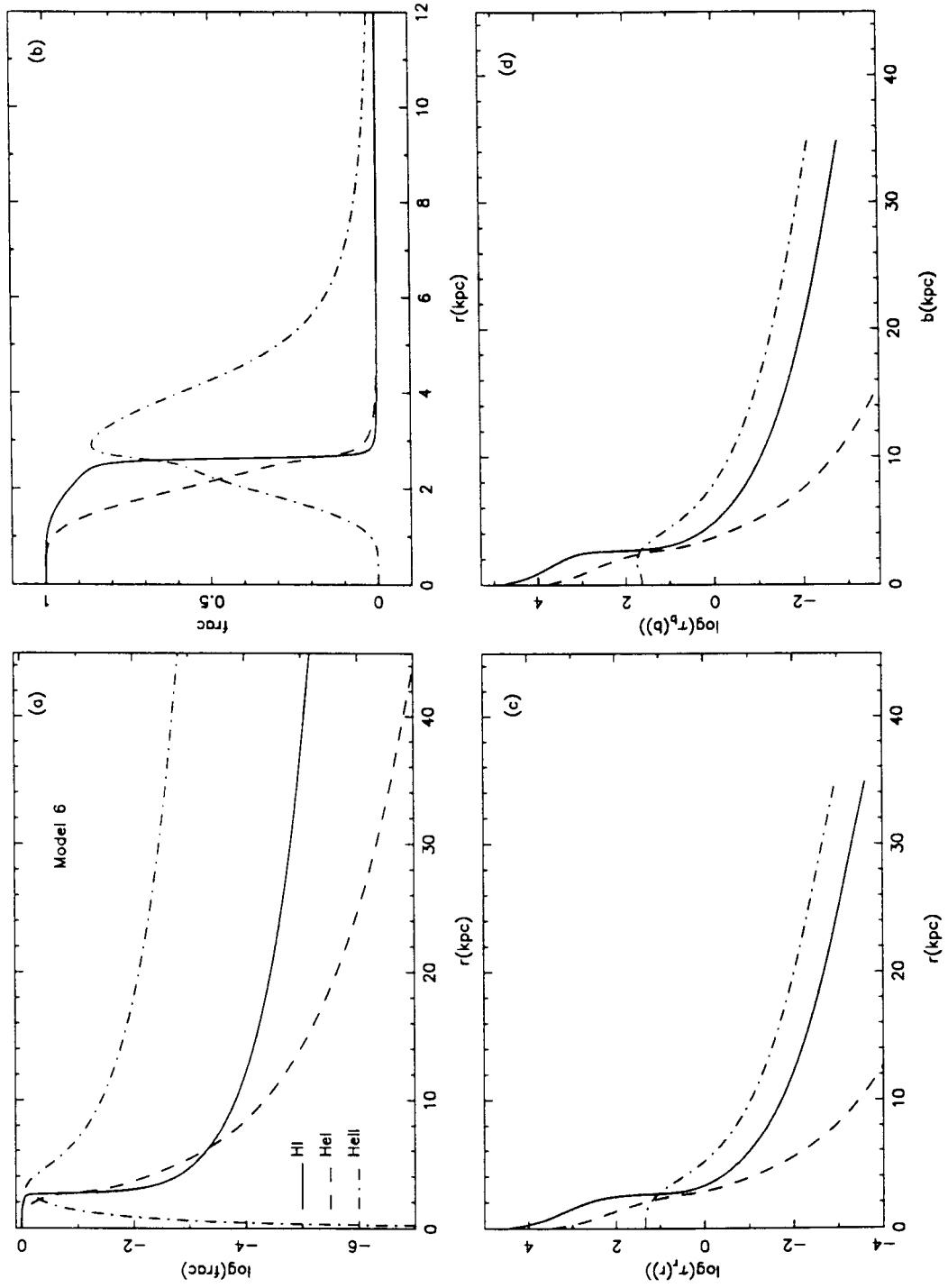
(a)
Model 6
HI
HeI
HeII
log(frac)
r(kpc)
(b)
frac
(c)
log(τ_r(r))
r(kpc)
(d)
log(τ_b(b))
b(kpc)

Figure 7